

https://dspace.org/

In situ conjugation-co-fabrication of bioarchetypes employing 3D print processing

Sithole, Mduduzi N

2019

https://hdl.handle.net/10539/29780

Sithole, Mduduzi Nkosinathi, In situ conjugation-co-fabrication of bio archetypes employing 3D print processing, University of the Witwatersrand, Johannesburg, <http://hdl.handle.net/10539/29780>

Downloaded from a DSpace repository. https://dspace.org/

IN SITU CONJUGATION-CO-FABRICATION OF BIOARCHETYPES EMPLOYING 3D PRINT PROCESSING

MDUDUZI NKOSINATHI SITHOLE

A thesis submitted to the Faculty of Health Sciences, University of the Witwatersrand, in fulfilment of the requirements for the degree of

Doctor of Philosophy



UNIVERSITY OF THE
WITWATERSRAND,
JOHANNESBURG

Supervisor:

Professor Viness Pillay

Department of Pharmacy and Pharmacology, Faculty of Health Sciences,

University of the Witwatersrand, South Africa

Co-Supervisors:

Professor Yahya Essop Choonara

Professor Lisa Claire du Toit

Professor Pradeep Kumar

Department of Pharmacy and Pharmacology, Faculty of Health Sciences,

University of the Witwatersrand, South Africa

Johannesburg

2019

DECLARATION

I, Mduduzi Nkosinathi Sithole, declare that this thesis is my own work. It has been submitted for the degree of Doctor of Philosophy in the Faculty of Health Sciences at the University of the Witwatersrand, Johannesburg, South Africa. It has not been submitted before for any degree or examination at this or any other University.

.....

Signed this 27 day of June 2019

ANIMAL ETHICS DECLARATION

I, Mduduzi Nkosinathi Sithole, hereby confirm the study entitled "*In vivo* assessment of 3D printed, *in situ* Conjugated-co-Fabricated, Alginate-PEI Scaffolds using New Zealand White Rabbits" was approved by the Animal Ethics Screening Committee (AESC) of the University of the Witwatersrand with Ethics Clearance Number 2017/10/64D.

APPENDIX A

RESEARCH OUTPUTS

Publications arising from PhD work

1. Mduduzi N. Sithole, Pradeep Kumar, Lisa C. du Toit, Thashree Marimuthu, Yahya E. Choonara, Viness Pillay. A 3D bioprinted *in situ* conjugated-co-fabricated scaffold for potential bone tissue engineering applications. Journal Biomedical Materials Research Part A, 2018, 106A:1311–1321 *[Research Article].*

APPENDIX B

2. Mduduzi N. Sithole, Pradeep Kumar, Lisa C. du Toit, Yahya E. Choonara, Viness Pillay. Reinforced, composite biomaterial 3D printed scaffold for bone tissue engineering: Tuning mechanical properties and cellular affinity (Submitted to Materials Science: Materials in Medicine) [Review Article].

APPENDIX C

3. Mduduzi N. Sithole, Pradeep Kumar, Yahya E. Choonara, Lisa C. du Toit, Kennedy H. Erlwanger, Viness Pillay. 3D bioprinted biomaterial scaffold for bone tissue engineering: *in vitro* cell assessment and *in vivo* animal studies (Submitted to Materials Science: Materials in Medicine) [Research Article].

APPENDIX D

Research presentations

1. Mduduzi N. Sithole, Pradeep Kumar, Lisa C. du Toit, Thashree Marimuthu, Yahya E. Choonara, Viness Pillay. A 3D bioprinted *in situ* conjugated-co-fabricated scaffold for potential bone tissue engineering applications. AAPS PharmSci 360, Washington DC, Walter E. Washington Convention Center, USA, November 4-7, 2018.

2. Mduduzi N. Sithole, Pradeep Kumar, Lisa C. du Toit, Thashree Marimuthu, Yahya E. Choonara, Viness Pillay. The impact of 3D printing in the health sector. TECH MEET UP 4 ADDITIVE MANUFACTURING, 3D printing, Tshimologong precint, 41 Juta Street, JHB. October 18, 2018.

3. Mduduzi N. Sithole, Pradeep Kumar, Lisa C. du Toit, Thashree Marimuthu, Yahya E. Choonara, Viness Pillay. The impact of 3D printing in the health sector. Global

Entrepreneurship. Medical Technology Talk, Tshimologong precint, 41 Juta Street, JHB. November 16, 2018.

APPENDIX E

ABSTRACT

Bone tissue has the natural ability to self-regenerate or self-heal, however, large-size (critical-sized) bone defects do not have the ability to self-heal to completion without external intervention. Traditional repair treatments for critical-sized or non-union bone defects have been centered on orthopaedic implants, allografts, and autografts. However, these techniques suffer from a number of limitations such as lack of available donors and inadequate biomechanical properties. A constructive development of novel fabrication methods and the design of novel composite 3D printed biomaterial scaffolds will address the challenge of complete healing of critical-sized bone defects. Furthermore, 3D printing technology have emerged as an innovative tool, with great potential in designing and fabrication of novel composite 3D biomaterial scaffolds. Recently, there has been a huge interest in 3D printing biomaterial scaffolds for bone tissue engineering application. A number of reinforced multi-biomaterials 3D printed scaffolds have been developed and investigated as a key solution for the mechanical and biological properties. But there is still a huge gap for appropriate composite biomaterials that will yield composite 3D biomaterial scaffolds with acceptable mechanical and biological properties for bone tissue engineering application. Developing novel fabrication methods, which will increase the limited printable biomaterial, yielding 3D printed biomaterial scaffolds for bone tissue engineering application, will be of great advantage in bone tissue engineering research and be a solution in the healing of critical-sized bone defect. The use of single-component biomaterials independently poses limitations in their properties as scaffolds for bone tissue engineering application. In this research, a composite 3D printed biomaterial scaffold was fabricated with desirable mechanical and biological properties for bone tissue application. This 3D biomaterial scaffold was engineered by modifying sodium alginate (NaAlg) with silica gel (Si), through *in situ* conjugated with polyethylenimine (PEI) yielding a composite 3D printed biomaterial scaffold to regulate the regeneration of new bone tissue formation. The method of fabrication was based on the novel single step *in situ* conjugation-co-fabrication of the biomaterial scaffold employing 3D bioprinter technology as an innovative tool. The 3D printed biomaterial scaffold maintained its 3D architecture for the duration of the 28 day degradation investigation, while potentially permitting the infiltration of nutrients, growth factor, and cells, evident by the increased solvent penetration into the scaffold observed via Magnetic Resonance Imaging (MRI) studies. The scaffold porosity and pore size were found to be 60% and 210µm, respectively. Biomechanical evaluation revealed a Young's modulus of 60MPa highlighting that the scaffold in its current form possesses the mechanical capabilities for certain bone tissue engineering applications. *In vitro* studies, which include: biomineralization (e.g. Ca-P) and biological parameters (such as cell viability, cell adhesion, and cell proliferation) were investigated and analysed. Osteoblast-like MG63 cells were used and cultured on the novel composite 3D printed biomaterial scaffolds to determine the various biological responses/parameters. Cells-scaffolds were cultured for seven days, thereafter, light microscopy and electron scanning microscopy (SEM) were used to qualitatively examine cell adhesion, cell proliferation and surface morphology; MTS assay was used to quantitatively determine cell viability. Therefore, the novel composite 3D printed biomaterial scaffold exhibited biomineralization (e.g. Ca-P) confirmed through the EDX and FTIR analysis. Light microscopy and scanning electron microscopy (SEM) revealed that the osteoblast-like MG63 cell cultured on the scaffold were clearly attached to its surface and proliferated within the scaffolds pores. Viability of cells cultured on the composite 3D printed biomaterial scaffold and on the control increased over time ($P < 0.05$), however, at respective time point, cell viability was not significantly different between the two groups ($P > 0.05$). Therefore, these results suggest that the novel composite 3D printed biomaterial scaffold is a biocompatible material. *In vivo* studies were performed using New Zealand White Rabbits model to assess new bone formation from the composite 3D printed biomaterial scaffold and control. Therefore, the final composite 3D printed biomaterial scaffold provided a pro-regenerative platform, rich in mechanical, topographical and biological cues and guides the cells towards functional regeneration. Histology results revealed that there was significant new bone formation especially at week 8 in all induced bone defects. It was also noted that the scaffold containing growth factors had complete bone formation (week 8 complete) compared to the scaffold without growth factors and the empty defect (the control). There was no sign of pain and advance tissue reaction, therefore; the composite 3D printed biomaterial scaffold proved to provide a pro-regenerative platform for bone tissue engineering application.

ACKNOWLEDGEMENTS

My highest thank you to the Lord for always loving me and his constant guidance through my research. God has blessed me with amazing parents, Cate Elizabeth Sithole and Zibuse Sithole, for their support in my academic journey. A special thanks to my mother for her guidance and prayers throughout my life.

A special thank you to my beautiful wife Linda Elizabeth Sithole who always supported me emotionally and sometimes edited my research papers for spelling errors plus she believed in me.

A thank you to my siblings, there are my best friends, they love me unconditionally. Such love keeps me going. I love you all.

This project would have not been possible without the mentoring and inspiration of my supervisor Professor Viness Pillay and my co-supervisors, Professor Yahya Choonara, Professor Lisa du Toit, and Professor Pradeep Kumar. I am most grateful for the knowledge and skills I have gained under your mentorship and look forward to another prosperous journey in the field of research which I intend on undertaking in the near future.

Thank you to Mr. Sello Ramarumo, Mr. Bafana Temba and Ms. Phumzile Madondo for their indispensable assistance with the running of the laboratories.

My sincere thanks to the staff of Wits Department of Pharmacy and Pharmacology and the staff of Central Animal Services (CAS) at the University of the Witwatersrand for their assistance and expertise during *in vivo* studies.

A special thanks to the National Research Foundation (NRF) for all their financial assistance throughout the duration of this research.

And we know that in all things God works for the good of those who love Him, who have been called according to His purpose
Romans 8:28

DEDICATION

This thesis is dedicated to the pillar of my existence, my motivator, my wife, Linda Elizabeth Sithole and my first born Uminathi Kate Aluta Sithole. Thank you for being there for me my love and being the catalyst for me to finish and give the two of you a better life.



TABLE OF CONTENTS

DECLARATION……i

ANIMAL ETHICS DECLARATION……..ii

RESEARCH OUTPUTS……iii

ABSTRACT……v

ACKNOWLEDGEMENTS……vi

DEDICATION……vii

TABLE OF CONTENTS……viii

LIST OF ABBREVIATIONS……xvi

LIST OF EQUATIONS……xviii

LIST OF FIGURES……xix

LIST OF TABLES……xxii

CHAPTER ONE

INTRODUCTION AND BACKGROUND

1.1. BACKGROUND OF THIS STUDY 1

1.2. RATIONALE AND MOTIVATION 3

1.3. AIM AND OBJECTIVES 6

1.4. NOVELTY OF THIS STUDY 6

1.5. OVERVIEW OF THE THESIS 7

1.6. REFERENCES 8

CHAPTER TWO

REINFORCED, COMPOSITE BIOMATERIAL 3D PRINTED SCAFFOLD FOR BONE TISSUE ENGINEERING: TUNING MECHANICAL PROPERTIES AND CELLULAR AFFINITY

2.1. INTRODUCTION 10

2.2. CHALLENGES WITH SINGLE-COMPONENT BIOMATERIALS FOR 3D PRINTING BONE TISSUE SCAFFOLD 14

2.3. RATIONALE FOR REINFORCEMENT OF MULTI-BIOMATERIALS FOR 3D PRINTED SCAFFOLDS 18

2.4. SCAFFOLD FABRICATION APPROACHES FOR BIOMATERIAL SCAFFOLD REINFORCEMENT 19

2.4.1. Post-3D Printed Biomaterial Scaffolds Dip Coating Modification 19

2.4.2. Modification by *in situ* Co-Fabrication via 3D Printing Method 20

2.4.3. Pre-Processed Biomaterials Modification Method for 3D Printing 20

2.5. REINFORCED, MULTI-BIOMATERIAL, 3D PRINTED SCAFFOLDS FOR IMPROVEMENT OF MECHANICAL PROPERTIES AND CELL AFFINITY 21

2.6. REPRESENTATIVE EXAMPLES OF REINFORCED, 3D PRINTED BIOMATERIALS SCAFFOLDS FOR BONE TISSUE ENGINEERING 24

2.6.1. Alginate-Based Reinforced 3D Printed Biomaterial Scaffolds for Bone Tissue Engineering 25

2.6.2. Silica Reinforced 3D Printed Biomaterial Scaffolds for Bone Tissue Engineering 28

2.7. CONCLUDING REMARKS 29

2.8. REFERENCES 30

CHAPTER THREE

A 3D BIOPRINTED *IN SITU* CONJUGATED-CO-FABRICATED SCAFFOLD FOR POTENTIAL BONE TISSUE ENGINEERING APPLICATION

3.1. INTRODUCTION 41

3.2. MATERIALS AND METHODS 43

3.2.1. Materials 43

3.2.2. Fabrication of the 3D Bioprinted *in situ* Conjugated-co-fabricated Scaffold Bioarchetypes 44

3.2.3. Determination of Chemical Transitions of the 3D Bioprinted Scaffolds and Native Biomaterials 45

3.2.4. Thermal Transition Analysis of the 3D Bioprinted Scaffold 46

3.2.5. Analysis of the Thermal Decomposition of the 3D Bioprinted Scaffold 46

3.2.6. Characterization of the 3D Bioprinted Scaffold Swelling and Structural Integrity Transitions 46

3.2.7. Surface Morphology Analysis of the 3D Bioprinted Scaffold 47

3.2.8. Porositometric Determination of the 3D Bioprinted Scaffolds 47

3.2.9. Comparative Degradation Rate Analysis of the 3D Bioprinted Scaffolds 47

3.2.10. Determination of the Biomechanical Properties of the 3D Bioprinted Scaffold 48

3.3. RESULTS AND DISCUSSION 48

3.3.1. Preliminary Evaluation of the 3D Bioprinted Scaffold 48

3.3.2. Chemical Transition Evaluation of the Bioprinted Scaffold 50

3.3.3. Assessment of Thermal Transitions and Stability of the Bioprinted Scaffold . 52

3.3.4. Evaluation of the Morphology, Porosity, Pore Size, Swelling and Structural Integrity of the Bioprinted Scaffold 55

3.3.5. Evaluation of Degradation of the Various Bioprinted Scaffolds 56

3.3.6. Evaluation of the Physicomechanical Strength of the Bioprinted Scaffold 57

3.4. CONCLUDING REMARKS 59

3.5. REFERENCES 60

CHAPTER FOUR

BIOCOMPATIBILITY AND BIOMINERALIZATION STUDY OF A NOVEL REINFORCED 3D PRINTED BIOMATERIAL SCAFFOLD

4.1. INTRODUCTION 65

4.2. MATERIALS AND METHODS 66

4.2.1 Materials 66

4.2.2. Determination of the Biomaterials Complexation and Gelation Kinetics 67

4.2.3. Preparation of the Novel *in situ* 3D Printed Biomaterial Scaffolds 67

4.2.4. Evaluation of the Biomechanical Properties of 3D Printed Biomaterial Scaffolds 68

4.2.5. Preliminary Mechanical Evaluation of the Different 3D Printed Biomaterial Scaffolds 69

4.2.6. Morphological Evaluation of the 3D Printed Porous Biomaterial Scaffold 70

4.2.7. Biomineralization Evaluation of the 3D Printed Biomaterial Scaffold 71

4.2.8. The *in vitro* Assessment using Osteoblast-like Cells 71

4.2.8.1. Cell culturing method for the osteoblast-like cell line 72

4.2.8.2. Seeding osteoblast-like cells onto the 3D printed biomaterial scaffold 72

4.2.8.3. Cell viability assay assessment for the novel 3D printed biomaterial scaffold 72

4.2.9. Osteoblast-like Cells Behaviour onto the 3D Printed Biomaterial Scaffold 73

4.2.9.1. Visualization of cell adhesion onto the 3D printed biomaterial scaffold 73

4.2.9.2. Osteoblast-like cell staining using methylene blue 73

4.3. RESULTS AND DISCUSSION 74

4.3.1. Complexation and Gelation Kinetics Evaluation of the Bio-Inks 74

4.3.2. Preliminary Mechanical Evaluation of the 3D Printed Biomaterial Scaffolds . 75

4.3.3. Surface Biomineralization Evaluation of the 3D Printed Biomaterial Scaffold 76

4.3.4. Evaluation of the Scaffold Pore Size, Pore Interconnectivity and Morphology 78

4.3.5. Evaluation of Cells Growth and Confluence before Seeding the Cells on the Scaffolds 79

4.3.6. Cell Viability and Cell Proliferation Evaluation on the Printed Scaffold 80

4.3.7. Evaluation of Cell Adhesion and Cells Confluence on the 3D Printed Porous Scaffold 81

4.4. CONCLUDING REMARKS 85

4.5. REFERENCES 85

CHAPTER FIVE

***IN VIVO* ASSESSMENT OF THE NOVEL *IN SITU* 3D PRINTED BIOMATERIAL SCAFFOLD FOR BONE REGENERATION IN NEW ZEALAND WHITE RABBITS**

5.1. INTRODUCTION 88

5.2. MATERIALS AND METHODS 90

5.2.1. Materials 90

5.2.2. Animal Welfare, Housing and Habituation Prior to Scaffold Study Experiment 90

5.2.3. The 3D Printed Biomaterial Scaffolds Preparation Prior Implantation 91

5.2.4. Design and Surgical Procedure for the Main Intervention 91

5.2.4.1. The procedure for the pilot study 92

5.2.4.2. The design of the main study 92

5.2.4.3. Surgical procedure for the intervention 95

5.2.5. Post-operative Care of the New Zealand White Rabbits 97

5.2.6. Procedure for Euthanasia and Sample Collection 97

5.2.7. Samples Preparation for Histological Examination 97

5.3. RESULTS AND DISCUSSION 98

5.3.1. Pilot Study Assessment 98

5.3.2. Clinical and Histological Analysis 98

5.3.2.1. Clinical examination 98

5.3.2.2. Histological analysis 98

5.3.2.2.1. Histological examination for group 1 (week 1) 98

5.3.2.2.2. Histological examination for group 2 (week 2) 101

5.3.2.2.3. Histological examination for group 3 (week 4) 103

5.3.2.2.4. Histological examination for group 4 (week 8) 105

5.4. DISCUSSION 107

5.5. CONCLUDING REMARKS 109

5.6. REFERENCES 109

CHAPTER SIX

CONCLUSIONS, RECOMMENDATIONS AND FUTURE OUTLOOK

6.1. CONCLUSIONS 114

6.2. RECOMMENDATIONS AND FUTURE OUTLOOK 115

APPENDICES

APPENDIX A……...116

APPENDIX B……..….117

APPENDIX C……..…….118

APPENDIX D……..…….119

APPENDIX E……120

LIST OF ABBREVIATIONS

AESC - Animal ethics screening committee

3D printer - Three dimensional printer

MRI - Magnetic Resonance Imaging

SEM - Scanning Electron Microscopy

XRD - X-ray diffraction

TGA - Thermo-Gravimetric Analysis

TEM - Transmission Electron Microscope

ATR-FTIR - Attenuated Total Reflectance Fourier-Transform Infrared Spectroscopy

FBS - Foetal bovine serum

DSC - Differential Scanning Calorimetry

DMEM - Dulbecco's Modified Eagles Medium

ECM - Extracellular matrix

RP - Rapid prototyping

FDL - Fused deposition modelling

MIW - Direct ink writing

SLS - Selective laser sintering

DLP - Digital laser printing

Ca-P - Calcium phosphate

PEI - Polyethyleimine

PIC - Polyelectrolyte

NaAlg - Sodium alginate

FBS - Fetal bovin serum

EDX - Energy-dispersive X-ray

CAD - Computer aided design

α-MEM - alpha minimum essential medium

SBF - Simulated body fluid

BMPs - Bone Morphogenetic Proteins

CAS - Central Animal Service

UV - Ultra-Violet

HA - Hydroxyapatite

H&E stain - Haematoxylin and eosin stain

GT - Granulation tissue

PR - Periosteal reaction

NB - New bone

SD - Scaffold

DMEM - Dulbecco's Modified Eagles Medium

LIST OF EQUATIONS

Equation 3.1: Scaffold porosity formula ……47
Equation 3.2: Degradation rate % ……48
Equation 4.1: Scaffold porosity formula ……71
Equation 4.2: % Relative cell viability ……73

LIST OF FUGURES

Figure 1.1: Simplified reaction schematic for the fabrication of the bioarchetype scaffolds. 4
Figure 1.2: Schematic representation of general synthetic route for tissue engineering..... 5
Figure 2.1: The schematic workflow of the multidisciplinary approach utilized in the 3D printing of scaffolds for tissue engineering applications (Devi *et al.*, 2018)..... 11
Figure 2.2: Schematic flowchart for the fabrication of the 3D printed constructs/implants (Mok *et al.*, 2016)..... 13
Figure 2.3: Schematic representation of scaffolds dip-coating method (Coan et al., 2013). 20
Figure 2.4: Light microscopy morphology of (a) original osteoblast-like MG63 cells; (b-d) SEM microscopy of osteoblast-like MG63 cells (arrows) on the pure akermanite scaffold and (e-g) 5wt% nano-TiO_2 reinforced akermanite scaffold; (b and e) after cell culture for 3 days;(c and f) 7 days and (d and g) 10 days 23
Figure 2.5: Photograph of prototype sample part 3D printed Fe–30Mn scaffold powder after sintering (Chou *et al.*, 2013). 24
Figure 3.1: Schematic and photographic depiction of formation of the 3D bioprinted and *in situ* conjugated-co-fabricated scaffold..... 49
Figure 3.2: FTIR spectra of (a) Pristine Si, (b) Pristine NaAlg, (c) Pristine PEI, and (d) Alg-PEI/Si scaffold 51
Figure 3.3: XRD spectra of the (a) Pristine Si, (b) Pristine NaAlg, and (c) Scaffold..... 52
Figure 3.4: The TGA spectra for, a) Pristine Si, b) Pristine NaAlg, and c) Alg-PEI/Si..... 53
Figure 3.5: DSC thermal behaviour of a) Pristine Si, b) Pristine NaAlg, and c) Alg-PEI/Si 54
Figure 3.6: (a) Surface schematic of the proposed design of the bioprinted scaffold, (b) Cross-section schematic of the proposed design of the bioprinted scaffold, (c) SEM image of the surface section of the bioprinted Alg-PEI/Si scaffold**.**..... 55
Figure 3.7: Magnetic resonance imaging of the bioprinted scaffold..... 56
Figure 3.8: *In vitro* degradation (mass loss, %) of the bioprinted scaffolds..... 57
Figure 3.9: BioTester images and corresponding real-time image analysis and force-displacement graphs representing scaffold strength (a) before application of force and (b) during maximum stretch. 58
Figure 3.10: Stress-strain curve depicting Young's modulus of the bioprinted scaffold. 59
Figure 4.1: Bar Chart depicting Young's modulus of the three 3D printed biomaterial scaffolds. 70
Figure 4.2: Complexation and gelation kinetics of the three biomaterial scaffolds, a) Alg-PEI/Si, b) Alg-PEI/HAP and c) Alg-PEI/Nanoclay..... 75

Figure 4.3: The SEM, EDX surface elements analysis of a) the scaffold before immersion and b) scaffold after immerse in SBF (pH 7.4, 37^{o}C). 77
Figure 4.4: The FTIR spectra of a) scaffold before immersion as a control and b) scaffold after immerse in SBF (pH 7.4, 37^{o}C). 78
Figure 4.5: Scanning electron microscopy (SEM) pictures of the 3D printed porous scaffold. 79
Figure 4.6: Assessment of osteoblast-like MG63 cell differentiation a) day zero, b) day 2 and c) day 3..... 80
Figure 4.7: Cell viability performed on the 3D cell-scaffold within seven days..... 81
Figure 4.8: Light microscopy images of the cell-scaffolds at different time intervals..... 82
Figure 4.9: SEM images of osteoblast-like MG63 cells adhered to the 3D printed biomaterial scaffold at day seven. 83
Figure 4.10: Images from light microscopy, a) the scaffold without cells (control) and b) the scaffold with cells both treated with methylene blue..... 84
Figure 5.1: Photographic representation of (a – b) housing of the New Zealand White Rabbits, (c) measurement of rabbit's weight at Wits CAS unit. 91
Figure 5.2: Schematic showing the *in vivo* studies model for the implanted scaffold..... 94
Figure 5.3: Schematic representation of the surgical procedure for induction of nasal critical-sized bone defects in the New Zealand White Rabbit. 96
Figure 5.4: Histological images, a) scaffold with growth factors, b) scaffold without growth factors, c) an empty nasal defect at week one post-operation, H&E staining (x10 magnification): GT = granulation tissue; SD = scaffold mostly representd by the empty space; yellow arrows = blood vessels within the scaffold. There was negligible osteoblastic activity observed in all the defects..... 100
Figure 5.5: Histological images of the, a) scaffold with growth factors, b) scaffold without growth factors, c) an empty nasal defect at week 2 post-operation, H&E staining (x10 magnification): GT = granulation tissue; SD = scaffold mostly represented by the empty space; Yellow arrows = blood vessels within the scaffold, ENB = early new bone development, Black arrows = osteoblast, PR = periosteal reactions. Osteoblastic activity was observed in all the defects. ... 102
Figure 5.6: Histological images of the, a) scaffold with growth factors, b) scaffold without growth factors, c) an empty nasal defect at week 4 post-operation, H&E staining (x10 magnification): GT = granulation tissue; SD = scaffold mostly represented by the empty space; Yellow arrows = blood vessels within the scaffold, NB = new bone development, Black arrows = osteoblast, PR = periosteal reactions, Green arrows = osteocytes. There was a major

osteoblastic activity accompanied by new bone formation observed in all the defects..... 104

Figure 5.7: Histological images of the, a) scaffold with growth factors, b) scaffold without growth factors, c) an empty nasal defect at week 8 post-operation, H&E staining (x10 magnification): GT = granulation tissue; SD = scaffold mostly represented by the empty space; NB = new bone development, Black arrows = osteoblast, PR = periosteal reactions, Green arrows = osteocytes, There was major osteoblastic activity observed in all the defects**.**..... 106

LIST OF TABLES

Table 2.1: Characteristics of human cortical and cancellous bones. 14

Table 2.2: Summary of different single-components biomaterials used for bone tissue scaffold (Turnbull *et al.*, 2018). 16

Table 3.1: Parameters used to print the desire bioarchetype scaffold 44

Table 3.2: 3D bioprinted scaffold combinations and preliminary characterization 45

Table 4.1: Modified parameters used for the 3D printing of the porous biodegradable scaffolds. 68

CHAPTER ONE
INTRODUCTION AND BACKGROUND

1.1. BACKGROUND OF THIS STUDY

The development of biological substitutes that maintain, restore or improve the function of tissue is currently necessitated by the combined effort of interdisciplinary fields such as materials science, cell biology, genetics, engineering, mathematics and clinical science through tissue engineering (Bártolo *et al.,* 2008). The main purpose of tissue engineering is to come up with ways or strategies to repair, regenerate, restore, replace and reorganize tissues and/or organs. The fabrication of biomaterial scaffolds substitutes plays a significant part in tissue engineering since biomaterial scaffolds serve as templates for cell adhesion, proliferation and recruitment to infiltrate the deeper or inner site of the scaffolds. Biomaterial scaffolds also offer mechanical support during tissue regeneration/healing/restoration. Therefore, there are on-going attempts by researchers to develop optimized biomaterial scaffolds environment that will mimic the natural extracellular matrix (ECM) of the tissue under investigation (e.g. bone tissue) (Wu and Hsu, 2015).

Hence, polymeric biomaterials are attractive materials to be used in the fabrication of scaffolds since they offer significant 3D support for cell growth and tissue or organ formation (Park *et al.,* 2010). Different conventional fabrication techniques have been developed to fabricate biomaterial scaffolds to be utilized in tissue engineering, that includes, but not limited to, solvent casting, gas foaming, phase separation and salt leaching (Mironov *et al.,* 2003; Sachlos and Czernuszka, 2003). However, fabricating biomaterial scaffold structures with controlled pores interconnectivity is difficult when utilizing the above conventional polymeric biomaterial scaffolds processing techniques, because these techniques are not easily adjusted to yield structures that will support cell ingrowth or to control pore size for cell migration (Seitz *et al.,* 2005).

Several rapid-prototyping (RP) computer-aided technologies such as selective laser sintering, stereolithography, fused deposition, and 3D printing have been introduced and accepted in the synthesis of 3D biomaterial scaffolds for specific geometric control (Park *et al.,* 2010; Wu and Hsu, 2015). Furthermore, this synthetic approach for 3D biomaterials provides great opportunities with significant potential for tissue engineering. Supplementary insight on structure/function relation and cellular interaction within the tissue may be gained by the extension of these studies to three-dimension cellular control (Chen *et al.,* 2006). The

3D printing technology provides great potential as mentioned, but there are some significant limitations to be overcome before it can be recognized as a common bio-fabrication technique. One major significant limitation in relation to the 3D biomaterial bioprinter capability is the non-availability of diverse 3D printable biomaterials hereafter referred to as bio-inks (Guvendiren *et al.,* 2016).

The 3D printing technology is known as additive manufacturing (Gu *et al.,* 2016) or solid free-form fabrication and it has become the driving force in various areas of research (Lee and Dai, 2015). 3D bioprinting technology has been utilized to fabricate scaffolds from biomaterials due to specific advantages *w.r.t*. customized production, high precision and rapid fabrication (Gu *et al.,* 2016). Scaffolds are 3D biomaterials that are required to be biocompatible and mimic the properties of the Extracellular Matrix (ECM) namely cellular activity and mechanical support. If the scaffold is appropriately designed employing various bio- and physicochemical cues; it can act as a template for cell attachment, cell proliferation and the stimulation of tissue formation *in vivo*. Biomaterial scaffolds performance is determined by parameters such as pore size, chemistry, mechanical strength and pore volume (Bose *et al.,* 2013; Li *et al.,* 2014).

There is a great need for the diversity of 3D printable biomaterials for the synthesis of bioarchetypes scaffolds that conforms to specific characteristics and parameters needed for specific tissue engineering applications such as bone tissue. The fabrication, analysis, and development of novel bioarchetypes scaffolds and biodegradable polymeric biomaterials will constitute a centrepiece for the research efforts in the field of tissue engineering (repair, regeneration, restoration, and reorganization) (Liu and Ma, 2004).

Extrusion-based 3D printing is the most common method for scaffold fabrication procedure for tissue engineering applications (such as bone tissue). There are two widespread extrusion methods, namely, fused deposition modelling (FDL) and direct ink writing (DIW). The procedure that is mainly used in extrusion-based additive manufacturing is that pressure is applied in the biomaterial ink to extrude it through a nozzle as a melt or viscous liquid to form lines that gelate or solidify onto the building reactive solvent or building plate. A nozzle containing biomaterial ink follows a pre-defined path which is determined by a computer model to fabricate structures layer-by-layer. The solvent-cast direct-writing ink is biomaterials solutions in a preferably low boiling solvent (such as dichloromethane and tetrahydrofuran) that evaporate rapidly upon extrusion leaving a solid polymer matrix (Guvendiren *et al.,* 2016).

This research proposes to develop a novel bioarchetype scaffold employing 3D bioprinter technology whereby two or more biomaterials will be conjugated via 3D print processing as an innovative tool towards one-step conjugation-co-fabrication of biomaterial scaffolds which will be further seeded with specific cells (osteoblast-like MG63 cells) to form a construct engineered bio-substitute for *in vitro* cellular investigations.

1.2. RATIONALE AND MOTIVATION

There are significant defects (critical-sized bone defects) resulting from trauma or tumors, that cannot be easily repaired by the body without external intervention. Hence, for these defects (e.g. critical-sized bone defects), synthetic replacement applications involving 3D biomaterial scaffolds have great clinical potential as a repairing solution. Using such bioarchetypes scaffolds may further result in the reduction of tissue rejection by the body since the implantable biomaterials used has to be biocompatible and to some extent biodegradable (Seitz *et al.,* 2005). However, fabrication of a “perfect” defect-filling and ECM-mimicking 3D biomaterial scaffold is a challenge as most conventional techniques lack tailor-made fabrication capabilities.

3D biomaterial printing refers to the physical extrusion of a bio-ink or biomaterial polymer-ink that rapidly stabilizes upon deposition via a specific different mechanism and is repeated layer-by-layer for fabrication of a construct intended to interact with cells or tissue environment. Mechanical stiffness, incompatibility of materials, complicated liquid medium densities to preserve shape, low resolution and critical timing of gelation or solidification are some of the disadvantages that hinder efficient production of desired 3D biomaterial scaffold structures when using 3D bioprinting technology (Jakus *et al.,* 2016). Advanced materials development, can be optimized for bio-factors and may provide the potential to fabricate constructs satisfying complex biological requirements of tissue engineering scaffolds (Chia and Wu, 2015). However, not every feature of the tissue needs to be printed, since the 3D printed biomaterial scaffold will guide the cellular organization into more ordered structures reminiscent of natural tissue. Hence, the structural integrity concerning the bio-ink, upon extraction of the biomaterial ink onto a substrate, should ideally maintain the user-defined pattern across all three dimensions. Meaning the used materials must be mechanically soft enough to be extruded, though at the same time be stiff enough to be self-supporting upon deposition - maintaining the as-printed architecture across many layers.

Though there is huge progress in tissue engineering, but the reality of on-demand fabrication of functional and transplantable biomaterial scaffolds or tissues and organs is not fulfilled

completely yet. There are two main technical challenges that need to be overcome in order to advance from this point of research onward: firstly, we must expand on the limited available 3D printable biomaterials (bio-ink) capable of satisfactorily representing the chemical, physical, biological complexity, and diversity of the tissue and organs within the human body. Secondly, the fabricated 3D biomaterial scaffolds from the developed bio-inks must have certain characteristics that will lead to optimal printing, structural and biological outcomes.

This research focuses on fabricating novel bioarchetype scaffolds employing a 3D bioprinter as an advanced innovative tool wherein the constituent biomaterials [natural polymers (alginates)] will be conjugated via in-print processing. The medium of the 3D bioprint reaction will be maintained and controlled externally to mold the bioarchetype scaffolds with varied mechanical properties and pore and surface morphologies. The mode of *in situ* polymerization will be critically engineered for the choice of polymers used and to control the resulting structural and mechanical architecture. This will be significant since the mechanics of the biomaterial scaffold needs to closely match the endogenous matrix of the cells or tissue niches investigated. The naturally derived polymers that will be used have their own inherited method of gelation or solidification, such as ionic (alginate) crosslinking (Bajaj *et al.,* 2014). Figure 1.1, highlights the generalized in-process polymeric reaction approach employing 3D printing.

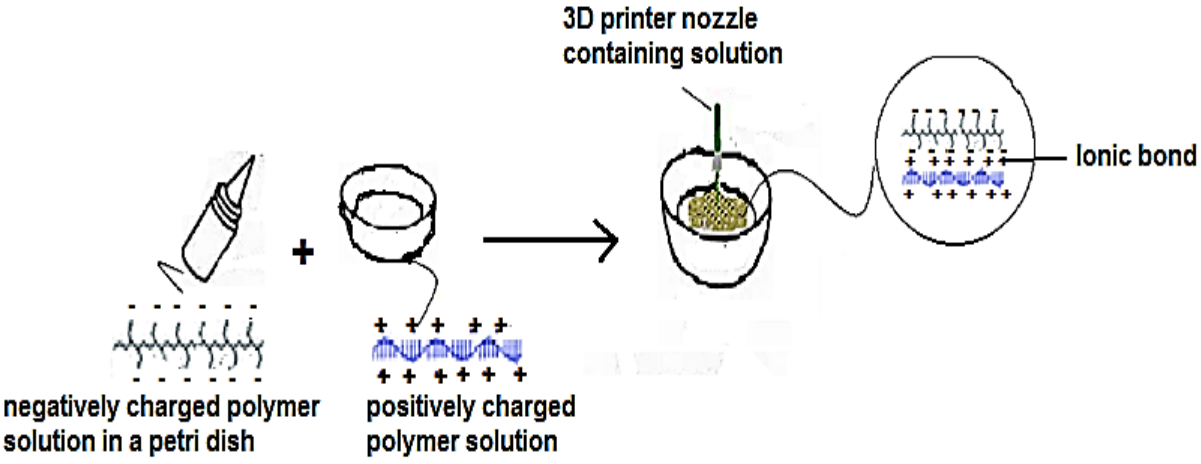


Figure 1.1: Simplified reaction schematic for the fabrication of the bioarchetype scaffolds.

For the 3D print processed biomaterials, the reaction mechanism may include thermal induced gelification, chemical conjugation, and complexation, precipitation induced solidification, and post-process solidification through sintering. Though, for the extruded biomaterials (bio-ink) to hold their shape during deposition, the rate of these reactions must be extremely high. By increasing polymer fraction or adding an inherently viscous

component one can increase the viscosity of the solution which can be utilized alone or in conjunction with layer-by-layer gelation or solidification. In another embodiment of this research, a cyto-conducing inorganic phase (e.g. silica) will be included via intermediate layering to form a robust substitute tissue. Hence, the aim was to fabricate a fully interconnected biocompatible bioarchetype scaffold that will be conjugated via innovative in-printing using the 3D bioprinter to form a variety of novel bioarchetypical scaffold matrices. The scaffold matrices were utilized in tissue engineering whereby osteoblast-like MG63 cells were seeded on the biomaterial scaffolds to generate specific tissue environment capable of enhanced cell attachment and complete tissue formation (Seitz *et al.,* 2005). Figure 1.2 represents the generalized synthetic route for tissue engineering.

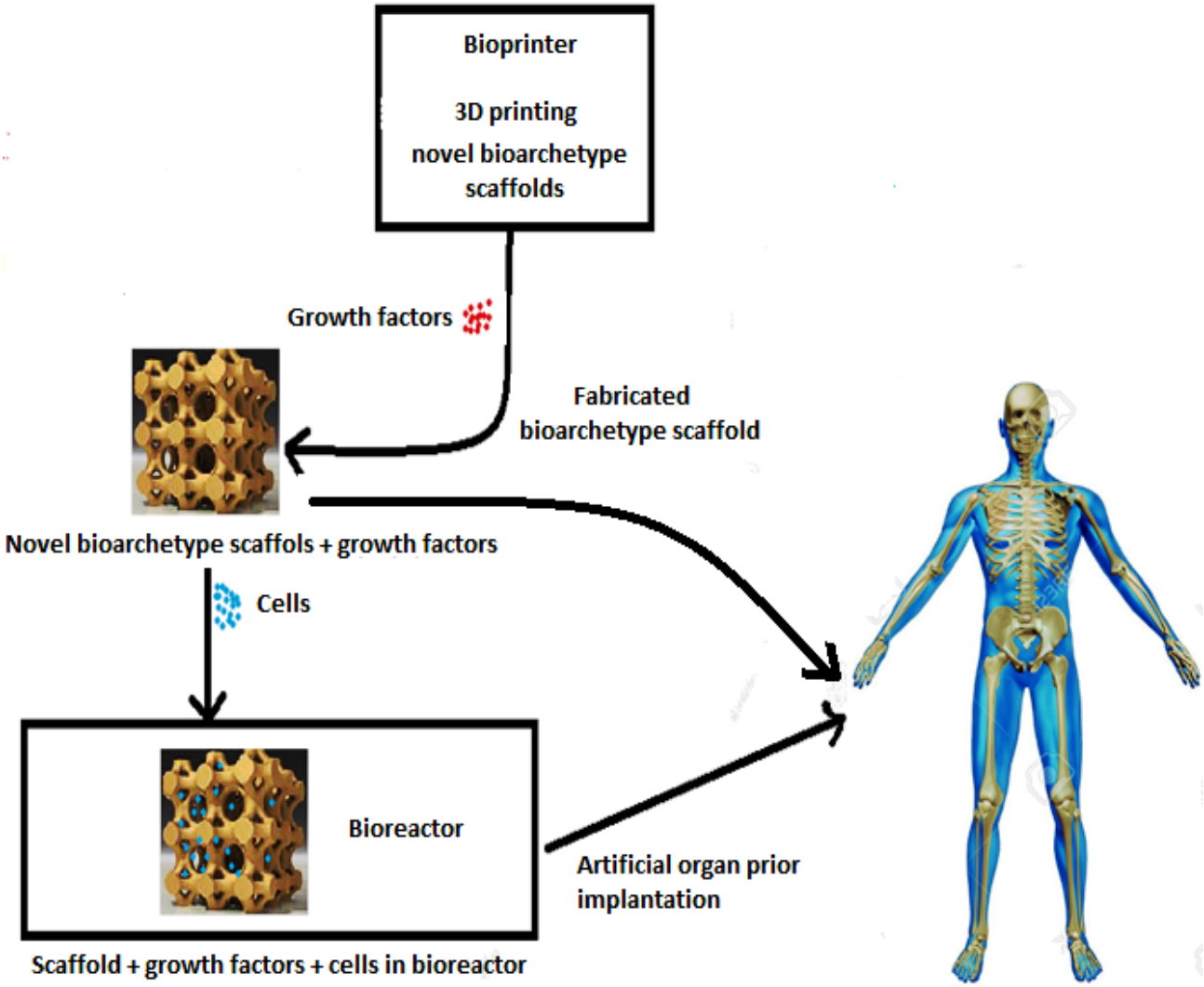


Figure 1.2: Schematic representation of general synthetic route for tissue engineering.

According to Guvendiren *et al., (*2016), none of the available biomaterial-inks (bio-inks) have the potential to be functionalized. The current attempt is to fabricate novel biodegradable

polymeric ink libraries with tunable and user-defined properties. Therefore, the deficiency of printable biomaterial with sufficient mechanical and chemical properties for construction of regenerative scaffolds or implants has been a huge barrier in medical 3D bioprinting.

1.3. AIM AND OBJECTIVES

The aim of this research was to fabricate a novel bioarchetype scaffolds employing 3D bioprinting as an advanced innovative tool wherein the constituent biomaterials were *in situ* conjugated *via* in-print processing and then the biomaterial scaffolds were seeded with osteoblast-like MG63 cells for bone tissue engineering *in vitro* analysis (cell viability, cell adhesion, and cell proliferation). The following objectives were undertaken to ensure the achievement of the proposed study.

1. Preliminary studies were conducted using the selected suitable polymeric biomaterials and cyto-conducive inorganic phase materials. Followed up by the complexation and conjugation reactions for optimization of reaction and formation conditions *w.r.t. in situ* biomaterial synthesis.
2. Development of the novel bioarchetype scaffold using the suitably selected biomaterials employing 3D bioprinting technology.
3. Characterization of the selected native biomaterials and the fabricated 3D printed biomaterial bioarchetype scaffold employing physicochemical, physicomechanical and morphological analyses. Then optimization of the fabricated 3D printed bioarchetype scaffold for tailored biodegradability, mechanical properties, and ECM-mimicking properties.
4. Seed the fabricated bioarchetype scaffold with osteoblast-like MG63 cells to assess the *ex vivo/in vitro* performance (cell viability, cell adhesion, and cell proliferation) of the cell-seeded onto the bioarchetype scaffolds for its application in bone tissue engineering.
5. Undertake *in vivo* studies, using New Zealand White Rabbits, in order to assess the performance of the 3D printed bioarchetype biomaterial scaffold on the living organism.

1.4. NOVELTY OF THIS STUDY

1. A novel composite 3D printed biomaterial scaffolds were synthesized in an effort to overcome the limitations associated with previously fabricated scaffolds for bone tissue engineering application. The composite 3D printed biomaterial scaffolds comprised at least two new different combination of integrated biomaterial: i.e. natural biomaterial e.g.

(Alginate), synthetic polymers (e.g. Polyethyleneimine) and inorganic biomaterial (Silica gel). The 3D printed biomaterial scaffold composite is completely novel and has not been formulated in previously published studies.

2. The novel 3D bioarchetype scaffold composite was fabricated employing an advanced innovative 3D bioprinting in-processing method.
3. The synthetic path and the design of the 3D bioarchetype scaffold composite are novel for bone tissue engineering.
4. This engineered bone tissue construct could solve the problem associated with the repair of critical-sized bone defects and replacement in bone tissues engineering application.

1.5. OVERVIEW OF THE THESIS

CHAPTER 1: This chapter provides an introduction and background of this current research study. The rationale for this research is stressed upon, and the aims and objectives outlined in detail for undertaking this research.

CHAPTER 2: A detailed literature review of the reinforced multi-biomaterial 3D printed scaffolds for bone tissue application. This chapter highlighted various biomaterials and 3D printing method used in fabricating composite 3D printed biomaterial scaffolds. It highlighted the critical factors to be considered when synthesizing bone tissue biomaterial scaffolds. The limitations associated with single-component biomaterials (natural or synthetic polymers, metals, and bioceramics) and the benefit of using hybrid or composite 3D printed biomaterial scaffolds in bone tissue engineering application are discussed in detail.

CHAPTER 3: This chapter provides preliminary experimental parameters for the 3D bioprinting synthesis of the 3D biomaterial scaffold, as well as physicochemical and physicomechanical characterization, in conjunction with *in vitro* analyses studies (e.g. degradation study). The pre-formulation complexation was investigated with various techniques used to characterize the interaction of the precursors and the newly-formed 3D biomaterial scaffold. Some of these characterization studies undertaken include magnetic resonance imaging (MRI), attenuated total reflection transform infrared spectroscopy (ATR-FTIR), differential scanning calorimetry (DSC), thermogravimetric analysis (TGA), X-ray powder diffraction (XRD) and scanning electron microscopy (SEM).

CHAPTER 4: This chapter describes in detail the analysis and optimization of the composite 3D printed biomaterial scaffolds, prepared according to different inorganic biomaterials (silica

gel, hydroxyapatite, and nanoclay). The 3D printed biomaterial scaffolds were analyzed and physicomechanical characterization optimization was determined. Proceeding from this founding, biomineralization, and biocompatibility studies were conducted.

CHAPTER 5: This chapter provides detailed *in vivo* animals studies, employing New Zealand White Rabbits for clinical bone regeneration observation at predetermined time intervals, rabbits were terminated and samples were collected and analyzed after surgical implantation of the 3D printed biomaterial scaffolds and comparative formulations. The regeneration progress of new bone formation was analyzed through histological examination, thereby determining the new bone formation and osteoblastic activities.

CHAPTER 6: This chapter concludes the thesis, providing the recommendations and future outlook in the field of 3D printing technology in bone tissue engineering applications

1.6. REFERENCES

Bajaj, P., Schweller, R. M., Khademhosseini, A., West, J. L. and Bashir, R. (2014) 3D biofabrication strategies for tissue engineering and regenerative medicine, *Annual Review of Biomedical Engineering*, 16, pp. 247–276. DOI:10.1146/annurev-bioeng-071813-105155.

Bártolo, P. J., Almeida, H. A., Rezende, R. A., Laoui, T. and Bidanda, B. (2008) Advanced Processes to Fabricate Scaffolds for Tissue Engineering, in: Bidanda, B. and Bártolo, P. (eds.) *Virtual Prototyping & Bio Manufacturing in Medical Applications*. Springer US, pp. 149–170. DOI: 10.1007/978-0-387-68831-2_8.

Bose, S., Vahabzadeh, S. and Bandyopadhyay, A. (2013) Bone tissue engineering using 3D printing, *Materials Today*, 16 (12), pp. 496–504. DOI:10.1016/j.mattod.2013.11.017.

Chen, A. A., Tsang, V. L., Albrecht, D. R. and Bhatia, S. N. (2006) 3-D Fabrication Technology for Tissue Engineering, in: Ferrari, M., Desai, T., and Bhatia, S. (eds.) *BioMEMS and Biomedical Nanotechnology*. Springer US, pp. 23–38. DOI: 10.1007/978-0-387-25844-7_2.

Chia, H. N. and Wu, B. M. (2015) Recent advances in 3D printing of biomaterials, *Journal of Biological Engineering*, 9, pp. 4. DOI:10.1186/s13036-015-0001-4.

Lee, V. and Dai, G. (2015) Three-dimensional bioprinting and tissue fabrication: prospects for drug discovery and regenerative medicine, *Advanced Health Care Technologies*, 1, pp. 23-35. DOI:10.2147/AHCT.S69191.

Gu, B. K., Choi, D. J., Park, S. J., Kim, M. S., Kang, C. M. and Kim, C.-H. (2016) 3-dimensional bioprinting for tissue engineering applications, *Biomaterials Research*, 20, pp. 12. DOI:10.1186/s40824-016-0058-2.

Guvendiren, M., Molde, J., Soares, R. M. D. and Kohn, J. (2016) Designing Biomaterials for 3D Printing, *ACS Biomaterials Science & Engineering,* 10 (2), pp.1679-1693 . DOI:10.1021/acsbiomaterials.6b00121.

Jakus, A. E., Rutz, A. L. and Shah, R. N. (2016) Advancing the field of 3D biomaterial printing, *Biomedical Materials (Bristol, England)*, 11 (1), pp. 014102. DOI:10.1088/1748-6041/11/1/014102.

Li, X., Cui, R., Sun, L., Aifantis, K. E., Fan, Y., Feng, Q., Cui, F. and Watari, F. (2014) 3D-Printed Biopolymers for Tissue Engineering Application, *International Journal of Polymer Science*, 2014, pp. e829145. DOI:10.1155/2014/829145.

Liu, X. and Ma, P. X. (2004) Polymeric scaffolds for bone tissue engineering, *Annals of Biomedical Engineering*, 32 (3), pp. 477–486. DOI: 10.1023/B:ABME.0000017544.36001.8e.

Mironov, V., Boland, T., Trusk, T., Forgacs, G. and Markwald, R. R. (2003) Organ printing: computer-aided jet-based 3D tissue engineering, *Trends in Biotechnology*, 21 (4), pp. 157–161. DOI:10.1016/S0167-7799(03)00033-7.

Park, S. A., Lee, S. H. and Kim, W. D. (2010) Fabrication of porous polycaprolactone/hydroxyapatite (PCL/HA) blend scaffolds using a 3D plotting system for bone tissue engineering, *Bioprocess and Biosystems Engineering*, 34 (4), pp. 505–513. DOI:10.1007/s00449-010-0499-2.

Sachlos, E. and Czernuszka, J. T. (2003) Making tissue engineering scaffolds work. Review: the application of solid freeform fabrication technology to the production of tissue engineering scaffolds, *European Cells & Materials*, 5, pp. 29–39 DOI: 10.22203/eCM.v005a03.

Seitz, H., Rieder, W., Irsen, S., Leukers, B. and Tille, C. (2005) Three-dimensional printing of porous ceramic scaffolds for bone tissue engineering, *Journal of Biomedical Materials Research Part B: Applied Biomaterials*, 74B (2), pp. 782–788. DOI:10.1002/jbm.b.30291.

Wu, G.-H. and Hsu, S. (2015) Review: Polymeric-Based 3D Printing for Tissue Engineering, *Journal of Medical and Biological Engineering*, 35 (3), pp. 285–292. DOI:10.1007/s40846-015-0038-3.

CHAPTER TWO
REINFORCED, COMPOSITE BIOMATERIAL 3D PRINTED SCAFFOLD FOR BONE TISSUE ENGINEERING: TUNING MECHANICAL PROPERTIES AND CELLULAR AFFINITY

2.1. INTRODUCTION

Bone tissue is the most extensive and ubiquitous organ, and its functional failure is amongst the main causes of reduced quality of life (Woolf and Pfleger, 2003). Tissue engineering encompasses the use of different biomaterials to fabricate 3D scaffold substitutes, to assist tissue regeneration or enhance host tissue self-healing (Chan and Leong, 2008; Yang *et al.,* 2001). Bone tissue engineering is an intricate and dynamic progression which is initiated by the recruitment and migration of osteoprogenitor cells followed by cell spreading (proliferation), cell differentiation, and then the matrix formation with the remodelling of bone tissue (Khan *et al.,* 2008). Furthermore, bone tissue engineering involves designing and fabricating novel biological substitutes, as solutions for critical-sized bone defects (non-union defects estimated to be 5mm diameter in rabbits bones) caused either by tumours, infections, trauma or congenital disorder since they cannot self-heal to completion without external intervention (Li *et al.,* 2015; Sun *et al.,* 2015). Therefore, bone tissue engineering is aimed at developing 3D biomaterial scaffolds with the necessary mechanical support and mimic the extracellular matrix (ECM) to aid in the formation of new bone tissue (De Witte *et al.,* 2018). Biomaterials have been used for the fabrication of external intervention and there is a great need to modify biomaterials to imitate natural tissues or tissue environments partially or absolutely (Green, 2008). The development and investigation of intelligent biomaterials that are not only responsive to biological fluid but also mimic ECM are amongst the current research that is undertaken in bone tissue engineering with regard to the fabrication of 3D biomaterial scaffolds (Peppas and Clegg, 2016). Hence, this leads to a combined work of different areas of science community to form a 3D structured scaffold, Figure 2.1 shown a schematic workflow of the multi-disciplinary approach in scaffold design.

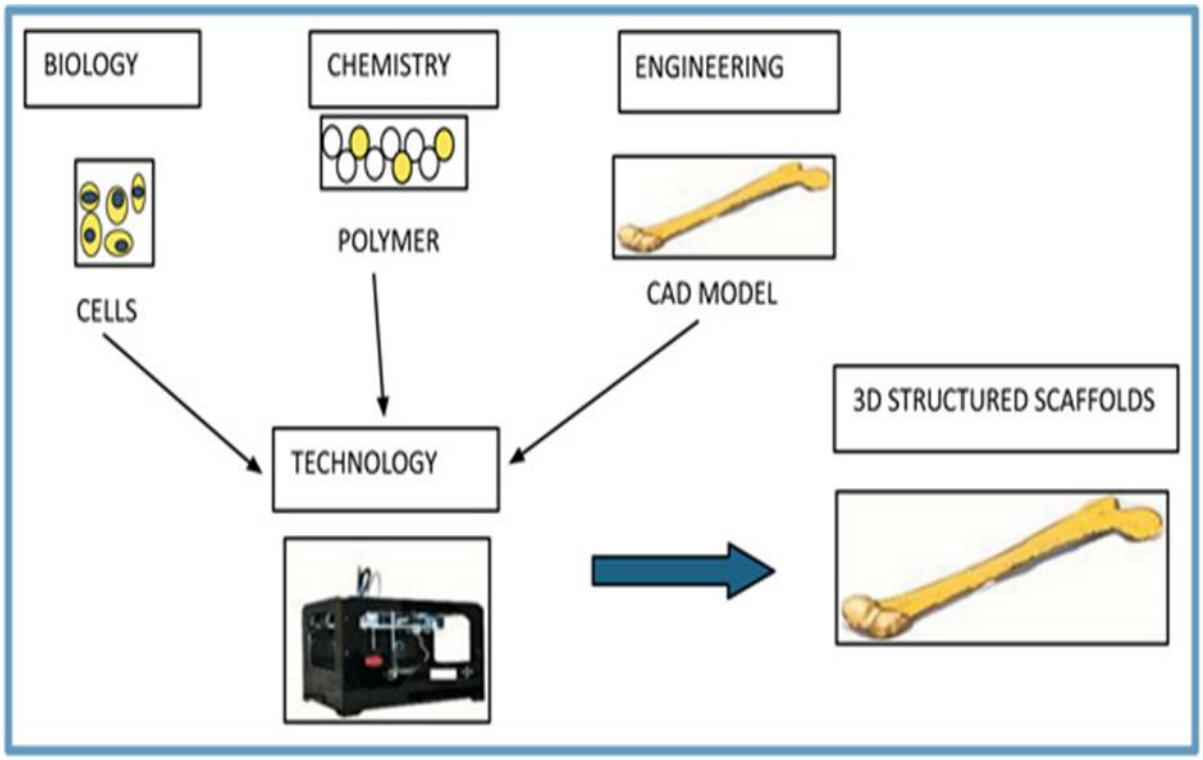


Figure 2.1: The schematic workflow of the multidisciplinary approach utilized in the 3D printing of scaffolds for tissue engineering applications (Devi *et al.*, 2018).

Biomaterials that are utilized specifically in bone tissue engineering have certain characteristics that are incorporated, such as; excellent biocompatibility, complete lack of antigenicity, osteoconductivity, good mechanical properties that match the native tissue, and good porosity (Misch *et al.,* 1999; Wang *et al.,* 2011). Ideally, the fabricated 3D biomaterial scaffolds should not only have the mechanical support similar to human bone, but it must also be resorbed as the new bone tissue growth occurs (Fielding *et al.,* 2012). The replacement or resorption of the 3D biomaterial scaffold by the regenerated tissue is mostly facilitated by the combination of the carefully selected biomaterials properties, stimulating the native *in vivo* mechanisms of tissue to regenerate thereby stimulating the body to self-heal (Costa *et al.,* 2007). Hence, biomaterial selection and the fabrication method are two of the most significant factors/elements that shape the utilization of 3D biomaterial scaffolds, promoting new tissue development or regeneration. In this review chapter, biomaterials are referred to as materials that interface with the biological systems (Freed *et al.,* 1994; Karp *et al.,* 2003; Nair and Laurencin, 2006; Navarro *et al.,* 2008). Different biomaterials have been engineered for the use in fabricating implantable 3D biomaterial scaffolds, which act as stimuli and guide for cell in-growth in a three-dimensional manner using 3D printing technology (Chang *et al.,* 2015; Costa *et al.,* 2007; Stumpf *et al.,* 2018). Furthermore, the choice of biomaterials for bone tissue 3D scaffolds has to also consider the bonding strength at the scaffold interface (Chang *et al.,* 2015).

Novel biomaterials development and modification have been explored through a variety of studies (Nair and Laurencin, 2006; Navarro *et al.,* 2008). Currently, most of the available biomaterials needs to be engineered in order to obtain biomimetic properties, for the use in medical applications (Khan and Tanaka, 2017) and appropriate mechanical properties. 3D printing technology referred to as additive manufacturing, includes; inkjet printing, selective laser sintering (SLS), extrusion, digital laser printing (DLP), fused deposition modelling (FDM), laser beam melting, bioprinting, polyjet, and electron beam melting (Khatiwala *et al.,* 2012; Wong and Hernandez, 2012) have been used in fabricating 3D biomaterial scaffolds. Regardless of the method/type of 3D printing technology, all 3D printing technology uses the same principle, where the desired structure/object is obtained through layer-by-layer patterning of material. 3D printing technological methods gives numerous advantages (which includes a precise control over shape, pore size, and their interconnectivity and also the fabrication time is minimized) (Jammalamadaka and Tappa, 2018). Therefore, 3D printing technology is the current preferred method of fabrication, to engineer 3D biomaterial scaffolds for bone tissue engineering in medical sciences. The flowchart for the creation/fabrication of 3D printed biomaterial scaffolds is depicted in Figure 2.2. Briefly, the selection of biomaterials is an essential process in the fabrication of scaffolds. During the fabrication process, the scaffolds are physically or chemically modified to meet the properties requirements ofspecific tissue properties, such as the mechanical properties, porosity, shape, size, bioactivity, and biodegradability. The material requirement varies according to the fabrication method and the nature of the biomaterials used. The 3D biomaterial scaffold will be implanted within the body after achieving the desired appropriate properties, for the host cells to infiltrate the scaffold (Jammalamadaka and Tappa, 2018; Mok *et al.,* 2016).

This review focuses on 3D printing technology as a preferred current method of 3D biomaterial scaffolds fabrication for bone tissue engineering application. Nevertheless, the 3D biomaterial scaffolds properties (e.g. mechanical properties) that match the native bone tissue and materials bioactivity are amongst the current existing major challenges in bone tissue regeneration. Hence, different 3D printed biomaterial scaffolds for different tissue applications have emerged in the past decades and significantly transformed the field of 3D printing technology. The 3D printing technology does not only provide an advantage for tissue engineering and medical device because of its capability to fabricate one-of-a-kind parts/structures on-demand based on patient specifications, but it also provides flexibility in the starting materials (Bandyopadhyay *et al.,* 2015).

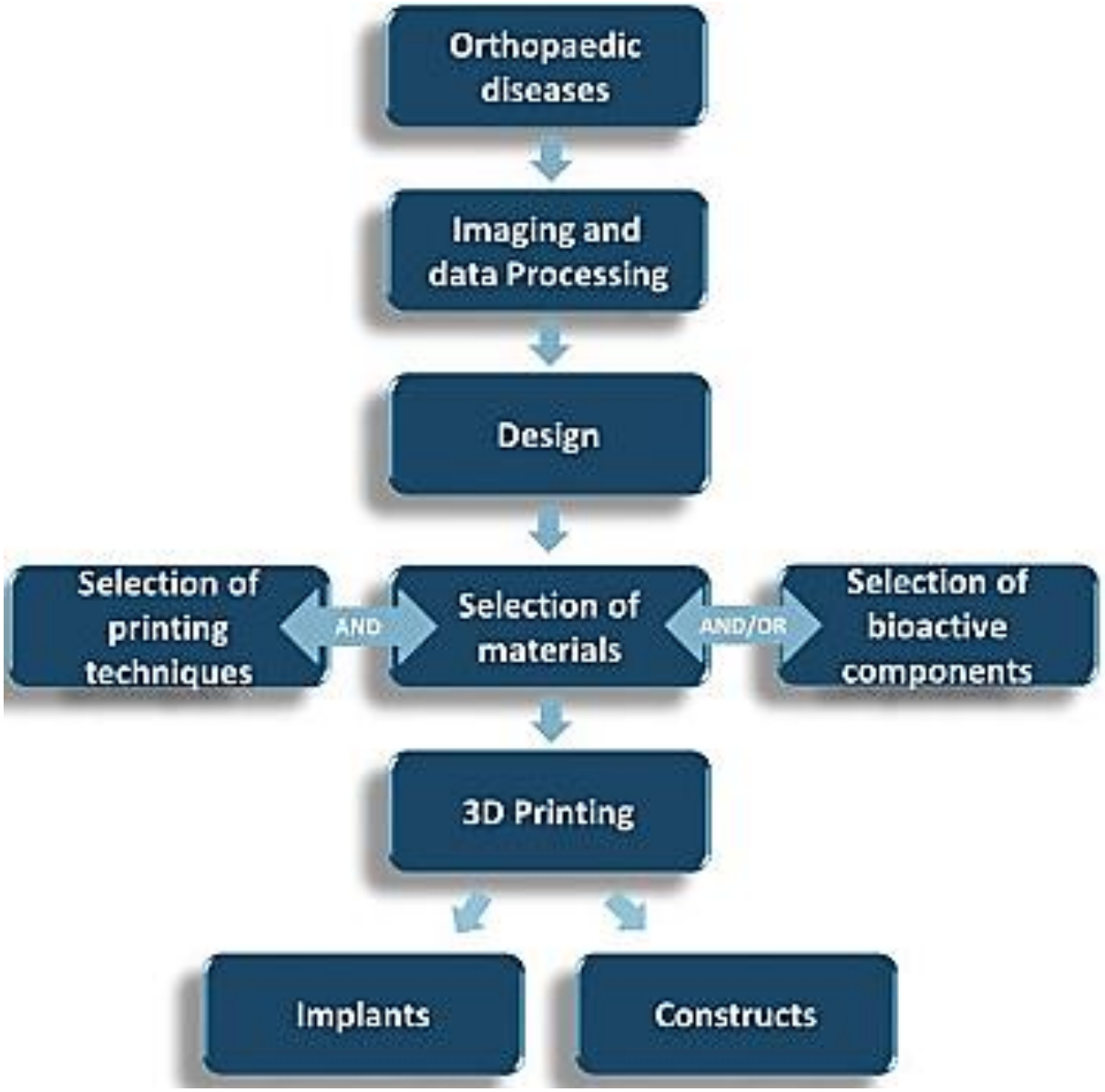


Figure 2.2: Schematic flowchart for the fabrication of the 3D printed constructs/implants (Mok *et al.*, 2016).

The review primarily aims at highlighting the advancements in reinforced multi-biomaterial 3D printed scaffolds, for the tuning of mechanical and cell affinity properties for bone tissue engineering application. Furthermore, also discuss the limitations associated with single-component biomaterials (pure biomaterials) in the fabrication of bone tissue scaffold and the challenges associated with their 3D printability .It is anticipated that this review inspires research scientist to develop novel printable biomaterials which will ultimately ensure the attainment of 3D printing of bone tissue 3D biomaterial scaffolds. Therefore, the chapter will offer a brief overview of advantage of the composite 3D printed biomaterial scaffolds for bone tissue application, along with selected representative biomaterials examples, including but not limited to 3D printed biomaterial scaffolds to give assistance to the reader in attaining

an understanding of the current state of art and to encourage future technical contributors and research scientists towards expanding the frontier of 3D printed biomaterial scaffolds for bone tissue applications.

2.2. CHALLENGES WITH SINGLE-COMPONENT BIOMATERIAL'S FOR 3D PRINTING BONE TISSUE SCAFFOLD

3D printing technologies are amongst fabrication methods that have grown significantly over the years and been used in developing novel 3D biomaterial scaffolds for bone application (Turnbull *et al.,* 2018). 3D biomaterial scaffolds are invented to act as template for cell attachment and stimulate functional bone tissue formation *in vivo* through tailored biophysical cues to direct the organization and behaviour of cells (Bose *et al.,* 2013; Ferrand *et al.,* 2014). Currently, different biomaterials such as bioceramics, metals and polymers are being utilised in medical 3D printing of biomaterial scaffolds, and novel biomaterials have been discovered by researchers to be applied in 3D printing technological methods (Jammalamadaka and Tappa, 2018).

As mentioned before, the current challenges in 3D printing scaffolds for bone tissue engineering is the limited appropriate mechanical property and cellular affinity of the available biomaterials, and also the challenge of limited available printable biomaterials. Furthermore, because most single-component (pure) biomaterials have limitations in their properties, to fully replicate the properties of the tissue under investigation and the nature of 3D printing technological methods, hence the printability and the properties of these single-component biomaterials mostly needs to be modified. Particularly for bone tissue application, the 3D printed biomaterial scaffold needs to have appropriate mechanical strength (see Table 2.1) in addition to the 3D porous structure that provides support during bone remodelling and bone growth (Wu *et al.,* 2008). Therefore, 3D printing techniques have been used in designing single-component biomaterial scaffolds for tissue engineering even though the properties that improve cell viability and functions are at odds with those that aid in 3D printing (Chimene *et al.,* 2016).

Table 2.1: Characteristics of human cortical and cancellous bones.

Bone type	Compressive strength (MPa)	Young's modulus (GPa)
Cortical bone	130-1225	3-30
Cancellous bone	4-12	0.01-0.5

The most investigated synthetic polymers for the synthesis/fabrication of biomaterial scaffolds for bone tissue engineering application, include but not limited to; poly (lactic acid) (PLA), poly (caprolactone) (PCL), poly (ethylene glycol) (PEG), and poly(glycolic acid) (PGA), due to their mechanical and biocompatibility properties (Dong *et al.,* 2017; Oh *et al.,* 2003; Sheikh *et al.,* 2016). However, most synthetic biomaterial polymers lack specific cell recognition sites and are restricted by their hydrophobicity when used as single-component for bone tissue engineering application (Dong *et al.,* 2017; Tallawi *et al.,* 2015; Wang *et al.,* 2016). Additionally, the most investigated natural polymers for bone tissue engineering application, include but not limited to; hyaluronic acid, alginate, chitosan, silk and collagen (Calabrese *et al.,* 2016). Nevertheless, natural polymers also have limitations when used as single-component for scaffolds fabrication, such as the presence of pathogenic impurities like endotoxin (Liu and Ma, 2004), lack of tuneability of the degradation rate and degradation related inhibition of local cells. Additionally, for bone tissue engineering, the mechanical properties of natural polymers are suboptimal (Ravi and Chaikof, 2010; Yoon and Fisher, 2009).

Biomaterials that are classified as bioceramics also attracted great attention in bone tissue engineering application, due to the unlimited availability, reported potential osteoinductivity, osteoconductivity and excellent biocompatibility, which are similar to the native bone inorganic components, namely bioactivity and hydrophilicity (LeGeros, 2002; Woodard *et al.,* 2007). Furthermore, bioceramics have the potential to instruct the surrounding *in vivo* environment to induce ectopic bone formation (Blokhuis and Arts, 2011). Hence, bioceramics such as bioactive glass and calcium phosphate (Ca-P) are well documented for their application as bone fillers in the dental field (Sarkar and Banerjee, 2010). Natural origin bioceramics such as calcium sulphate and Ca-P have been extensively studied over the years as a bone tissue substitute biomaterial and Ca-P was proven to be the prominent part of the skeletal tissue. The Ca-P has the ability to be osteoconductive, osteoinductive and bioactive material, beside organizational occurrence (Dadhich *et al.,* 2016). However, most single-component or pure bioceramics have unsatisfactory mechanical properties and low wear resistance, resulting in limited application in bone tissue engineering (Dadhich *et al.,* 2016). Although on the other hand, bioceramics such as amorphous glass, crystalline ceramics, and bioceramics composite have also shown great potential for bone tissue engineering application, due to their strong mechanical properties with favourable bioactivity (Bonfield *et al.,* 1981). The use of these bioceramics has increased due to properties, such as stiffness and biocompatibility leading to widespread use within clinical orthopaedics (Kurtz *et al.,* 2007; Pasold *et al.,* 2017). These bioceramics also have limitations in bone tissue engineering application resulting from their weakness to shear and tensile strength, leading

to brittleness and resistance to compression (Ho and Matinlinna, 2011). Therefore, in general bioceramics based scaffold are prone to brittleness in perspective of bone tissue engineering application. Likewise, biomaterials such as metals have also been investigated for bone tissue engineering. However, metallic based biomaterial scaffolds have difficulties in finely controlling degradation rate (Turnbull *et al.,* 2018).

The synthetic and natural polymers when used as single-component biomaterials (individually) for scaffolds fabrication, have low elastic moduli with poor loading capacity compared to pure single-component metallic and some bioceramic biomaterials (Ma and Choi, 2001; Woodruff and Hutmacher, 2010). The mechanical requirements are complex for bone tissue engineering biomaterial scaffolds, with fatigue, compressive, and tensile properties all required for load bearing (Hollister and Murphy, 2011). An example of a single-component natural biomaterial polymer; namely collagen, is amongst the most used natural biomaterial polymer for the synthesis/fabrication of biomaterial scaffolds intended for bone tissue engineering application, because of its excellent biodegradability and biocompatibility. However, single-component (pure) collagen has limitations which hinder it from being widely used in bone regeneration field. Pure collagen has low mechanical strength and low osteoinductivity (Calabrese *et al.,* 2016; Zhang *et al.,* 2018), reducing its applicability for bone tissue engineering. Therefore, the mechanical property of pure collagen scaffold was improved through the reinforcement of bioceramic (such as hydroxyapatite (HAP)). The mechanical strength was found to be proportional or related to the concentration of the amount of HAP, collagen, the crosslinking methods and composite methods (Calabrese *et al.,* 2016). Through reinforcing different biomaterials, collagen matrix properties such as the structural stability, porosity, osteogenicity and osteoinductivity can be improved (Zhang *et al.,* 2018). Furthermore, Table 2.2 summarises the limitations of groups (classes) of biomaterials for scaffolds fabrication and their advantages in bone tissue engineering application.

Table 2.2: Summary of different single-components biomaterials used for bone tissue scaffold (Turnbull *et al.*, 2018).

Biomaterials	Potential advantages	Potential limitations
Natural polymers	• They have low toxicity and high biocompatibility since they are mostly derived from extracellular matrix. • On their surface they often contain bio-functional molecules • They are biodegradable	• For load bearing, it has poor mechanical properties. • Endotoxins maybe present (Pathological impurities).

Synthetic polymers	• Offer improved control over physical properties	• Lacks mechanical properties for loading bearing. • Lack cell recognition site and mostly hydrophobic.
Bioceramics	• Have strong integration with the host tissue due to their osteocoductive and osteoinductive properties. • Can be delivered as paste, injectable format or granules. • Their composition is similar to the host bone mineral content. .	• When used individually, they are brittle and hard. • Inappropriate resorption/degradation rate may be exhibited with decreased mechanical properties as a result.
Bioactive glasses	• Have osteoinductive and osteoconductivity properties. • Adapted into clinical prosthesis already.	• They are brittle. • Very difficult to adjust the rate of resorption. • It is a challenge to manipulate the scaffolds/constructs into 3D shape for specific treatment defects. • Toxic metal ion release is highly possible.
Metals	• Biocompatible and superior strength • Superior mechanical properties can be advantageous in situations where slow bone growth is likely.	• Stress-shielding resulting from superior modulus. • Tissue in-growth implantation/surgery results from poor biodegradability. • Distal and local toxicity maybe caused by secondary release of metal ions. .

Finally, the majority of single-component biomaterial (excluding metals) degrade easily and lack the necessary mechanical stability to be used as 3D printable biomaterial (Jang *et al.,*

2018) and to be applied in bone tissue engineering. Therefore, most single-component (pure) biomaterials are unable to fully replicate the properties of bone tissue when used alone (Turnbull *et al.,* 2018). That is why it is an urgent necessity to develop reinforced multi-biomaterials 3D scaffolds that will fulfil the mechanical and cell affinity of bone tissue and be printable using the 3D printing technologies.

2.3. RATIONALE FOR REINFORCEMENT OF MULTI-BIOMATERIALS FOR 3D PRINTED SCAFFOLDS

3D printed biomaterial scaffolds can be implanted either as cellular or acellular, wherein the former (cellular) involves the implantation of the biomaterial scaffold combined with cells (e.g. stem cell and/or osteoprogenitor cells) (Kinoshita and Maeda, 2013), where the cells are encapsulated during biomaterial scaffold fabrication made of hydrogel polymer matrix (Nicodemus and Bryant, 2008). The former technique protects cells from the immune system (Murua *et al.,* 2008) and permits uniform cell distribution within the scaffold (Bryant and Anseth, 2003). On the other hand, the latter (acellular), the overall architecture and geometry of the biomaterial scaffold promote the recruitment of local/host cells, which is possible with "smart" cues and attachment motifs within the biomaterial scaffold architecture (Kinoshita and Maeda, 2013). This review will investigate and highlight mostly the acellular 3D printed biomaterial scaffolds for bone tissue engineering application.

Biomaterial properties can be improved through the combination of two or more biomaterials to form composite multi-biomaterial 3D scaffolds (Turnbull *et al.,* 2018). Hence, different biomaterials are combined or reinforced to yield a multi-biomaterial 3D scaffolds with appropriate properties for bone tissue engineering application (Costa *et al.,* 2007; Stumpf *et al.,* 2018). The reinforcement of bioactive components (such as bioceramics amongst others) is also a popular strategy to improve osteogenesis, bioactivity and mechanical strength of pure or single-component polymeric scaffolds (Zhang *et al.,* 2018). Therefore, the physical/chemical bonding of the reinforced biomaterial into the polymeric/biomaterial scaffolds can solve the mechanical properties limitations of pure biomaterial or single-component biomaterials. Recently most bioceramics are combined with polymers (natural or synthetic polymers) to enhance their printability. Furthermore, most of the biomaterials that are polymer-based are 3D printed using the extrusion-based printing technology, and there a broader range of application in regenerative medicine (Jammalamadaka and Tappa, 2018). Biomaterials possess great influence on the overall properties of the developed 3D biomaterial scaffolds. Therefore, it is very important to study and understand individual biomaterials properties, and allow a suitable selection process of the biomaterials for a

specific tissue application; since biomaterials differ in their mechanical and cellular affinity (Khang, 2015); which also influences cell proliferation, cell adhesion, and overall tissue regeneration outcome (Asa'ad *et al.,* 2016).

2.4. SCAFFOLD FABRICATION APPROACHES FOR BIOMATERIAL SCAFFOLD REINFORCEMENT

Three selected methods are discussed, which are used to improve the 3D printed/printing of biomaterial scaffolds properties, for suitability in bone tissue engineering application. Below are brief descriptions of how each method is carried out.

2.4.1. Post-3D Printed Biomaterial Scaffolds Dip Coating Modification

The dip-coating technique, described as a process where the substrate (e.g. 3D printed biomaterial scaffolds) is immersed in a liquid solution (containing the coating materials) and then withdrawn in a pre-defined speed, under controlled temperature and atmospheric conditions (Figure 2.3). Therefore, the dip-coating of the 3D printed biomaterial scaffolds is amongst the techniques used to enhance biomaterials scaffold properties, such that the mechanical and biological properties are improved partially or wholly to match the tissue under investigation. Figure 2.3 is the representation of the schematic instrument utilized in the process of biomaterial scaffolds dip-coating method. Briefly, after the 3D biomaterial scaffolds are fabricated using the 3D printing technique, it is coated with a thin layer (e.g. solution) via dip coating. Prior the dip-coating, the 3D biomaterial scaffolds of equal size are cleaned in an ultrasound (e.g. using acetone or ethanol) and then dried at room temperature. To apply the coating (solution) to the 3D printed biomaterial scaffolds, the dip-coating method RDC 15 (Relamatic, Glattburg, Switzerland) can be utilized. The scaffolds will be immersed in the coating solution for a specified period and withdrawn with a specific hosting speed as per the specifically developed protocol. Finally, the coated 3D biomaterial scaffolds will be dried (Coan *et al.,* 2013; Motealleh *et al.,* 2016). The thickness varies depending on the dipping time (Li *et al.,* 1996).

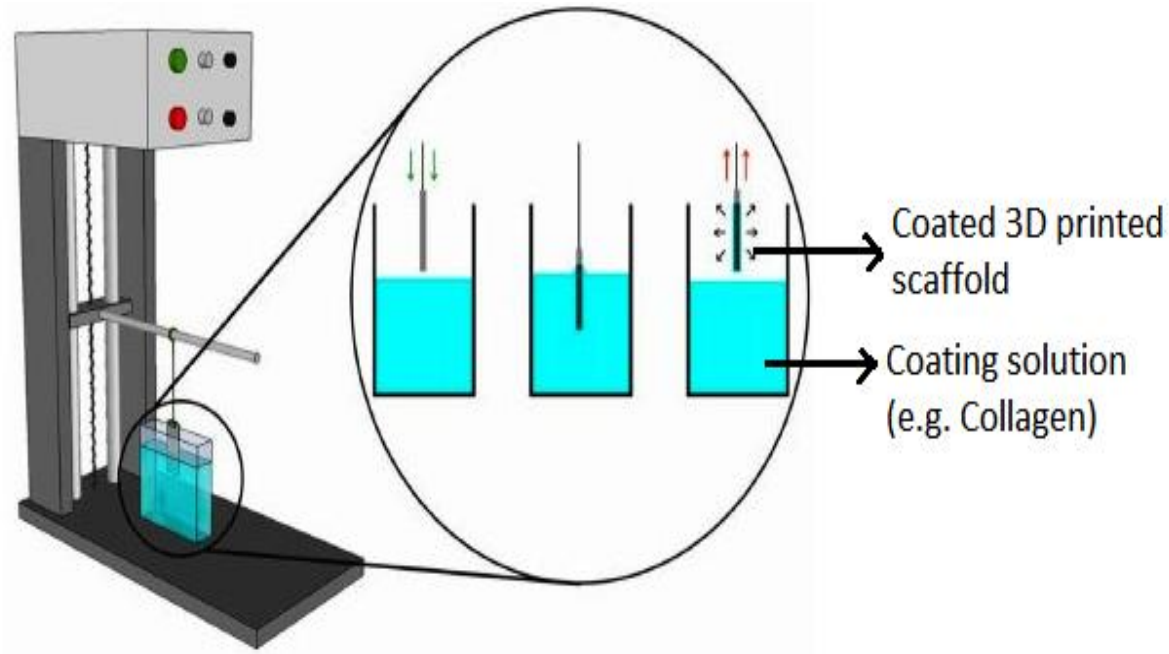


Figure 2.3: Schematic representation of scaffolds dip-coating method (Coan *et al.,* 2013).

2.4.2. Modification by *in situ* Co-Fabrication via 3D Printing Method

The *in situ* co-fabrication/precipitation/mineralization is amongst the current effective methods to reinforce biomaterials/biomolecules for the enhancement of 3D printed biomaterial scaffolds properties. Briefly, a polymeric solution is prepared as a hydrogel (e.g. Sodium alginate/nanoHAP or alginate/SiO_2), then added to a 3D print cartridge and printed into a solution made of biomaterials that enhance the precursor biomaterial properties (e.g. PEI). Figure 3.1 (Section 3.3.1, chapter 3), is the pictorial simplified synthetic demonstration of the *in situ* co-fabrication method (Sithole *et al.,* 2018). This method is believed to efficiently distribute minerals within polymer matrixes. Hence, alginate/nanoHAP (Rajkumar *et al.,* 2011), chitosan/nanoHAP (Azami *et al.,* 2012), gelatin/nanoHAP (Zandi *et al.,* 2010) and collagen/nanoHAP composite (Hoyer *et al.,* 2012) have been fabricated through a similar technique.

2.4.3. Pre-Processed Biomaterials Modification Method for 3D Printing

This method is also amongst the most used biomaterials modification techniques, it includes the pre-processing of biomaterials to be 3D printable as 3D biomaterial scaffolds and have desired properties for bone tissue engineering application. Briefly, the biomaterials are modified through chemical/physical means such as blending, crosslinking and grafting to be 3D printable and at the same time have biological and mechanical properties that are suitable for the tissue under investigation such as bone tissue engineering application.

2.5. REINFORCED, MULTI-BIOMATERIAL, 3D PRINTED SCAFFOLDS FOR IMPROVEMENT OF MECHANICAL PROPERTIES AND CELL AFFINITY

The mechanical integrity of the 3D printed biomaterial scaffolds remains a challenge in successfully achieving a balance *in vivo* properties (Chan and Leong, 2008; Hollister *et al.,* 2002). As highlighted above, single-component biomaterials (which include bioceramics, metals and polymers), when utilised alone are unable to fully replicate the properties of bone tissue when used alone or 3D printed as single-component biomaterial (Jang *et al.,* 2018). The type of biomaterial used and architectural properties are the driving force for scaffold mechanical behaviour (Wu *et al.,* 2017). Hence, pure biomaterials or single-component biomaterials mechanical properties and cell affinity limitations can be addressed by introducing bioceramics or physical/chemical bonding biomaterials into the polymeric/biomaterial composite scaffolds. In most cases, bioceramics are introduced as filler or are coated to the polymer matrix to improve the mechanical properties and its bioactivity properties (Gloria *et al.,* 2010; Liu and Ma, 2004; Rezwan *et al.,* 2006). Porosity is introduced to the composite biomaterial scaffolds through various levels of precision using techniques such as 3D printing technology (Do *et al.,* 2015), since the scaffolds pore size have an effect on its mechanical properties and cell behaviour (Loh and Choong, 2013). Below are selected examples of reinforced composite 3D printed scaffolds for bone tissue engineering application, to enhance either the mechanical properties, cell affinity or both.

Chou *et al.,* (2013), 3D printed a metallic scaffold using iron (Fe) and magnesium (Mn), resulted in tensile mechanical properties scaffold being similar to cancellous bone tissue. The composite 3D printed iron-magnesium (Fe-Mn) scaffold was also found to have good cell viability, cell adhesion (cell affinity) and the cells infiltrated the 3D printed biomaterial scaffold pores upon exposure through *in vitro* analysis. But the reported mechanical properties of pure or single-component Fe (Young modulus 211GPa) (Ghassemi *et al.,* 2018) is significantly higher than the measured mechanical properties of the composite 3D printed Fe-30Mn scaffold (Young's modulus 32.47GPa). The reduction in the mechanical properties suggested that the 3D printed metallic biomaterial scaffold under investigation may be more appropriate for craniofacial bone scaffolds application. The measured Young's modulus (32.47GPa) was found to be twice that of the natural bone, hence, the composite 3D printed Fe-30Mn should possess reduced risk for stress shielding compared to other metallic biomaterials of higher stiffness such as Ti and Co-Cr systems (Chou *et al.,* 2013). Furthermore, a stainless metallic composite 3D printed scaffold made of the combination of cobalt chromium and titanium alloy was 3D printed through selective laser sintering (SLS), which was then secondarily modified using phosphoric acid. The resulted composite 3D

printed metallic scaffold composed of a biocompatible phosphoric acid layer on the metallic scaffold surface. Hence, this allowed a successful reinforcement of biomolecules and antibiotics to improve bioactivity on the printed scaffold phosphoric acid surfaces (Kruth *et al.,* 2005; Vaithilingam *et al.,* 2015).

Feng *et al.,* (2015), fabricated a composite akermanite ($Ca_2MgSi_2O_7$) biomaterial scaffold, which was reinforced/modified with nano-titania (nano-TiO_2) particles using selective laser sintering (SLS) 3D printing technology. The composite 3D printed biomaterial scaffold had shown a high compressive strength of 23 MPa when reinforced/modified with nano-TiO_2. Hardness, stiffness, compressive strength and fracture toughness were significantly enhanced with increase nano-TiO_2 content. Additionally, on the surface of the composite 3D printed biomaterial scaffold, a bone-like apatite was formed *in vitro* with osteoblast-like MG63 cells proliferated and adhere to the biomaterial scaffold (Feng *et al.,* 2015). Figure 2.4a depicted the morphology of the original osteoblast-like MG63 cells viewed under light microscopy. The original osteoblast-like MG63 cells were uniform in size and polygon/fusiform shaped. Figure 2.4(b-d and e-g) depicted the morphologies of osteoblast-like MG63 cells cultured on the pure akermanite scaffold and the 5wt% nano-TiO_2 reinforced porous akermanite scaffold for different days respectively. Figure 2.4(b and e) depicted the attachment of osteoblast-like MG63 cells and spread well on the surface of the scaffold after culturing for 3 days. Figure 2.4(c-d and f-g), shows that as the cell-scaffold culture days increases, it significantly increases the number of osteoblast-like MG63 cells attachment on the scaffold surface. The cells were observed to be flattened and tightly attached on the surface of the scaffolds with their lamellipodium and filopodium, suggesting good cell viability on all akermanite scaffolds.

Wu *et al.,* (2006), previously showed that Si, Mg and Ca ions, resulted from the scaffold made of akermanite dissolution could stimulate osteoblast-like MG63 cells to proliferate and this may be considered as one of the stimulatory effects in evaluation criteria for bioactivity of the biomaterial scaffold. The nano-TiO_2 reinforced akermanite biomaterial scaffold has enhanced cell growth and attachment, since the results indicated excellent scaffold biocompatibility. Additionally, Liu *et al.,* (2013), used metal titanium and silica to fabricate a composite titanium-silica composite scaffold using a selective laser sintering (SLS) 3D printing techniques (Liu *et al.,* 2013). The compressive strength of the composite 3D printed scaffold was enhanced by the heat treatment, post-3D printing. Osteoblast-like MG63 cells were utilized to study the cell proliferation for seven days and the result supported good cell viability (Huang *et al.,* 2013).

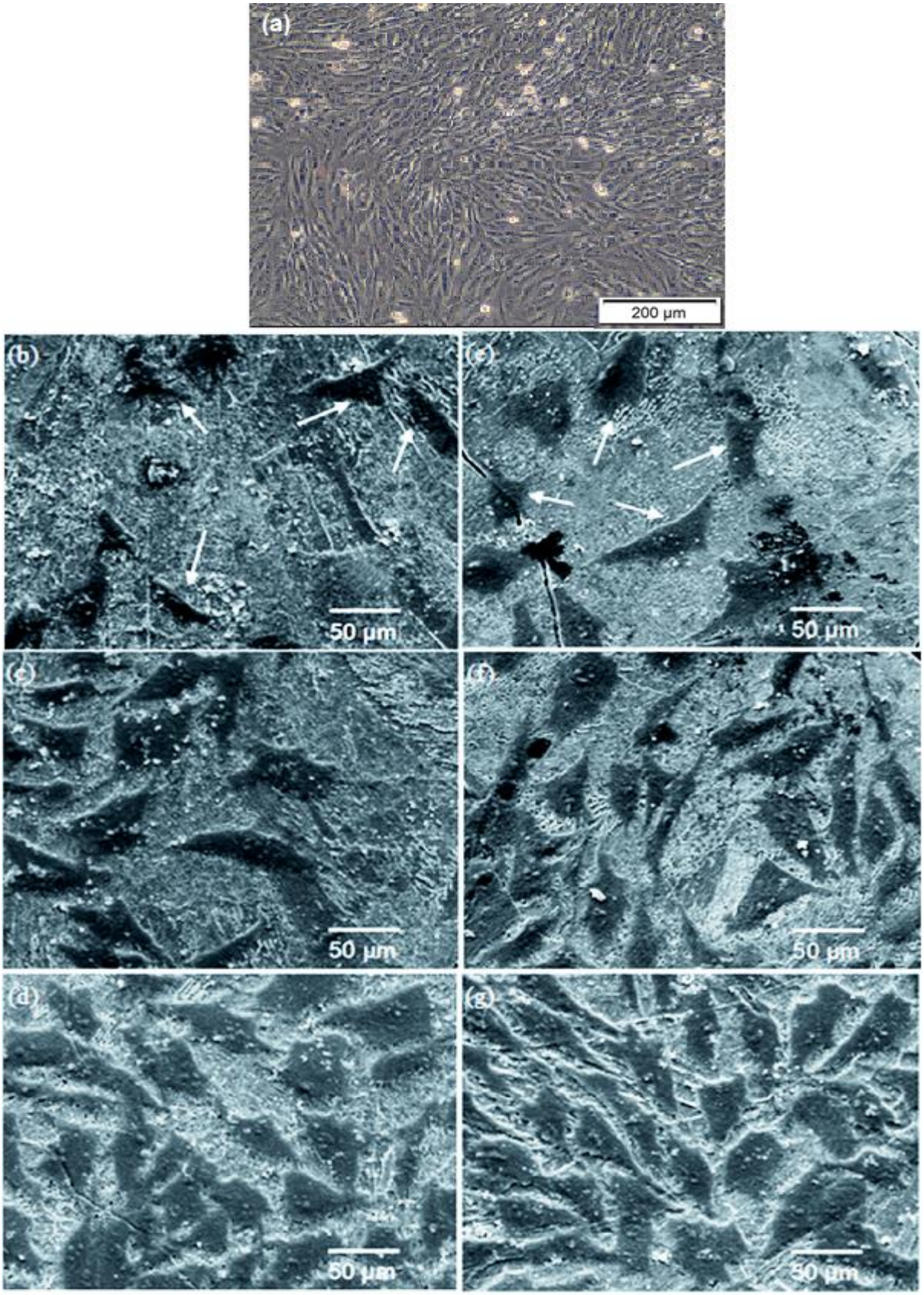


Figure 2.4: Light microscopy morphology of (a) original osteoblast-like MG63 cells; (b-d) SEM microscopy of osteoblast-like MG63 cells (arrows) on the pure akermanite scaffold and (e-g) 5wt% nano-TiO_2 reinforced akermanite scaffold; (b and e) after cell culture for 3 days;(c and f) 7 days and (d and g) 10 days (Feng *et al.,* 2015).

However, there are few challenges encountered by using metals for 3D printed biomaterial scaffolds in bone tissue application. Most 3D printed metallic scaffolds are sintered at 1200^{o}C, very high-temperature conditions. High-temperature conditions are not good for the inclusion of bioactive polymers or bone growth factors, and biomolecules directly during scaffolds fabrication. Attempts such as reinforcement of HAP or calcium silicate through coating the surface of the metallic scaffold post-3D printing are encouraged (Huang *et al.,* 2013) in these cases. The other encountered challenge in 3D printed metallic scaffold, involved the removal of unbound powder after 3D printing, especially within the pores size of 500µm as displayed in Figure 2.5 (Chou *et al.,* 2013).



Figure 2.5: Photograph of prototype sample part of the 3D printed Fe–30Mn scaffold powder after sintering (Chou *et al.*, 2013).

However, currently, there is increased attention focused on the development of polymer/bioceramic or copolymer/ceramic composite scaffolds, which has been reviewed in detail (Turnbull *et al.,* 2018). Because they possess the most ideal characteristics appropriate for bone tissue engineering application and the use of heat is eliminated as to incorporate biomolecules directly during fabrication and biological polymers will not lose their biological integrity since the fabrication temperature conditions are low and appropriate for the inclusion of bone growth factors and bioactive.

2.6. REPRESENTATIVE EXAMPLES OF REINFORCED, 3D PRINTED BIOMATERIALS SCAFFOLDS FOR BONE TISSUE ENGINEERING

A huge number of biomaterials have been investigated for bone tissue engineering application over the year. Different fabrication methods have been explored to produce bone biomaterial scaffolds, but this review focused on 3D printing biomaterial scaffolds fabrication methods as mentioned above. In this review, two mostly and currently used biomaterials for scaffolds fabrication in bone tissue engineering – alginate and silica are discussed in detail.

2.6.1. Alginate-Based Reinforced 3D Printed Biomaterial Scaffolds for Bone Tissue Engineering

Alginate is a natural biomaterial polymer, widely used for biomaterial scaffold fabrication in tissue engineering because of its high water content mimicking natural ECM, innate biocompatibility and low cytotoxicity (Yang *et al.,* 2018; You *et al.,* 2017). Alginates easily degrade and consist of two monosaccharides units, namely; mannoronic acid and gulunoric acid. When mixed with trivalent cations or divalent cation such as Ca^{2+}, it can possibly form a stable hydrogel. The negatively charged carbonyl groups of guluronic acid of alginate chain can easily interact ionically with cations (e.g. Ca^{2+}) and the noncovalent interaction mostly led to gelation (Bajpai and Tankhiwale, 2006; Gombotz and Wee, 1998). Alginate is also widely used because it easily and quickly encapsulate growth factors and cells (Cui *et al.,* 2013; Freeman and Cohen, 2009; George and Abraham, 2006; Lee and Mooney, 2012; Tønnesen and Karlsen, 2002; Axpe and Oyen, 2016; Kim *et al.,* 2016; Yeo and Kim, 2017). Therefore, alginate-based scaffolds holds great potential in bone tissue engineering application, due to the easy delivery of living cells and growth factors, even though it has low compressive strength, lacking bioactivity and low modulus.

The introduction of inorganic materials (such as Silica or Hydroxyapatite) as alginate modification biomaterials is an option to enhance the bioactivity and mechanical properties of alginate-based scaffolds (Lin and Yeh, 2004; Turco *et al.,* 2009). Traditional reinforcements of inorganic materials are based on physical interactions with the hydrogel matrix in which secondary or van der Waals forces including dipolar interactions, hydrogen bonding and London dispersion forces are involved (Ehrburger, 1980). These physical interactions generate strong adhesion between the reinforcements and hydrogel matrix, and the enhancement of hydrogel properties (Jeong *et al.,* 2016). However, alginate as a natural biomaterial polymer lacks cell adhesion site, consequence limiting cell adhesion and it also easily degrade. Hence, cell-recognition peptide such as RGD peptides and/or other biomaterials can be mixed/added into the alginate hydrogel as alternative bioactive hydrogel to be incorporated in alginate hydrogel to provide biochemical functionality for cell growth (You *et al.,* 2017). Therefore, this leads to the wide use of alginate in 3D printing of scaffolds mostly used for cartilage tissue engineering application. For an example, Müller *et al.,* (2017) 3D printed a scaffold for cartilage tissue engineering application using sodium alginate in combination with nano-cellulose (Müller *et al.,* 2017). Cell proliferation was reported to be accelerated by alginate-based 3D bioprinted scaffold overlaid with agarose and calcium salt of polyphosphate compounds (Neufurth *et al.,* 2014).The reinforcement of inorganic phase

into polymer-based biomaterial scaffold structure is a great strategy to improve bioactivity in tissue engineering as suggested (Egorov *et al.,* 2016).

Sodium alginate is a biocompatible polyanionic, having shear thinning properties that's result from alginate solution, which leads to alginate being often utilized as precursor solution in 3D printing of tissue engineering constructs/products. The 3D printed hydrogel shape and structural integrity are often difficult to guarantee because of the insufficient viscosity of the maximum concentration of alginate hydrogel, hence the deposited layers can easily collapse and fuse. Furthermore, crosslinking alginate hydrogel with Ca^{2+} mostly results in a mechanically weak alginate construct and due to gravity the deposited layers can easily collapse, this also has influence on the shape and structural integrity of the 3D printed hydrogel construct. Therefore, alginate as a biocompatible polyanionic, can easily form a polyion complex (PIC) when crosslinked with a polycation as mentioned in the text. But the changing reactive ion pairs mostly control the mechanical strength of the PIC hydrogels, which are prepared from two opposite charged polyelectrolytes. The inhomogeneous precipitations are usually the result of mixing bulk solutions of polyanion and polycation, where at the interface of the two solutions a strong PIC is formed, which quenches further reaction. Consequentially, due to the limited ion pairs that are reactive in the reaction site, this may lead to a low crosslinking density of the biomaterial internal network. As a solution to this problem, Luo *et al.,* (2015) used a polyelectrolyte to polymerize it from a monomer solution in the presence of an oppositely charged 1:1 charged ratio polymer (Luo *et al.,* 2015). The monomer 3-(methacryloylamino) propyl-trimethylammonium chloride (MPTC) which is cationic, was homopolymerized first and then mixed with monomer sodium p-styrenesulfonate (NaSS) which is anionic. In the second step, the anionic monomer is polymerized after good dispersion, forming a soft PIC hydrogel. The hydrogel that was formed from the oppositely charged polyelectrolyte are self-healing, rebuildable and tough as usually indicated by the compression and tensile test (Liu *et al.,* 2018). Below, few studies on reinforced 3D printed biomaterial scaffolds have been highlighted.

A 3D printed biomaterial scaffold was fabricated from novel hydrogel composite for bone tissue engineering, using biomaterials such as alginate, hydroxyapatite (HAP) and gelatin. (Wüst *et al.*, 2014). A huge widow of using this hydrogel in tissue engineering was opened. The hydrogel resulted from the two-step process of chemical crosslinking alginate and mixing the thermosensitive properties of gelatin, to achieve a long term structural integrity and a fast crosslinking with human mesenchymal stem cells performed during the 3D printing of hydroxyapatite. Furthermore, alginate was combined with polycaprolatone due to its excellent mechanical properties for bone tissue application to fabricate/create a 3D

osteochondral tissue from a 3D bioprinter (Shim *et al.*, 2012). Hence, the combination of these two biomaterials results in the mechanical properties that is necessary for bone tissue engineering application. Armstrong *et al.*, (2016) fabricated a 3D alginate-based scaffolds with enhance mechanical properties, from a hydrogel made of sodium alginate and poloxamer as a sacrificial guest. On the other hand, a 3D biomaterial scaffold made of sodium alginate and gelatin mixed with bone-related SaOS-2 cells, then overlayed by agarose and calcium salt of polyphosphate was fabricated. An increase in cell mineralization and higher cell proliferation was observed from the resultant biomaterial scaffold (Neufurth *et al.*, 2014). Wang *et al.*, (2014) used the same cell phenotype to investigate the effect of bioglass on SaOS-2 cells biomineralization and growth in the 3D printed alginate/gelatin scaffolds. Cell mineralization and cell proliferation were increased by the presence biosilica and polyphosphate. Jang *et al.*, (2016) fabricated a 3D biomaterial scaffold from mixing nanofibers, polycaprolactone microfibers, collagen and mesenchymal stem cell-laden alginate, utilizing a 3D bioprinter. The resultant 3D biomaterial scaffold accelerated new bone formation *in vivo* and promoted osteogenesis after mastoid obliteration. Daly *et al.*, (2016) firstly used stem cells supported by gamma-irradiated alginate hydrogel with Arg-Gly-Asp adhesion peptides to make cartilage templates. The template was modified/reinforced by 3D printed polycaprolactone, the resultant printed biomaterial scaffold was approximately 350-fold high in compressive modulus, which will be advantageous for bone tissue engineering application.

Therefore, alginate mechanical properties for bone tissue scaffold is low in 3D bioprinting (for instance, the stiffness during elastic deformations of the bone ranges between 15–25 GPa (Ritchie *et al.,* 2009), whereas alginates is so much lower which is 150–550 kPa (Kaklamani *et al.,* 2014)). Even though there exists limitations such as modulus, low compressive strength and the lack of bioactivity, the scaffolds made from alginate still holds great potential in bone tissue engineering application due to their potential to deliver living cells and growth factors. Hence, the combination of biomaterial such as biosilica, polycaprolatone and hydroxyapatite amongst others, with alginate improves the mimicking of the mechanical properties of the 3D printed biomaterial scaffold for bone tissue. Hence, alginate-based scaffolds mechanical properties and bioactivity can be improved by the introduction of inorganic materials such as hydroxyapatite (HAP) amongst others (Luo *et al.,* 2015).

2.6.2. Silica Reinforced 3D Printed Biomaterial Scaffolds for Bone Tissue Engineering

Silica-based bioceramics composite scaffolds have gained great attention in bone tissue engineering, due to the ionic breakdown of Si-containing biomaterial scaffolds, making it possess osteoconductive properties (Huang *et al.,* 2013; Wu *et al.,* 2008; Xue *et al.,* 2005). Furthermore, silica has good biocompatibility, bioactivity and mechanical properties making advantageous for bone restoration and bone tissue engineering application (Chang *et al.,* 2015; Torres *et al.,* 2013). Though, it was reported that the compressive strength of SiO_2 scaffold was found to be 4.2MPa, which is insufficient to support bone structure since the compressive strength of human bone is reported in a range of 100- 230MPa (Chang *et al.,* 2015; Kokubo *et al.,* 2003; Lei *et al.,* 2014). But silica has good mechanical properties, even though it is not sufficient to support bone structures when used alone, therefore, it is significant to reinforce the silica biomaterials in order to achieve appropriate mechanical properties for bone tissue engineering application. Feng *et al.,* (2014) 3D printed a potential bone scaffold using calcium silica via SLS, the mechanical strength was improved by the reinforcement of HAP. Therefore, the 3D printed biomaterial scaffold compressive strength increased from 15MPa to 27MPa with the reinforcement of 20wt% HAP whiskers. Furthermore, apatite mineralization was observed on the surface of the 3D printed biomaterial scaffold *in vitro* analysis and osteoblast-like cell infiltration and cell proliferation increased with culture time (Feng *et al.,* 2014).

Furthermore, few examples to highlight silica-reinforced scaffolds advantages with multi-biomaterials 3D printed scaffolds for bone tissue engineering application, special for good mechanical properties improvement. Bioceramic silica ceramic slurry (SiO_2) was 3D printed through a self-developed 3D printer and its mechanical strength was improved by reinforcing $CaCO_3$ in order to blend it into a homogenous SiO_2-sol. The prepared $CaCO_3$/SiO_2-sol bi-component was 3D printed as biomaterial scaffold (Chang *et al.,* 2015). The 3D printed bioceramic-based scaffold presented an improved mechanical property and showed good cell affinity when osteoblast-like MG63 cells were used, demonstrating good biocompatibility, no cytotoxicity and improved mechanical properties (Chang *et al.,* 2015). The reinforcement of ZnO and SiO_2 dopants to the 3D interconnected porous tricalcium phosphate (TCP) scaffolds influenced both mechanical and biological properties of the scaffolds. These means that, the reinforced dopants decreases the phase transformation of TCP sintered at 1250^{o}C, increasing densification and the result showed up to 250% increase in compressive strength when compared to pure TCP scaffolds. The maximum compressive strength of 10.21 ± 0.33MPa was achieved in doped scaffolds (Fielding *et al.,* 2012). Tarafder and Bose, (2014) 3D printed TCP scaffold from the combination of polycaprolactone (PCL) and

alendronic acid (AL), performed post-fabrication (Tarafder and Bose, 2014). Through *in vivo* investigation by local delivery of AL from PCL-coated TCP scaffold, it shows an increase in early bone formation compared to bare TCP and PCL coated TCP scaffolds. Additional studies of 3D printing of 3D TCP scaffold reinforced with silicon dioxide and magnesium oxide doping into the scaffold design was conducted (Bose *et al.,* 2017). Hence, significantly great blood vessel and bone formation were observed in scaffolds reinforce with Si and Mg compared to bare TCP scaffolds through *in vivo* investigation. But these hard materials based scaffolds lack a soft niche to support neo-angiogenesis *in vivo*. The findings of the study suggested that silicon and magnesium reinforce into the 3D printed TCP scaffolds could have the potential for future bone tissue repair and regeneration (Turnbull *et al.,* 2018).

2.7. CONCLUDING REMARKS

3D printing technology has solved a great number of 3D biomaterials scaffolds fabrication limitations in tissue engineering applications. Though, the mechanical properties and cell affinity are still the existing challenges, especially for bone tissue engineering applications. This review chapter highlighted a number of attempted potential solutions to address the limitation associated with mechanical strength and cell affinity of the 3D printed biomaterial scaffolds specifically for bone tissue engineering application. The review chapter also highlighted briefly the limitation associated with pure or single-component biomaterials for bone tissue scaffolds application and printability. It was also noted that some synthetic conditions (e.g. high temperatures) of the 3D printed biomaterials scaffold (mostly metallic) are not appropriate for inclusion of biomolecules during 3D printing fabrication stage. Therefore, the biomaterial scaffolds printed in high temperatures condition makes it impossible to work with most biological materials as precursors. Furthermore, the methods of sterilization before implantation in living organism (such as animals) are not well investigated and studied. The 3D bioprinter can work in low temperatures and biological materials (including living cells) can be printed or be incorporated in the printing of biomaterial. In our lab, we published a paper on alginate-based 3D printed biomaterial scaffold for bone tissue engineering application. Our lab, focused on the novel synthetic methods using novel biomaterial combination, yielding a composite 3D printed polymer-bioceramic scaffold for bone tissue engineering application (Sithole *et al.,* 2018). Therefore, recently polymer-bioceramics composites are under investigation as a best composite biomaterial to be 3D bioprinted for bone tissue engineering application.

2.8. REFERENCES

Armstrong, J. P., Burke, M., Carter, B. M., Davis, S. A. and Perriman, A. W. (2016) 3D bioprinting using a templated porous bioink, *Advanced Healthcare Materials*, 5 (14), pp. 1724–1730. DOI: 10.1002/adhm.201600022.

Asa'ad, F., Pagni, G., Pilipchuk, S. P., Giannì, A. B., Giannobile, W. V. and Rasperini, G. (2016) 3D-Printed Scaffolds and Biomaterials: Review of Alveolar Bone Augmentation and Periodontal Regeneration Applications, *International Journal of Dentistry*, 4, pp. 1-15. DOI:10.1155/2016/1239842.

Axpe, E. and Oyen, M. L. (2016) Applications of Alginate-Based Bioinks in 3D Bioprinting, *International Journal of Molecular Sciences*, 17 (12), pp. 1-11. DOI:10.3390/ijms17121976.

Azami, M., Moosavifar, M. J., Baheiraei, N., Moztarzadeh, F. and Ai, J. (2012) Preparation of a biomimetic nanocomposite scaffold for bone tissue engineering via mineralization of gelatin hydrogel and study of mineral transformation in simulated body fluid, *Journal of Biomedical Materials Research Part A*, 100A (5), pp. 1347–1355. DOI:10.1002/jbm.a.34074.

Bajpai, S. K. and Tankhiwale, R. (2006) Investigation of water uptake behavior and stability of calcium alginate/chitosan bi-polymeric beads: Part-1, *Reactive and Functional Polymers*, 66 (6), pp. 645–658. DOI:10.1016/j.reactfunctpolym.2005.10.017.

Bandyopadhyay, A., Bose, S. and Das, S. (2015) 3D printing of biomaterials, *MRS Bulletin*, 40 (2), pp. 108–115. DOI:10.1557/mrs.2015.3.

Blokhuis, T. J. and Arts, J. J. C. (2011) Bioactive and osteoinductive bone graft substitutes: definitions, facts and myths, *Injury*, 42 Suppl 2, pp. S26-29. DOI:10.1016/j.injury.2011.06.010.

Bonfield, W., Grynpas, M. D., Tully, A. E., Bowman, J. and Abram, J. (1981) Hydroxyapatite reinforced polyethylene--a mechanically compatible implant material for bone replacement, *Biomaterials*, 2 (3), pp. 185–186. DOI:10.1016/0142-9612(81)90050-8.

Bose, S., Tarafder, S. and Bandyopadhyay, A. (2017) Effect of Chemistry on Osteogenesis and Angiogenesis Towards Bone Tissue Engineering Using 3D Printed Scaffolds, *Annals of Biomedical Engineering*, 45 (1), pp. 261–272. DOI:10.1007/s10439-016-1646-y.

Bose, S., Vahabzadeh, S. and Bandyopadhyay, A. (2013) Bone tissue engineering using 3D printing, *Materials Today*, 16 (12), pp. 496–504. DOI:10.1016/j.mattod.2013.11.017.

Bryant, S. J. and Anseth, K. S. (2003) Controlling the spatial distribution of ECM components in degradable PEG hydrogels for tissue engineering cartilage, *Journal of Biomedical Materials Research Part A*, 64A (1), pp. 70–79. DOI:10.1002/jbm.a.10319.

Calabrese, G., Giuffrida, R., Fabbi, C., Figallo, E., Furno, D. L., Gulino, R., *et al.* (2016) Collagen-Hydroxyapatite Scaffolds Induce Human Adipose Derived Stem Cells Osteogenic Differentiation In Vitro, *PLOS ONE*, 11 (3), pp. e0151181. DOI:10.1371/journal.pone.0151181.

Chan, B. P. and Leong, K. W. (2008) Scaffolding in tissue engineering: general approaches and tissue-specific considerations, *European Spine Journal: Official Publication of the European Spine Society, the European Spinal Deformity Society, and the European Section of the Cervical Spine Research Society*, 17 Suppl 4, pp. 467–479. DOI:10.1007/s00586-008-0745-3.

Chang, C.-H., Lin, C.-Y., Liu, F.-H., Chen, M. H.-C., Lin, C.-P., Ho, H.-N. and Liao, Y.-S. (2015) 3D Printing Bioceramic Porous Scaffolds with Good Mechanical Property and Cell Affinity, *PLOS ONE*, 10 (11), pp. e0143713. DOI:10.1371/journal.pone.0143713.

Chimene, D., Lennox, K. K., Kaunas, R. R. and Gaharwar, A. K. (2016) Advanced Bioinks for 3D Printing: A Materials Science Perspective, *Annals of Biomedical Engineering*, 44 (6), pp. 2090–2102. DOI:10.1007/s10439-016-1638-y.

Chou, D.-T., Wells, D., Hong, D., Lee, B., Kuhn, H. and Kumta, P. N. (2013) Novel processing of iron–manganese alloy-based biomaterials by inkjet 3-D printing, *Acta Biomaterialia*, 9 (10), pp. 8593–8603. DOI:10.1016/j.actbio.2013.04.016.

Coan, T., Barroso, G. S., Motz, G., Bolzán, A. and Machado, R. a. F. (2013) Preparation of PMMA/hBN composite coatings for metal surface protection, *Materials Research*, 16 (6), pp. 1366–1372. DOI:10.1590/S1516-14392013005000140.

Costa, V. C., Costa, H. S., Vasconcelos, W. L., Pereira, M. de M., Oréfice, R. L. and Mansur, H. S. (2007) Preparation of hybrid biomaterials for bone tissue engineering, *Materials Research*, 10 (1), pp. 21–26. DOI:10.1590/S1516-14392007000100006.

Cui, W., Cui, Y., Zhao, J. and Li, J. (2013) Fabrication of tumor necrosis factor-related apoptosis inducing ligand (TRAIL)/ALG modified CaCO3 as drug carriers with the function of tumor selective recognition, *Journal of Materials Chemistry B*, 1 (9), pp. 1326–1332. DOI:10.1039/C2TB00293K.

Dadhich, P., Das, B., Pal, P., Srivas, P. K., Dutta, J., Ray, S. and Dhara, S. (2016) A simple approach for an eggshell-based 3D-printed osteoinductive multiphasic calcium phosphate scaffold, *ACS Applied Materials & Interfaces*, 8 (19), pp. 11910–11924. DOI: 10.1021/acsami.5b11981.

Daly, A. C., Cunniffe, G. M., Sathy, B. N., Jeon, O., Alsberg, E. and Kelly, D. J. (2016) 3D bioprinting of developmentally inspired templates for whole bone organ engineering, *Advanced Healthcare Materials*, 5 (18), pp. 2353–2362. DOI: 10.1002/adhm.201600182.

De Witte, T.-M., Fratila-Apachitei, L. E., Zadpoor, A. A. and Peppas, N. A. (2018) Bone tissue engineering via growth factor delivery: from scaffolds to complex matrices, *Regenerative Biomaterials*, 5 (4), pp. 197–211. DOI:10.1093/rb/rby013.

Devi, M. G., Amutheesan, M., Govindhan, R. and Karthikeyan, B. (2018) A Review of Three-dimensional Printing for Biomedical and Tissue Engineering Applications, *The Open Biotechnology Journal*, 12 (1), pp. 241-255. DOI:10.2174/1874070701812010241.

Do, A.-V., Khorsand, B., Geary, S. M. and Salem, A. K. (2015) 3D Printing of Scaffolds for Tissue Regeneration Applications, *Advanced Healthcare Materials*, 4 (12), pp. 1742–1762. DOI:10.1002/adhm.201500168.

Dong, L., Wang, S.-J., Zhao, X.-R., Zhu, Y.-F. and Yu, J.-K. (2017) 3D- Printed Poly(ε-caprolactone) Scaffold Integrated with Cell-laden Chitosan Hydrogels for Bone Tissue Engineering, *Scientific Reports*, 7 (1), pp. 13412. DOI:10.1038/s41598-017-13838-7.

Egorov, A. A., Fedotov, A. Y., Mironov, A. V., Komlev, V. S., Popov, V. K. and Zobkov, Y. V. (2016) 3D printing of mineral–polymer bone substitutes based on sodium alginate and calcium phosphate, *Beilstein Journal of Nanotechnology*, 7, pp. 1794-1799. DOI: 10.3762/bjnano.7.172..

Ehrburger, P. (1980) Interface in composite materials, *Phil. Trans. R. Soc. Lond. A*, 294 (1411), pp. 495–505. DOI:10.1098/rsta.1980.0059.

Feng, P., Gao, C., Shuai, C. and Peng, S. (2015) Toughening and strengthening mechanisms of porous akermanite scaffolds reinforced with nano-titania, *RSC Advances*, 5 (5), pp. 3498–3507. DOI:10.1039/C4RA12095G.

Feng, P., Wei, P., Li, P., Gao, C., Shuai, C. and Peng, S. (2014) Calcium silicate ceramic scaffolds toughened with hydroxyapatite whiskers for bone tissue engineering, *Materials Characterization*, Complete (97), pp. 47–56. DOI:10.1016/j.matchar.2014.08.017.

Ferrand, A., Eap, S., Richert, L., Lemoine, S., Kalaskar, D., Demoustier-Champagne, S., *et al.* (2014) Osteogenetic properties of electrospun nanofibrous PCL scaffolds equipped with chitosan-based nanoreservoirs of growth factors, *Macromolecular Bioscience*, 14 (1), pp. 45–55. DOI:10.1002/mabi.201300283.

Fielding, G. A., Bandyopadhyay, A. and Bose, S. (2012) Effects of silica and zinc oxide doping on mechanical and biological properties of 3D printed tricalcium phosphate tissue engineering scaffolds, *Dental Materials*, 28 (2), pp. 113–122. DOI:10.1016/j.dental.2011.09.010.

Freed, L. E., Vunjak-Novakovic, G., Biron, R. J., Eagles, D. B., Lesnoy, D. C., Barlow, S. K. and Langer, R. (1994) Biodegradable polymer scaffolds for tissue engineering, *Bio/Technology (Nature Publishing Company)*, 12 (7), pp. 689–693. DOI:

10.1038/nbt0794-689.

Freeman, I. and Cohen, S. (2009) The influence of the sequential delivery of angiogenic factors from affinity-binding alginate scaffolds on vascularization, *Biomaterials*, 30 (11), pp. 2122–2131. DOI:10.1016/j.biomaterials.2008.12.057.

George, M. and Abraham, T. E. (2006) Polyionic hydrocolloids for the intestinal delivery of protein drugs: alginate and chitosan--a review, *Journal of Controlled Release: Official Journal of the Controlled Release Society*, 114 (1), pp. 1–14. DOI:10.1016/j.jconrel.2006.04.017.

Ghasemi, T., Shahroodi, A., Ebrahimzadeh, M. H., Mousavian, A., Movaffagh, J. and Moradi, A. (2018) Current Concepts in Scaffolding for Bone Tissue Engineering, *Archives of Bone and Joint Surgery*, 6 (2), pp. 90–99. DOI: 10.22038/ABJS.2018.26340.1713.

Gloria, A., De Santis, R. and Ambrosio, L. (2010) Polymer-based composite scaffolds for tissue engineering, *Journal of Applied Biomaterials & Biomechanics: JABB*, 8 (2), pp. 57–67. DOI: 10.1177/228080001000800201.

Gombotz, W. R. and Wee, S. (1998) Protein release from alginate matrices, *Advanced Drug Delivery Reviews*, 31 (3), pp. 267–285. DOI:10.1016/S0169-409X(97)00124-5.

Green, D. W. (2008) Tissue bionics: examples in biomimetic tissue engineering, *Biomedical Materials (Bristol, England)*, 3 (3), pp. 034010. DOI:10.1088/1748-6041/3/3/034010.

Ho, G. W. and Matinlinna, J. P. (2011) Insights on Ceramics as Dental Materials . Part I : Ceramic Material Types in Dentistry, *Silicon*, 3 (3), pp. 109-115. DOI: 10.1007/s12633-011-9078-7.

Hollister, S. J., Maddox, R. D. and Taboas, J. M. (2002) Optimal design and fabrication of scaffolds to mimic tissue properties and satisfy biological constraints, *Biomaterials*, 23 (20), pp. 4095–4103. DOI:10.1016/S0142-9612(02)00148-5.

Hollister, S. J. and Murphy, W. L. (2011) Scaffold Translation: Barriers Between Concept and Clinic, *Tissue Engineering. Part B, Reviews*, 17 (6), pp. 459–474. DOI:10.1089/ten.teb.2011.0251.

Hoyer, B., Bernhardt, A., Heinemann, S., Stachel, I., Meyer, M. and Gelinsky, M. (2012) Biomimetically mineralized salmon collagen scaffolds for application in bone tissue engineering, *Biomacromolecules*, 13 (4), pp. 1059–1066. DOI:10.1021/bm201776r.

Huang, Y., Han, S., Pang, X., Ding, Q. and Yan, Y. (2013) Electrodeposition of porous hydroxyapatite/calcium silicate composite coating on titanium for biomedical applications, *Applied Surface Science*, 271, pp. 299–302. DOI:10.1016/j.apsusc.2013.01.187.

Jammalamadaka, U. and Tappa, K. (2018) Recent Advances in Biomaterials for 3D Printing and Tissue Engineering, *Journal of Functional Biomaterials*, 9 (1). DOI:10.3390/jfb9010022.

Jang, C. H., Ahn, S. H., Yang, G.-H. and Kim, G. H. (2016) A MSCs-laden polycaprolactone/collagen scaffold for bone tissue regeneration, *RSC Advances*, 6 (8), pp. 6259–6265. DOI: 10.1039/C5RA20627H.

Jang, T.-S., Jung, H.-D., Pan, H. M., Han, W. T., Chen, S. and Song, J. (2018) 3D printing of hydrogel composite systems: Recent advances in technology for tissue engineering, *International Journal of Bioprinting*, 4 (1). DOI:10.18063/ijb.v4i1.126.

Jeong, S.-H., Koh, Y.-H., Kim, S.-W., Park, J.-U., Kim, H.-E. and Song, J. (2016) Strong and Biostable Hyaluronic Acid-Calcium Phosphate Nanocomposite Hydrogel via in Situ Precipitation Process, *Biomacromolecules*, 17 (3), pp. 841–851. DOI:10.1021/acs.biomac.5b01557.

Kaklamani, G., Cheneler, D., Grover, L. M., Adams, M. J. and Bowen, J. (2014) Mechanical properties of alginate hydrogels manufactured using external gelation, *Journal of the Mechanical Behavior of Biomedical Materials*, 36, pp. 135–142. DOI: 10.1016/j.jmbbm.2014.04.013.

Karp, J. M., Dalton, P. D. and Shoichet, M. S. (2003) Scaffolds for Tissue Engineering, *MRS Bulletin*, 28 (4), pp. 301–306. DOI:10.1557/mrs2003.85.

Khan, F. and Tanaka, M. (2017) Designing Smart Biomaterials for Tissue Engineering, *International Journal of Molecular Sciences*, 19 (1), pp. 17. DOI:10.3390/ijms19010017.

Khan, Y., Yaszemski, M. J., Mikos, A. G. and Laurencin, C. T. (2008) Tissue engineering of bone: material and matrix considerations, *The Journal of Bone and Joint Surgery. American Volume*, 90 Suppl 1, pp. 36–42. DOI:10.2106/JBJS.G.01260.

Khang, G. (2015) Evolution of gradient concept for the application of regenerative medicine, *Biosurface and Biotribology*, 1 (3), pp. 202–213. DOI:10.1016/j.bsbt.2015.08.004.

Khatiwala, C., Law, R., Shepherd, B., Dorfman, S. and Csete, M. (2012) 3d cell bioprinting for regenerative medicine research and therapies, *Gene Therapy and Regulation*, 07 (01), pp. 1230004. DOI:10.1142/S1568558611000301.

Kim, S., Hwang, Y., Kashif, M., Jeong, D. and Kim, G. (2016) Evaluation of Bone Regeneration on Polyhydroxyethyl-polymethyl Methacrylate Membrane in a Rabbit Calvarial Defect Model, *In Vivo*, 30 (5), pp. 587–591.

Kinoshita, Y. and Maeda, H. (2013) Recent Developments of Functional Scaffolds for Craniomaxillofacial Bone Tissue Engineering Applications, *The Scientific World Journal*, 23, pp. 1-12. DOI:10.1155/2013/863157.

Kokubo, T., Kim, H.-M. and Kawashita, M. (2003) Novel bioactive materials with different mechanical properties, *Biomaterials*, 24 (13), pp. 2161–2175. DOI:10.1016/S0142-9612(03)00044-9.

Kruth, J. P., Mercelis, P., Vaerenbergh, J. V., Vaerenbergh, J. van, Froyen, L. and Rombouts, M. (2005) Binding Mechanisms in Selective Laser Sintering and Selective Laser Melting, *Rapid prototyping journal*, 11 (1), pp. 26–36. DOI:10.1108/13552540510573365.

Kurtz, S., Ong, K., Lau, E., Mowat, F. and Halpern, M. (2007) Projections of primary and revision hip and knee arthroplasty in the United States from 2005 to 2030, *The Journal of Bone and Joint Surgery. American Volume*, 89 (4), pp. 780–785. DOI:10.2106/JBJS.F.00222.

Lee, K. Y. and Mooney, D. J. (2012) Alginate: properties and biomedical applications, *Progress in Polymer Science*, 37 (1), pp. 106–126. DOI:10.1016/j.progpolymsci.2011.06.003.

LeGeros, R. Z. (2002) Properties of osteoconductive biomaterials: calcium phosphates, *Clinical Orthopaedics and Related Research*, (395), pp. 81–98. DOI: 10.1097/00003086-200202000-00009.

Lei, B., Shin, K.-H., Koh, Y.-H. and Kim, H.-E. (2014) Porous gelatin-siloxane hybrid scaffolds with biomimetic structure and properties for bone tissue regeneration, *Journal of Biomedical Materials Research. Part B, Applied Biomaterials*, 102 (7), pp. 1528–1536. DOI:10.1002/jbm.b.33133.

Li, T., Lee, J., Kobayashi, T. and Aoki, H. (1996) Hydroxyapatite coating by dipping method, and bone bonding strength, *Journal of Materials Science: Materials in Medicine*, 7 (6), pp. 355–357. DOI:10.1007/BF00154548.

Li, Y., Chen, S.-K., Li, L., Qin, L., Wang, X.-L. and Lai, Y.-X. (2015) Bone defect animal models for testing efficacy of bone substitute biomaterials, *Journal of Orthopaedic Translation*, 3 (3), pp. 95–104. DOI:10.1016/j.jot.2015.05.002.

Lin, H.-R. and Yeh, Y.-J. (2004) Porous alginate/hydroxyapatite composite scaffolds for bone tissue engineering: preparation, characterization, and in vitro studies, *Journal of Biomedical Materials Research. Part B, Applied Biomaterials*, 71 (1), pp. 52–65. DOI:10.1002/jbm.b.30065.

Liu, C., Carrera, R., Flamini, V., Kenny, L., Cabahug-Zuckerman, P., George, B. M., *et al.* (2018) Effects of mechanical loading on cortical defect repair using a novel mechanobiological model of bone healing, *Bone*, 108, pp. 145–155. DOI:10.1016/j.bone.2017.12.027.

Liu, F.-H., Lee, R.-T., Lin, W.-H. and Liao, Y.-S. (2013) Selective Laser Sintering of Bio-Metal Scaffold, *Procedia CIRP*, 5, pp. 83–87. DOI:10.1016/j.procir.2013.01.017.

Liu, X. and Ma, P. X. (2004) Polymeric scaffolds for bone tissue engineering, *Annals of Biomedical Engineering*, 32 (3), pp. 477–486. DOI: 10.1023/B:ABME.0000017544.36001.8e.

Loh, Q. L. and Choong, C. (2013) Three-Dimensional Scaffolds for Tissue Engineering Applications: Role of Porosity and Pore Size, *Tissue Engineering Part B: Reviews*, 19 (6), pp. 485–502. DOI:10.1089/ten.teb.2012.0437.

Luo, F., Sun, T. L., Nakajima, T., Kurokawa, T., Zhao, Y., Sato, K., *et al.* (2015) Oppositely Charged Polyelectrolytes Form Tough, Self-Healing, and Rebuildable Hydrogels, *Advanced Materials*, 27 (17), pp. 2722–2727. DOI: 10.1002/adma.201500140.

Ma, P. X. and Choi, J. W. (2001) Biodegradable polymer scaffolds with well-defined interconnected spherical pore network, *Tissue Engineering*, 7 (1), pp. 23–33. DOI:10.1089/107632701300003269.

Misch, C. E., Qu, Z. and Bidez, M. W. (1999) Mechanical properties of trabecular bone in the human mandible: implications for dental implant treatment planning and surgical placement, *Journal of Oral and Maxillofacial Surgery: Official Journal of the American Association of Oral and Maxillofacial Surgeons*, 57 (6), pp. 700–706, DOI: 10.1016/S0278-2391(99)90437-8.

Mok, S.-W., Nizak, R., Fu, S.-C., Ho, K.-W. K., Qin, L., Saris, D. B. F., Chan, K.-M. and Malda, J. (2016) From the printer: Potential of three-dimensional printing for orthopaedic applications, *Journal of Orthopaedic Translation*, 6, pp. 42–49. DOI:10.1016/j.jot.2016.04.003.

Motealleh, A., Eqtesadi, S., Perera, F. H., Pajares, A., Guiberteau, F. and Miranda, P. (2016) Understanding the role of dip-coating process parameters in the mechanical performance of polymer-coated bioglass robocast scaffolds, *Journal of the Mechanical Behavior of Biomedical Materials*, 64, pp. 253–261. DOI:10.1016/j.jmbbm.2016.08.004.

Müller, M., Öztürk, E., Arlov, Ø., Gatenholm, P. and Zenobi-Wong, M. (2017) Alginate Sulfate–Nanocellulose Bioinks for Cartilage Bioprinting Applications, *Annals of Biomedical Engineering*, 45 (1), pp. 210–223. DOI:10.1007/s10439-016-1704-5.

Murua, A., Portero, A., Orive, G., Hernández, R. M., de Castro, M. and Pedraz, J. L. (2008) Cell microencapsulation technology: towards clinical application, *Journal of Controlled Release: Official Journal of the Controlled Release Society*, 132 (2), pp. 76–83. DOI:10.1016/j.jconrel.2008.08.010.

Nair, L. S. and Laurencin, C. T. (2006) Polymers as biomaterials for tissue engineering and controlled drug delivery, *Advances in Biochemical Engineering/Biotechnology*, 102, pp. 47–90. DOI: 10.1007/b137240.

Navarro, M., Michiardi, A., Castaño, O. and Planell, J. . (2008) Biomaterials in orthopaedics, *Journal of the Royal Society Interface*, 5 (27), pp. 1137–1158. DOI:10.1098/rsif.2008.0151.

Neufurth, M., Wang, X., Schröder, H. C., Feng, Q., Diehl-Seifert, B., Ziebart, T., Steffen, R., Wang, S. and Müller, W. E. G. (2014) Engineering a morphogenetically active hydrogel for bioprinting of bioartificial tissue derived from human osteoblast-like SaOS-2 cells, *Biomaterials*, 35 (31), pp. 8810–8819. DOI:10.1016/j.biomaterials.2014.07.002.

Nicodemus, G. D. and Bryant, S. J. (2008) Cell encapsulation in biodegradable hydrogels for tissue engineering applications, *Tissue Engineering. Part B, Reviews*, 14 (2), pp. 149–165. DOI:10.1089/ten.teb.2007.0332.

Oh, S. H., Kang, S. G., Kim, E. S., Cho, S. H. and Lee, J. H. (2003) Fabrication and characterization of hydrophilic poly(lactic-co-glycolic acid)/poly(vinyl alcohol) blend cell scaffolds by melt-molding particulate-leaching method, *Biomaterials*, 24 (22), pp. 4011–4021. DOI: 10.1016/S0142-9612(03)00284-9.

Pasold, J., Markhoff, J., Tillmann, J., Krogull, M., Pisowocki, P. and Bader, R. (2017) Direct influence of titanium and zirconia particles on the morphology and functionality of mature human osteoclasts, *Journal of Biomedical Materials Research. Part A*, 105 (9), pp. 2608–2615. DOI:10.1002/jbm.a.36114.

Peppas, N. A. and Clegg, J. R. (2016) The challenge to improve the response of biomaterials to the physiological environment, *Regenerative Biomaterials*, 3 (2), pp. 67–71. DOI:10.1093/rb/rbw012.

Rajkumar, M., Meenakshisundaram, N. and Rajendran, V. (2011) Development of nanocomposites based on hydroxyapatite/sodium alginate: Synthesis and characterisation, *Materials Characterization*, 62 (5), pp. 469–479. DOI: 10.1016/j.matchar.2011.02.008.

Ravi, S. and Chaikof, E. L. (2010) Biomaterials for vascular tissue engineering, *Regenerative Medicine*, 5 (1), pp. 107–120. DOI:10.2217/rme.09.77.

Rezwan, K., Chen, Q. Z., Blaker, J. J. and Boccaccini, A. R. (2006) Biodegradable and bioactive porous polymer/inorganic composite scaffolds for bone tissue engineering, *Biomaterials*, 27 (18), pp. 3413–3431. DOI:10.1016/j.biomaterials.2006.01.039.

Sarkar, R. and Banerjee, G. (2010) Ceramic based bio-medical implants, *Interceram*, 59 (2), pp. 98–102.

Sheikh, F. A., Ju, H. W., Moon, B. M., Lee, O. J., Kim, J.-H., Park, H. J., *et al.* (2016) Hybrid scaffolds based on PLGA and silk for bone tissue engineering, *Journal of Tissue Engineering and Regenerative Medicine*, 10 (3), pp. 209–221. DOI:10.1002/term.1989.

Shim, J.-H., Lee, J.-S., Kim, J. Y. and Cho, D.-W. (2012) Bioprinting of a mechanically enhanced three-dimensional dual cell-laden construct for osteochondral tissue

engineering using a multi-head tissue/organ building system, *Journal of Micromechanics and Microengineering*, 22 (8), pp. 085014.

Sithole, M. N., Kumar, P., Toit, L. C. du, Marimuthu, T., Choonara, Y. E. and Pillay, V. (2018) A 3D bioprinted in situ conjugated-co-fabricated scaffold for potential bone tissue engineering applications, *Journal of Biomedical Materials Research Part A*, 106 (5), pp. 1311–1321. DOI:10.1002/jbm.a.36333.

Stumpf, T. R., Yang, X., Zhang, J. and Cao, X. (2018) In situ and ex situ modifications of bacterial cellulose for applications in tissue engineering, *Materials Science and Engineering: C*, 82, pp. 372–383. DOI:10.1016/j.msec.2016.11.121.

Sun, M., Liu, A., Ma, C., Shao, H., Yu, M., Liu, Y., Yan, S. and Gou, Z. (2015) Systematic investigation of β-dicalcium silicate-based bone cements in vitro and in vivo in comparison with clinically applied calcium phosphate cement and Bio-Oss®, *RSC Advances*, 6 (1), pp. 586–596. DOI:10.1039/C5RA21340A.

Tallawi, M., Rosellini, E., Barbani, N., Cascone, M. G., Rai, R., Saint-Pierre, G. and Boccaccini, A. R. (2015) Strategies for the chemical and biological functionalization of scaffolds for cardiac tissue engineering: a review, *Journal of the Royal Society, Interface*, 12 (108), pp. 20150254. DOI:10.1098/rsif.2015.0254.

Tappa, K. and Jammalamadaka, U. (2018) Novel Biomaterials Used in Medical 3D Printing Techniques, *Journal of Functional Biomaterials*, 9 (1). DOI:10.3390/jfb9010017.

Tarafder, S. and Bose, S. (2014) Polycaprolactone-coated 3D printed tricalcium phosphate scaffolds for bone tissue engineering: in vitro alendronate release behavior and local delivery effect on in vivo osteogenesis, *ACS Applied Materials & Interfaces*, 6 (13), pp. 9955–9965. DOI:10.1021/am501048n.

Tønnesen, H. H. and Karlsen, J. (2002) Alginate in drug delivery systems, *Drug Development and Industrial Pharmacy*, 28 (6), pp. 621–630. DOI:10.1081/DDC-120003853.

Torres, A. L., Gaspar, V. M., Serra, I. R., Diogo, G. S., Fradique, R., Silva, A. P. and Correia, I. J. (2013) Bioactive polymeric–ceramic hybrid 3D scaffold for application in bone tissue regeneration, *Materials Science and Engineering: C*, 33 (7), pp. 4460–4469. DOI:10.1016/j.msec.2013.07.003.

Turco, G., Marsich, E., Bellomo, F., Semeraro, S., Donati, I., Brun, F., Grandolfo, M., Accardo, A. and Paoletti, S. (2009) Alginate/Hydroxyapatite Biocomposite For Bone Ingrowth: A Trabecular Structure With High And Isotropic Connectivity, *Biomacromolecules*, 10 (6), pp. 1575–1583. DOI:10.1021/bm900154b.

Turnbull, G., Clarke, J., Picard, F., Riches, P., Jia, L., Han, F., Li, B. and Shu, W. (2018) 3D bioactive composite scaffolds for bone tissue engineering, *Bioactive Materials*, 3 (3), pp. 278–314. DOI:10.1016/j.bioactmat.2017.10.001.

Vaithilingam, J., Kilsby, S., Goodridge, R. D., Christie, S. D. R., Edmondson, S. and Hague, R. J. M. (2015) Functionalisation of Ti6Al4V components fabricated using selective laser melting with a bioactive compound, *Materials Science & Engineering. C, Materials for Biological Applications*, 46, pp. 52–61. DOI:10.1016/j.msec.2014.10.015.

Wang, J., Ma, H., Jin, X., Hu, J., Liu, X., Ni, L. and Ma, P. X. (2011) The effect of scaffold architecture on odontogenic differentiation of human dental pulp stem cells, *Biomaterials*, 32 (31), pp. 7822–7830. DOI:10.1016/j.biomaterials.2011.04.034.

Wang, J., Wang, L., Zhou, Z., Lai, H., Xu, P., Liao, L., *et al.* (2016) Biodegradable Polymer Membranes Applied in Guided Bone/Tissue Regeneration: A Review, *Polymers*, 8 (4), pp. 115. DOI:10.3390/polym8040115.

Wang, P., Zhao, L., Liu, J., Weir, M. D., Zhou, X. and Xu, H. H. K. (2014) Bone tissue engineering via nanostructured calcium phosphate biomaterials and stem cells, *Bone Research*, 2, pp. 14017. DOI:10.1038/boneres.2014.17.

Wong, K. V. and Hernandez, A. (2012) A Review of Additive Manufacturing, *International Scholarly Research Notices*. Research article. DOI:10.5402/2012/208760.

Woodard, J. R., Hilldore, A. J., Lan, S. K., Park, C. J., Morgan, A. W., Eurell, J. A. C., *et al.* (2007) The mechanical properties and osteoconductivity of hydroxyapatite bone scaffolds with multi-scale porosity, *Biomaterials*, 28 (1), pp. 45–54. DOI:10.1016/j.biomaterials.2006.08.021.

Woodruff, M. A. and Hutmacher, D. W. (2010) The return of a forgotten polymer : Polycaprolactone in the 21st century, *Progress in Polymer Science*, 35, pp. 1217–1256. DOI: 10.1016/j.progpolymsci.2010.04.002.

Woolf, A. D. and Pfleger, B. (2003) Burden of major musculoskeletal conditions, *Bulletin of the World Health Organization*, 81, pp. 646–656. DOI:10.1590/S0042-96862003000900007.

Wu, A. S., Iv, W. S., Bryson, T. M., Cheng, E., Metz, T. R., Schulze, S. E., Duoss, E. B. and Wilson, T. S. (2017) 3D Printed Silicones with Shape Memory, *Scientific Reports*, 7 (1), pp. 4664. DOI:10.1038/s41598-017-04663-z.

Wu, C., Chang, J., Zhai, W., Ni, S. and Wang, J. (2006) Porous akermanite scaffolds for bone tissue engineering: preparation, characterization, and in vitro studies, *Journal of Biomedical Materials Research. Part B, Applied Biomaterials*, 78 (1), pp. 47–55. DOI:10.1002/jbm.b.30456.

Wu, C., Ramaswamy, Y., Boughton, P. and Zreiqat, H. (2008) Improvement of mechanical and biological properties of porous CaSiO3 scaffolds by poly(d,l-lactic acid) modification, *Acta Biomaterialia*, 4 (2), pp. 343–353. DOI:10.1016/j.actbio.2007.08.010.

Wüst, S., Godla, M. E., Müller, R. and Hofmann, S. (2014) Tunable hydrogel composite with two-step processing in combination with innovative hardware upgrade for cell-based three-dimensional bioprinting, *Acta Biomaterialia*, 10 (2), pp. 630–640. DOI: 10.1016/j.actbio.2013.10.016.

Xue, W., Liu, X., Zheng, X. and Ding, C. (2005) In vivo evaluation of plasma-sprayed wollastonite coating, *Biomaterials*, 26 (17), pp. 3455–3460. DOI:10.1016/j.biomaterials.2004.09.027.

Yang, S., Leong, K. F., Du, Z. and Chua, C. K. (2001) The design of scaffolds for use in tissue engineering. Part I. Traditional factors, *Tissue Engineering*, 7 (6), pp. 679–689. DOI:10.1089/107632701753337645.

Yang, X., Lu, Z., Wu, H., Li, W., Zheng, L. and Zhao, J. (2018) Collagen-alginate as bioink for three-dimensional (3D) cell printing based cartilage tissue engineering, *Materials Science and Engineering: C*, 83, pp. 195–201. DOI:10.1016/j.msec.2017.09.002.

Yeo, M. G. and Kim, G. H. (2017) A cell-printing approach for obtaining hASC-laden scaffolds by using a collagen/polyphenol bioink, *Biofabrication*, 9 (2), pp. 025004. DOI: 10.1088/1758-5090/aa6997.

Yoon, D. M. and Fisher, J. P. (2009) Natural and Synthetic Polymeric Scaffolds, in: Narayan, R. (ed.) *Biomedical Materials*. Boston, MA: Springer US, pp. 415–442. DOI: 10.1007/978-0-387-84872-3_15.

You, F., Wu, X. and Chen, X. (2017) 3D printing of porous alginate/gelatin hydrogel scaffolds and their mechanical property characterization, *International Journal of Polymeric Materials and Polymeric Biomaterials*, 66 (6), pp. 299–306. DOI:10.1080/00914037.2016.1201830.

Zandi, M., Mirzadeh, H., Mayer, C., Urch, H., Eslaminejad, M. B., Bagheri, F. and Mivehchi, H. (2010) Biocompatibility evaluation of nano-rod hydroxyapatite/gelatin coated with nano-HAp as a novel scaffold using mesenchymal stem cells, *Journal of Biomedical Materials Research Part A*, 92A (4), pp. 1244–1255. DOI:10.1002/jbm.a.32452.

Zhang, D., Wu, X., Chen, J. and Lin, K. (2018) The development of collagen based composite scaffolds for bone regeneration, *Bioactive Materials*, 3 (1), pp. 129–138. DOI:10.1016/j.bioactmat.2017.08.004.

CHAPTER THREE
A 3D BIOPRINTED *IN SITU* CONJUGATED-CO-FABRICATED SCAFFOLD FOR POTENTIAL BONE TISSUE ENGINEERING APPLICATION

Published in Journal of Biomedical Materials Research Part A

Mduduzi N. Sithole, Pradeep Kumar, Lisa C. du Toit, Thashree Marimuthu, Yahya E. Choonara, Viness Pillay. A 3D bioprinted *in situ* conjugated-co-fabricated scaffold for potential bone tissue engineering applications. Journal Biomedical Materials Research Part A, 2018, 106A:1311–1321

3.1. INTRODUCTION

The traditional repair treatments for critical-sized or non-union bone defects due to trauma or disease have centered on orthopedic implants, allografts, and autografts. However, these techniques suffer from a number of limitations (Inzana *et al.*, 2014; Mallick *et al.*, 2015) such as lack of available donors and inadequate biomechanical properties (Sarkar *et al.*, 2006). Hence, bone tissue engineering employing scaffolds has emerged as an innovative and growing field of research in tissue engineering as an alternative technique to overcome the limitations of current approaches (Mallick *et al.*, 2015). Tissue engineering techniques involve the use of an appropriate scaffold biomaterial, relevant growth factor and/or cells (Cohen *et al.*, 2010; Tang *et al.*, 2016). Polymers have been investigated as biomaterials for a range of medical applications due to their biological properties (Karageorgiou and Kaplan, 2005). Major breakthroughs in tissue engineering is owing to the success in development of novel biomaterial-based approaches that simulate native organ and tissue parts (Bajaj *et al.*, 2014). Manipulation of materials and their biorelevant characterization has been the fundamental to their application in tissue engineering (Naebe and Shirvanimoghaddam, 2016).

The properties of the scaffold depend mainly on the fabrication methods and the nature of the biomaterial (Karageorgiou and Kaplan, 2005). Two-dimensional (2D) patterns of biochemical and mechanical cues have been generated through the development of numerous intricate methods, but for many cell types, the 2D culture condition may not be appropriate for propagating tissue regeneration. Additionally, 2D fabrication methods cannot be easily transformed into 3D methods, hence, there is a need for more progressive methods to precisely capture the intricate 3D cellular environment (Bajaj *et al.*, 2014). Scaffolds with controlled surface chemistry, pore size distribution, pore volume, pore interconnectivity and architecture cannot be fabricated with traditional processing techniques

(Gu *et al.*, 2016; Liu *et al.*, 2007) such as solvent casting or particle leaching, freeze-drying and gas foaming (Bajaj *et al.*, 2014). Therefore, additive manufacturing processing technologies such as 3D printing have been explored as an innovative tool since 1988 for the production of 3D structures, such as medical devices and tissue engineering scaffolds (Mehrban *et al.*, 2016). The advantages of 3D printed scaffolds for bone tissue engineering includes the fabrication of well-defined architecture with patient-specific geometries as well as enabling the necessary spatial organization (e.g., of bioactives or cells) within the scaffold or enhancing biological functionality (Inzana *et al.*, 2014). However, appropriate material selection is a major challenge in bioprinting. This could be addressed through conceptualizing tunable bio-inks with a range of material properties; this may be achieved through creation of novel composite mixtures to incorporate desirable features or properties (Mandrycky *et al.*, 2016). This approach is enabled via 3D printing which allows multiple biomaterials to be simultaneously plotted (Mandrycky *et al.*, 2016). During 3D printing of hydrogel scaffolds, further co-fabrication approaches, such as chemical or physical crosslinking reactions, could be implemented to influence the 3D structural integrity and properties (Khan *et al.*, 2015).

In considering the biomaterial composition of a bone scaffold it must be noted that bone is a nanostructured inorganic-organic composite (nanocomposite) or multiphase solid material. Alginate has been actively explored in the fabrication of scaffolds due to its capability to enable tissue and organ regeneration (Hashimoto *et al.*, 2005; Kataoka *et al.*, 2004; Levenberg *et al.*, 2005; Li *et al.*, 2006; Prang *et al.*, 2006; Suzuki *et al.*, 2000). For the fabrication of scaffolds using alginate, traditional methods such as electrospinning, crosslinking and lyophilization have been extensively studied. The most commonly employed traditional method for the production of alginate biopolymer scaffolds is via lyophilization (Venkatesan *et al.*, 2015). Alginate displays distinct efficacy due its high water absorbing ability, biodegradability and high biocompatibility. Hence, it has been widely studied for 3D cell culture, tissue regeneration and drug delivery (Shang *et al.*, 2017). Modification of alginate via diverse approaches is also possible, and a requirement for enhancement of its biomechanical properties for tissue engineering applications. Sun *et al.,* (2013) provided an in depth review of alginate hydrogels for regenerative medicine applications through click reaction, free radical polymerization, cell crosslinking, phase transition and ionic crosslinking (Sun and Tan, 2013; Venkatesan *et al.*, 2015). Polyethyleneimine (PEI) is a branched polycationic polymer that contains a high density of ionizable tertiary, secondary and primary amino groups and has a strong interaction with proteins. It has been employed widely in tissue engineering and promotes cell growth. It has also been utilized to enhance protein loading on solid surfaces and it has been introduced onto the surfaces of organic or

inorganic solid spheres using techniques such as covalent grafting, spray drying, electrostatic adsorption and layer-by-layer assembly. Murakami *et al.*, (2011) produced PEI-coated hydroxyapatite with various fractions of PEI via a spray drying technique. Further, Xia *et al.*, (2011) employed a layer-by-layer technique to produce chemically crosslinked PEI using glutaraldehyde. Therefore, PEI can form a polyelectrolyte (PEC) layer following electrostatic adsorption on a negative substrate (Wang *et al.*, 2012), such as alginate to create a complex with potentially enhanced capabilities. Silica gel is an exemplary inorganic component commonly included in bone scaffolds. Bioactive materials containing silicon species have demonstrated enhancement of osteogenesis. Silica could thus be included in the bio-ink for improved bone tissue biosimulation.

The 3D printing technology, as discussed, holds great potential, but there are some important limitations that need to be overcome. There is a great need for an increased diversity of printable biomaterials for the synthesis of bioarchetypes and biodegradable polymeric biomaterials that will fulfil the requirements of tissue repair, regeneration, restoration and reorganization (Guvendiren *et al.*, 2016; Liu and Ma, 2004). This study proposed to develop a novel bioarchetype employing 3D-printing technology as an innovative co-fabrication tool for single-step conjugation of scaffolds. A polymeric scaffold was engineered *in situ* employing sodium alginate as a bio-ink which interacted with PEI to form a polyelectrolyte complex while the scaffold was simultaneously bioprinted, with inclusion of silica gel as a temporal inorganic bone tissue supporting component for bioarchitectural simulation of bone tissue. Physicochemical and physicomechanical characterizations were undertaken to assess the potential of the scaffold for bone tissue engineering. Ultimately, this research proposes a novel approach for bio-ink design and scaffold bioprinting to address the limited availability of printable biomaterials for bone tissue engineering applications.

3.2. MATERIALS AND METHODS

3.2.1. Materials

Sodium alginate (NaAlg, Product number: W201502, sodium alginate), demonstrated to be suitable for biofabrication of 3D hydrogel (Tabriz *et al.*, 2017), was obtained from Sigma-Aldrich, Gilling-ham,UK. silica gel (Si, M_w = 60 000), poly(ethyleneimine) solution (PEI, 50%$^{w}/_{v}$ in water, M_w = 750 000), Dulbucco's Modified Eagle's Medium (DMEM), Fetal bovin serum (FBS), ethanol, deionized water and additional reagents were purchased from Sigma-

Aldrich (Cleveland, OH, USA). Chemicals were utilized without further purification unless stated.

3.2.2. Fabrication of the 3D Bioprinted *in situ* Conjugated-co-fabricated Scaffold Bioarchetypes

The Alg-PEI/Si scaffold was engineered as follows: Sodium alginate (200mg/mL) was prepared as a component of the bio-ink following hydration in ultra-filtrated purified deionized water (Millipore, France). Silica gel (200mg/mL) as an inorganic component was combined with the sodium alginate hydrogel. Separately, PEI solution was prepared by adding 40mL of PEI to 100mL of ethanol. A 3D Bioplotter® (EnvisionTEC, GmBH) was employed to engineer an Alg-PEI/Si 3D porous scaffold. The 3D printing of these polymeric scaffolds utilized computer aided design (CAD) to create the desired structure to be printed. The importing software of the STL data and the control of the 3D Bioplotter® consisted of two modules: (i) the 3D Bioplotter® software for STL data importation and structure (e.g. scaffold) fabrication; and (ii) the VisualMachine software for material parameters and machine control. The scaffold was printed at a temperature of 37^{o}C where the Alg/Si bio-ink was fed into a 30cm^{3} cartridge and dispensed through a plastic needle (nozzle diameter 0.41mm), under a pressure of 0.5Bar and deposition speed of 8mm/s into a petri dish containing the solidifying solution of PEI dissolved in ethanol. The layers were deposited at 90 degree angle to the underlying layer in PEI solution. Layers were successively printed with the average solidification time per layer noted. The scaffold was printed using parameters as described in Table 3.1. The bioprinted scaffold was subsequently washed thrice with double deionized water and dried to constant weight at room temperature (25°C). Table 3.2 provides visual results of the solidification behavior of the various preliminary solidified scaffolds evaluated, where deionized water and PEI, ethanol and PEI, or ethanol alone were investigated as the solidifying solutions. The preferred scaffold was identified and subjected to further characterizations.

Table 3.1: Parameters used to print the desire bioarchetype scaffold

Parameter	Value
Temperature	37^{o}C
Pressure	0.5Bar
Speed	8mm/s
Platform temperature	20^{o}C

Table 3.2: 3D bioprinted scaffold combinations and preliminary characterization

Bio-Ink	Solidification Solution	Visual Characterization
Sodium Alginate + Silica gel	Ethanol	Rapid solidification (within 30s); Stable scaffold (maintains 3D architecture for successive layers to be printed); Scaffold degrade within a day (see Comparative Degradation Rate Analysis of the Bioprinted Scaffold section).
Sodium Alginate + Silica gel	PEI dissolved in ethanol	Moderate solidification time (within 60s); Stable scaffold structure (maintains 3D architecture for successive layers to be printed); Scaffold maintains it 3D network structure over 28-day period of study (see Comparative Degradation Rate Analysis of the 3D Bioprinted Scaffolds section).
Sodium Alginate + Silica gel	PEI dissolved in deionised water	Very slowly solidification (does not maintain 3D architecture for successive layers to be printed); Nonstable scaffold structure (failed to maintain 3D structure); Scaffold did not form –erosion studies could not be undertaken

3.2.3. Determination of Chemical Transitions of the 3D Bioprinted Scaffolds and Native Biomaterials

The chemical transitions of the scaffold fabricated employing the 3D Bioplotter® (EnvisionTEC, GmBH) and the native materials used were determined utilizing a Fourier Transform Infrared (FT-IR) spectrometer (PerkinElmer Spectrum 100, FT-IR Spectrometer)

fitted with a universal ATR Polarization Accessory (PerkinElmer Ltd., Beconfield UK). The samples were weighed (1-3mg) and analyzed at high resolution with the wavelength ranging from 4000-650cm^{-1} on a Nicolet Impact 400D FT-IR Spectrophotometer coupled with Omnic FT-IR research grade software (Nicolet Instrument Corp., Madiso, WI, USA) and the presence and absence of specific functional groups were evaluated.

3.2.4. Thermal Transition Analysis of the 3D Bioprinted Scaffold

The thermal properties of all the native materials and the bioprinted scaffold were ascertained via differential scanning calorimetry (DSC) (Mettler Toledo, Schwerzernback, Switzerland). Dried samples of 5-10mg were weighed into aluminium crucible pans (40µL) and a small (0.2mm) hole in aluminium lid was induced to create an open system. The samples were heated under nitrogen atmosphere (Afrox, Germiston, Gauteng, South Africa) with 200mL/min flow rate acting as the purge gas to decrease oxidation. The samples were exposed to a temperature range between 25^{o}C and 400^{o}C at the rate of 10^{o}C/min and the thermal profiles were analyzed.

3.2.5. Analysis of the Thermal Decomposition of the 3D Bioprinted Scaffold

A thermogravimetric analyzer (TGA 400, PerkinElmer Inc., MA) was used to analyze the thermal decomposition of the newly formed scaffolds and the native materials. Samples (10-20mg) were placed in a ceramic pan under nitrogen gas atmosphere. Thermograms were recorded in a range of 30^{o}C to 900^{o}C and revealed the thermal decomposition of the materials.

3.2.6. Characterization of the 3D Bioprinted Scaffold Swelling and Structural Integrity Transitions

The swelling and structural integrity behavior of the 3D bioprinted scaffold matrices was imaged using a 0.5T open configuration Magnetic Resonance Imaging (MRI) system (Signa SP, General Electric Medical Systems, Milwaukee, WI). The dried scaffold was placed in a prepared phosphate buffered saline (pH 7.4) and positioned within the flow equipped with 0.5T permanent magnet system, stabilized at 37^{o}C. After duly configuring, optimizing the shims and probe tuning, the cone-like lower part of the cell was filled with glass beads to provide laminar flow at 16mL/min of the solvents employed. The scaffold was placed in

position and magnetic resonance images were taken at set time intervals with MARAN-I version 1.0 software. The image was acquired after setting the frequency offset and testing gain employing RINMR version 5.7 under continuous solvent conditions. MARAN-I software comprises image acquisition software and image analysis software. MR images were acquired over 24 hours.

3.2.7. Surface Morphology Analysis of the 3D Bioprinted Scaffold

Surface morphology of the fabricated scaffold was examined utilizing scanning electron microscopy (SEM) FEI Nova NanoLab SEM (FEI Company, Hillsboro, Oregon). Gold isotope was used to sputter coat the samples while the sample was mounted on the aluminium spud with an EPI coater (SPI Model sputter-coater and control unit, Hester, PA). After coating the samples for 60s, under constant nitrogen gas conditions, the samples were analysed using a FEI Nova NanoLab SEM (FEI Company, Hillsboro, Oregon).

3.2.8. Porositometric Determination of the 3D Bioprinted Scaffolds

The 3D plotted scaffold porosity was calculated from the microscopic images of the scaffold using (Equation 3.1), in accordance with the theoretical approach of (Landers *et al.*, 2002):

$$\boldsymbol{P = 1 - \frac{V_{scaffolds}}{V_{cube}} = 1 - \frac{\pi}{4} \cdot \frac{(d)^2}{d_1 d_2}} \qquad \textbf{(Equation 3.1)}$$

Where;

P = scaffold porosity,

d = scaffold fiber diameter,

d_1 = scaffold fiber spacing and d_2 = layer thickness within each different structure(Pan *et al.*, 2016).

3.2.9. Comparative Degradation Rate Analysis of the 3D Bioprinted Scaffolds

The degradation rates of the bioprinted Alg/Si and Alg-PEI/Si scaffolds were compared. UV-light was used to sterilize the pre-weighed dry scaffolds, which were subsequently soaked in Dulbecco's modified Eagle's medium (DMEM), supplemented with 10% fetal bovin serum (FBS), and incubated in an atmosphere of 5% CO_2 at 37^{o}C (pH 7.4) to simulate the

environment in a living organism. Scaffolds were removed at various time intervals and weighed after being dried. The medium was replaced every second day since the degraded residues may contaminate the scaffold because in a living organism degraded residues are eliminated through different processes such as urinating amongst others and the study was performed for a period of 28 days (Pan *et al.*, 2016). The degradation rate was calculated according to Equation 3.2 as follow:

$$\boldsymbol{Degradation\ rate}\ (\%) = \frac{\boldsymbol{W_0 - W'}}{\boldsymbol{W_0}}\boldsymbol{X\ 100} \qquad (\textbf{Equation 3.2})$$

Where;

W' = final weight of the scaffold

W_0 = initial weight of the scaffold

3.2.10. Determination of the Biomechanical Properties of the 3D Bioprinted Scaffold

The scaffold mechanical properties were measured utilizing a BioTester 5000. This enabled Biaxial testing of the scaffold which is critical for investigating the mechanical properties of biomaterials due to their directionally oriented microstructures. The BioRankes system permits the mounting of samples tissue into the BioTester. The fabricated scaffold was equilibrated by first soaking it in Dulbecco's modified Eagle's medium (DMEM), supplemented with 10% fetal bovin serum (FBS) and incubated at an atmosphere of 5% CO_2 at 37^{o}C (pH 7.4) for 24 hours. The sharp BioRankes pierces the most delicate and tough samples as to afford a constant dispersing site of attachment across the shape of the samples. Following positioning of the samples, a manually-functioning crown press exerted pressure onto the sample.

3.3. RESULTS AND DISCUSSION

3.3.1. Preliminary Evaluation of the 3D Bioprinted Scaffold

As depicted in Figure 3.1, a novel polyelectrolyte complex (PEC) scaffold was designed and printed using a 3D Bioplotter® (EnvisionTEC, GmBH). PEI was the cationic polymer of choice in this investigation, owing to its potential to interact with anionic functional groups to form complexes. Sodium alginate was a favorable anionic polymer selection, since it contains very reactive anionic functional groups (COO^-), rendering ionic bonding through

electrostatic interaction between the positively charged amino groups of PEI with the negatively charged COO^- of sodium alginate possible.

The 3D bioprinting highlights a novel application for the Alg-PEI PEC incorporating silica. The challenge was to investigate a biologically nontoxic solvent that would dissolve PEI, which upon contact with NaAlg/Si bio-ink, would cause it to undergo solifdification while enabling the interaction of NaAlg with PEI. Stable solidification is required to enable the next layer to be printed on top of the previous layer, implicit to this layer-by-layer fabrication approach. Ethanol was found to be the solvent of choice because it is nontoxic as well as enabling *in situ* co-fabrication of the PEC with solidification of the bioplotted strands. When water, however, was employed as solvent it did not effectively form or maintain a solid structure for the subsequent layer to be printed upon.

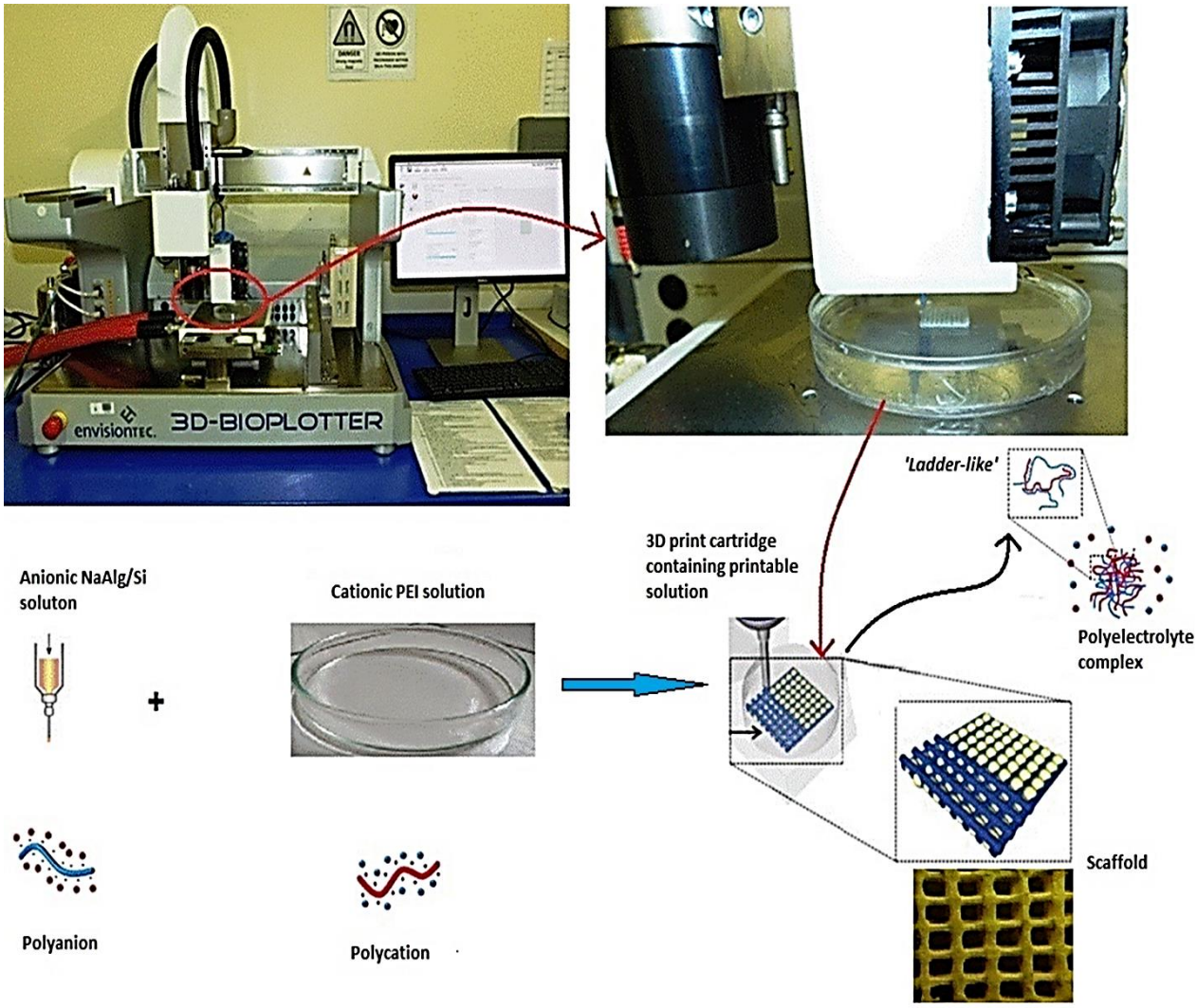


Figure 3.1: Schematic and photographic depiction of formation of the 3D bioprinted and *in situ* conjugated-co-fabricated scaffold.

3.3.2. Chemical Transition Evaluation of the Bioprinted Scaffold

The 3D bioprinted scaffolds composed of sodium alginate; PEI and silica gel were successfully fabricated using 3D Bioplotter® (EnvisionTEC, GmBH). Its fabrication was validated through various techniques as discussed below.

The FTIR spectrum in Figure 3.2a depicted a significant band at 1054cm^{-1} which is indicative of Si-O-Si in the spectrum of pristine silica gel. This band is overlapped by other vibrational modes in the FTIR spectrum of the bioprinted scaffold (Figure 3.2d). Figure 3.2b represents the spectrum of pristine sodium alginate, which displayed a broad stretch at 3500cm^{-1} to 3000cm^{-1} associated with O-H stretching and two distinct peaks at 1595cm^{-1} and 1397cm^{-1} which are attributed to the asymmetrical and symmetrical vibration of COO^- functional groups, respectively. The vibration stretch peak at 1021cm^{-1} is associated with C-O-C functional groups (Konwar *et al.*, 2015).

Figure 3.2c represents the pristine PEI FTIR spectrum, which possessed the following significant bands: the two peaks at 3348 and 3287cm^{-1} arise from NH_2 stretching vibration; the strong peaks at 2944 and 2844 cm^{-1} are associated with asymmetrical and symmetrical vibrations of CH_2 groups, respectively; and the peaks at 1599cm^{-1} and 1645cm^{-1} are associated with N-H bending. The peak at 1465cm^{-1} is associated with CH_2 bending and the peak from 1311cm^{-1} to 1000cm^{-1} is associated with C-N stretching (Li *et al.*, 2014).

Figure 3.2d depicts the spectrum of the bioprinted polymeric scaffold (Alg-PEI/Si). There are still two bands at 2948cm^{-1} and 2811cm^{-1} that are associated with CH_2 stretching vibrations, originating from the presence of PEI; in addition there is a peak at 1465cm^{-1} associated with the CH_2 bending vibration of PEI. Further interpretation highlighted bands at 3262cm^{-1} to 3350cm^{-1} associated with an NH_2 stretching vibration, as well as a new broad peak at 1562cm^{-1} which is due to the newly formed ionic bond between COO^- and NH_3^+, of NaAlg and PEI, respectively, which resulted in the absence of the peak at 1645cm^{-1} observed in Figure 3.2c. This partially confirms the formation of the polyelectrolyte complex (PEC), however further physicochemical analyses were undertaken to support this finding.

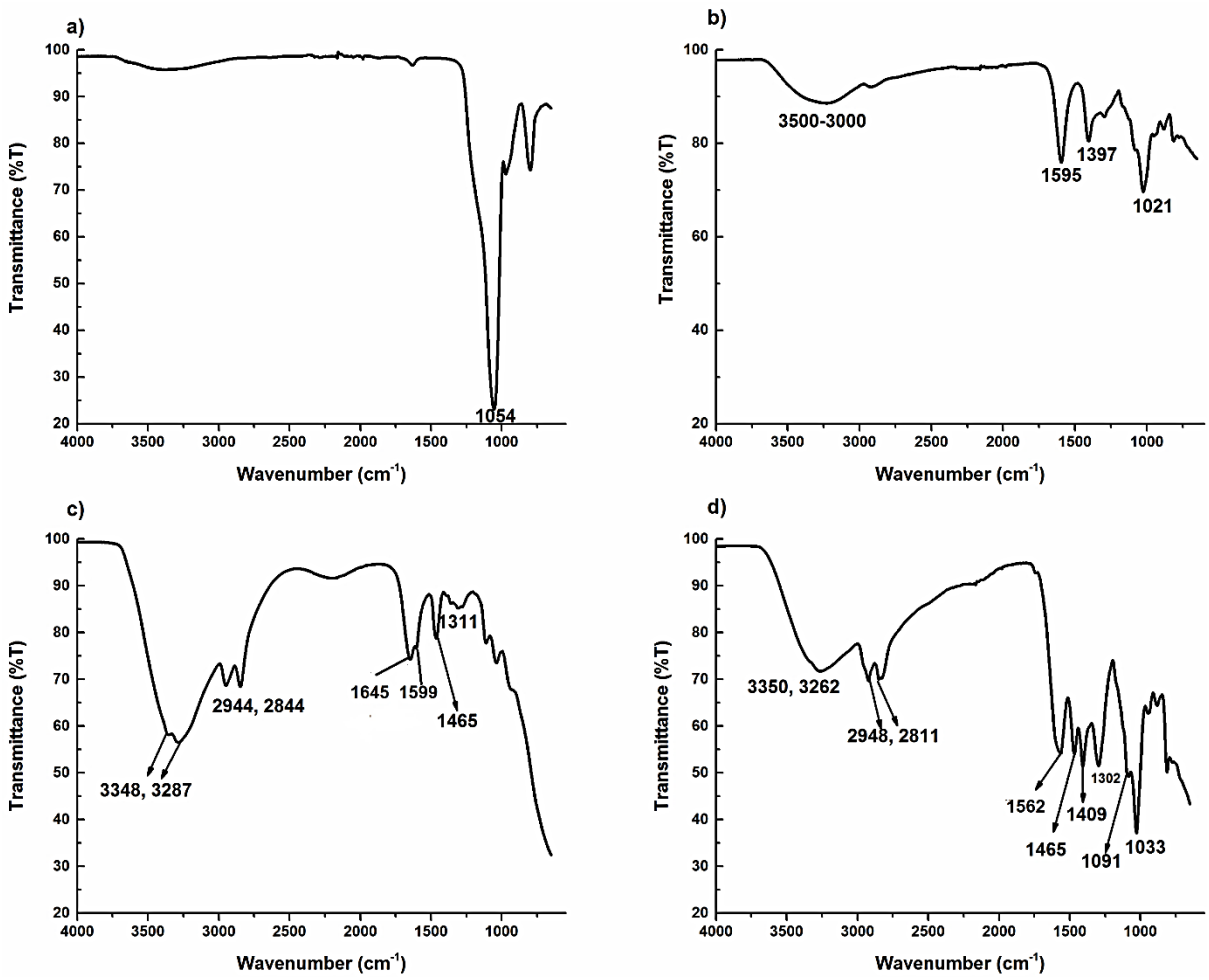


Figure 3.2: FTIR spectra of (a) Pristine Si, (b) Pristine NaAlg, (c) Pristine PEI, and (d) Alg-PEI/Si scaffold

Figure 3.3 represents the XRD diffractograms of pristine Si, pristine NaAlg and the Alg-PEI/Si scaffold for ascertaining the scaffold physicochemical state. The observed XRD patterns of pristine Si (Figure 3.3a) displayed a broad band centred at 22^{o} as an indication of its amorphous nature (Antony *et al.*, 2014). Figure 3.3b represents pristine NaAlg displaying characteristic peaks at 14^{o}, 22^{o} and 38^{o} confirming its semi-crystalline nature (Qi *et al.*, 2015). Figure 3.3c depicts the XRD for the bioplotted scaffold which had bands at 14^{o}, 23^{o} and at 38^{o}, reminiscent of pristine NaAlg, but with a more amorphous nature.

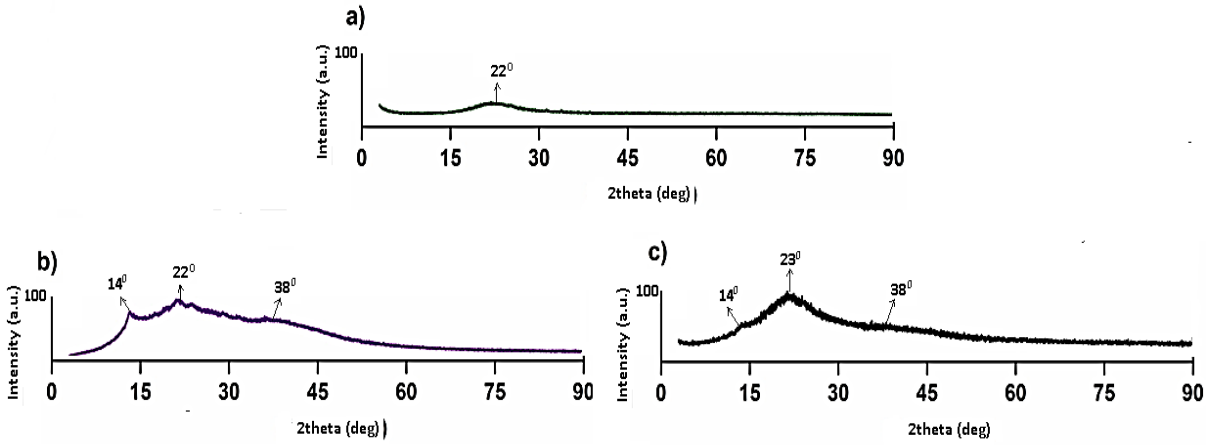


Figure 3.3: XRD spectra of the (a) Pristine Si, (b) Pristine NaAlg, and (c) Scaffold

3.3.3. Assessment of Thermal Transitions and Stability of the Bioprinted Scaffold

The thermal stability of the pristine Si, pristine NaAlg and Alg-PEI/Si scaffold was assessed using TGA. Figure 3.4a depicts the thermal degradation of pristine Si; there is a gradual loss of mass toward 100ºC due to the evaporation of water and it proved to be stable up to 400ºC. With regard to the TGA of pristine PEI, (Wang *et al.*, 2012) highlighted that the weight loss is first observed between 106ºC and 162ºC corresponding to the evaporation of water from PEI, and between 253ºC and 298ºC corresponding to the endothermic peak ascribed to the decomposition of PEI (Wang *et al.*, 2012). Figure 3.4b shows the TGA curve for pristine NaAlg where the loss of moisture was distinctly observed at temperatures below 100ºC. The major degradation of NaAlg occurred at 242ºC. Figure 3.4c represents the TGA curve of the Alg-PEI/Si scaffold, where the evaporation of water was observed at temperatures below 100ºC. There are two major degradations which occurred at 242ºC corresponding to Alg and the other at 298ºC which may correspond to the ionically cross-linked PEI confirming the presence of both polymers in the product.

The DSC curves of pristine NaAlg, pristine Si and the Alg-PEI/Si scaffold under N_2 are shown in Figure 3.5. The dehydration was evidenced by an endothermic peak at ~100ºC in all the thermal curves and the pristine Si is stable up to 400ºC as evidence in Figure 3.5a. The decomposition of pristine NaAlg in Figure 3.5b is represented by an exothermic peak at 240-250°C. Finally, the decomposition of the carbonaceous material occurred at 375ºC (Soares *et al.*, 2004). Figure 3.5c represents the thermogram of the bioprinted scaffold, which also exhibits an exothermic decomposition at 240-250ºC corresponding to initial NaAlg decomposition and a small endothermic peak close to 400ºC, but lack of a second

decomposition peak. There is delay in eventual decomposition of the scaffold compared to the individual components due to the ionic interaction (Shen *et al.*, 2013). These results are consistent with the thermal stability findings of the TGA spectra above.

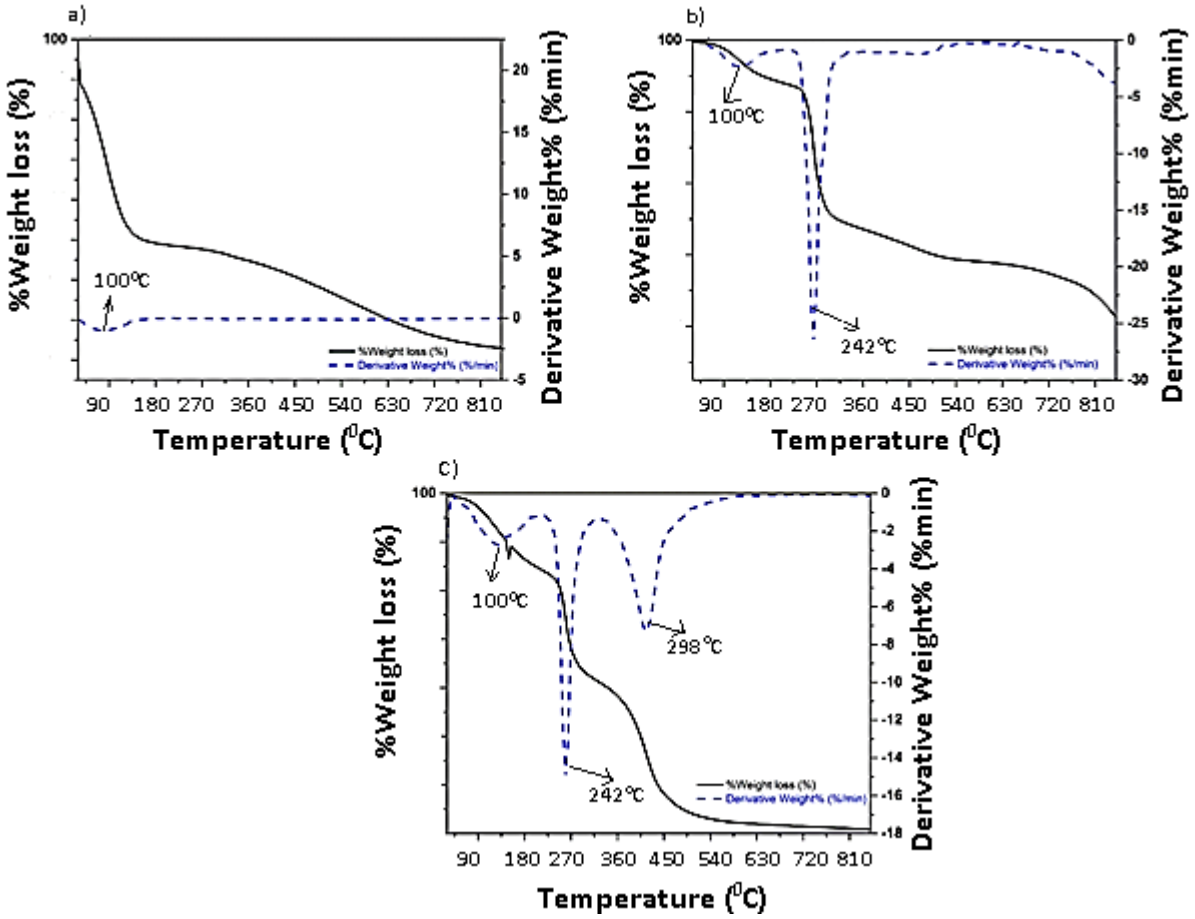


Figure 3.4: The TGA spectra for, a) Pristine Si, b) Pristine NaAlg, and c) Alg-PEI/Si

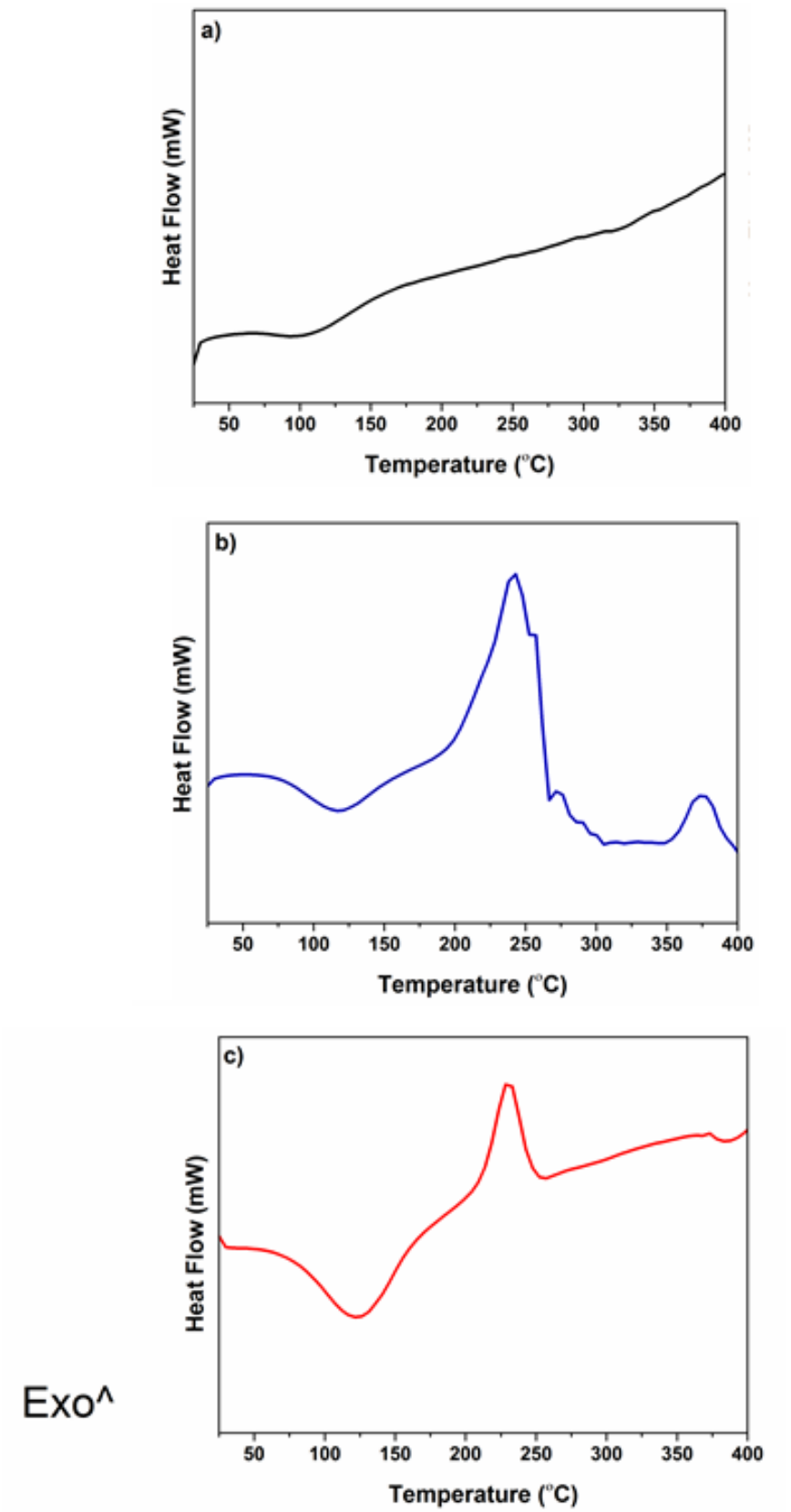


Figure 3.5: DSC thermal behaviour of a) Pristine Si, b) Pristine NaAlg, and c) Alg-PEI/Si

3.3.4. Evaluation of the Morphology, Porosity, Pore Size, Swelling and Structural Integrity of the Bioprinted Scaffold

Figure 3.6 depicted the scaffold dimensions and morphology for printing. Figure 3.6a highlighted the thickness of each printed bio-ink strand, which was observed to be 0.4mm, and the length of the space between the strands was visualized to be 0.2mm. The final dried Alg-PEI/Si bioprinted scaffold possessed dimensions of 3.6mmx4.5mmx1mm. Figure 3.6c provides the SEM of the dried printed scaffold which highlighted the roughness and porous nature of the bioprinted scaffold with consistent channelling of pores which are favorable for nutrient flow and material transfer, as well as providing a large surface area for attachment and proliferation of cells. The porosity of the scaffold was calculated to be 60% while the pore size was found to be 360±20µm, highlighting shrinkage of the scaffold strands on complex formation and drying. In general the acceptable pore size is in a range of 50 to 1000µm (Li *et al.*, 2014) for bone tissue engineering applications.

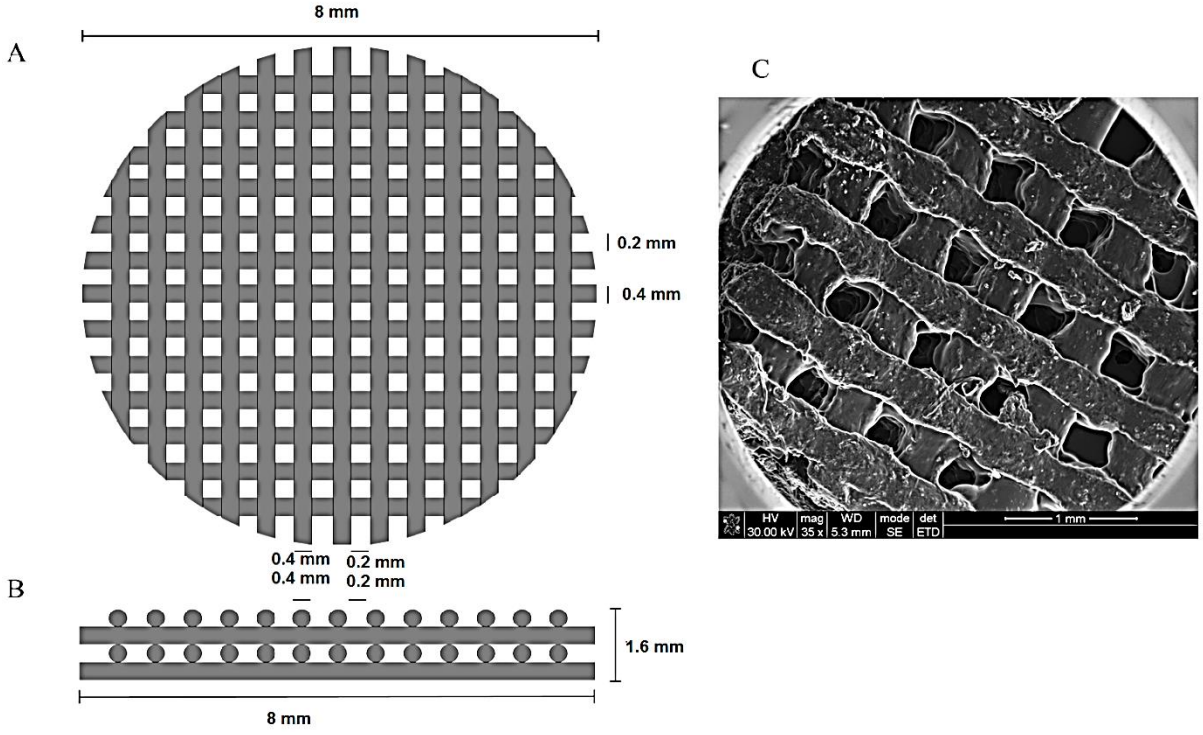


Figure 3.6: (a) Surface schematic of the proposed design of the bioprinted scaffold, (b) Cross-section schematic of the proposed design of the bioprinted scaffold, (c) SEM image of the surface section of the bioprinted Alg-PEI/Si scaffold**.**

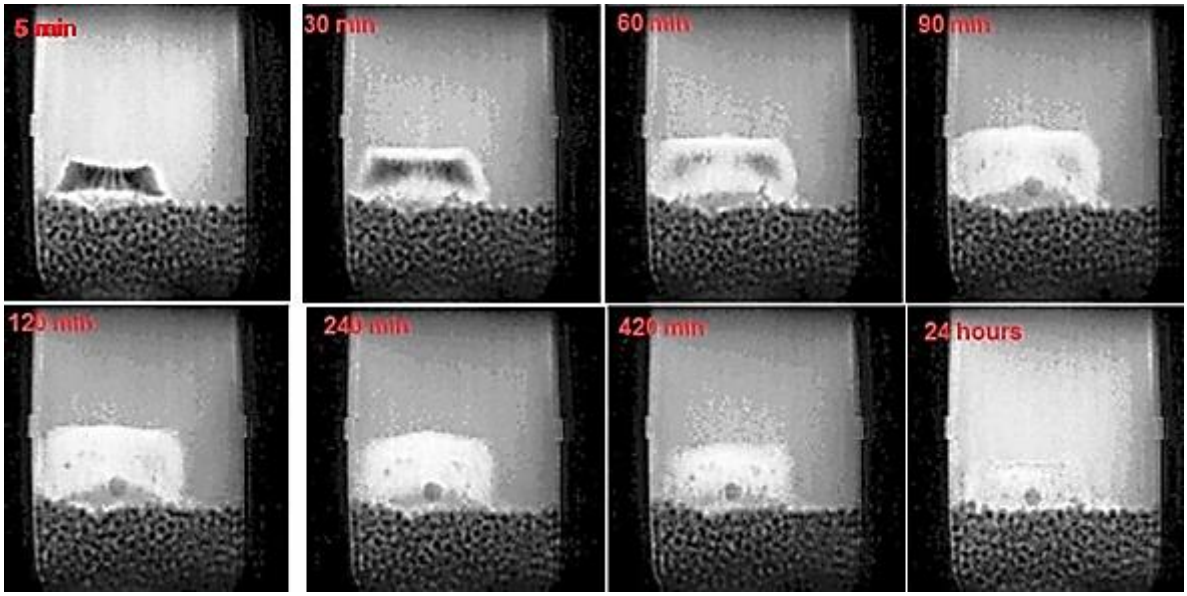


Figure 3.7: Magnetic resonance imaging of the bioprinted scaffold

This study utilized magnetic resonance imaging (MRI) to observe the swelling and structural integrity behavior of the bioprinted polymeric scaffold in phosphate buffered saline (pH 7.4). The observed images were captured at various time intervals. The light grey area that surrounds the scaffold matrix is the dissolution medium (buffer), while the contrasting black area within the scaffold matrix is the non-gelled non-hydrated region of the polymeric scaffold matrix. It is observed from Figure 3.7 that, as the scaffold matrix hydrated, it progressively gelled and swelled represented by the white region of the scaffold matrix with each printed strand becoming thicker. Initially there was increased erosion, with loss of some of the incorporated silica gel; thereafter that the scaffold maintained its 3D network (shape) over the 24 hour period of investigation.

3.3.5. Evaluation of Degradation of the Various Bioprinted Scaffolds

The degradation behavior of Alg/Si and Alg-PEI/Si scaffolds are depicted in Figure 3.8. The NaAlg/Si scaffold displayed complete erosion in the medium (pH 7.4) within a day (24 hours) as shown in the Figure 3.8 and this can be attributed to the solubility of NaAlg in water and the fact that the pristine silica gel is not chemically bonded to the pristine NaAlg; the silica gel primarily acts as a bioactive and support structure. The Alg-PEI/Si scaffold demonstrated an initial mass loss of 50% within a day due to the high silica gel content incorporated within the scaffold, but subsequently the scaffold maintained a near constant mass up to day 28. The fact that scaffold maintained it 3D network structure for the 28 day period of investigation highlights that the degradation of the scaffold has the potential to occur over

time at a controlled resorption rate correlating with the bone tissue reformation rate (~3-6 months).

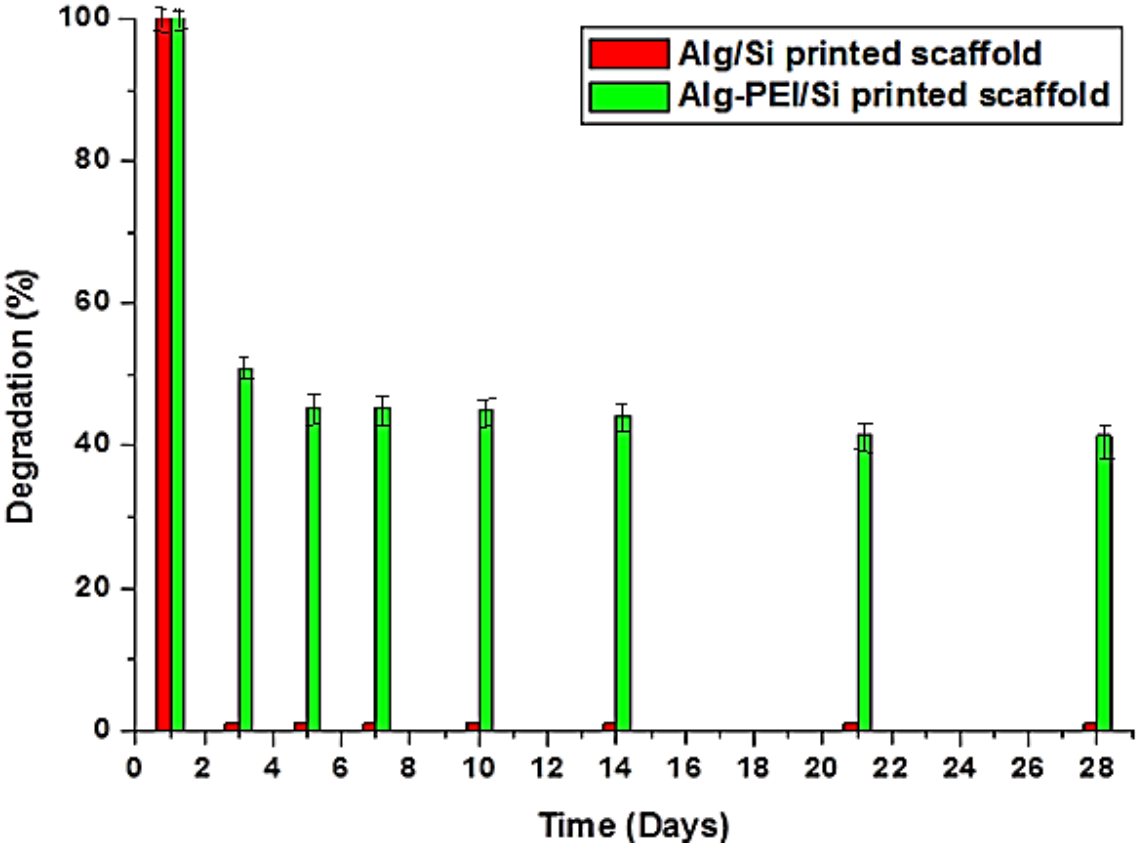


Figure 3.8: *In vitro* degradation (mass loss, %) of the bioprinted scaffolds

3.3.6. Evaluation of the Physicomechanical Strength of the Bioprinted Scaffold

Matrix hardness is the force required to deform scaffold matrices in the presence of an external pressure, while deformation energy is the energy required to withstand the forces within the matrices. Analysis of the physicomechanical strength is employed to indicate the stability of the matrices and their ability to withstand applied pressure, which a bone scaffold would ultimately encounter *in vivo*. A harder and more resilient matrix indicates a more compact matrix which is likely to have higher Young's modulus. The hardness of the scaffold is also influenced by the inherent properties of the polymers employed in the formulation of the scaffold.

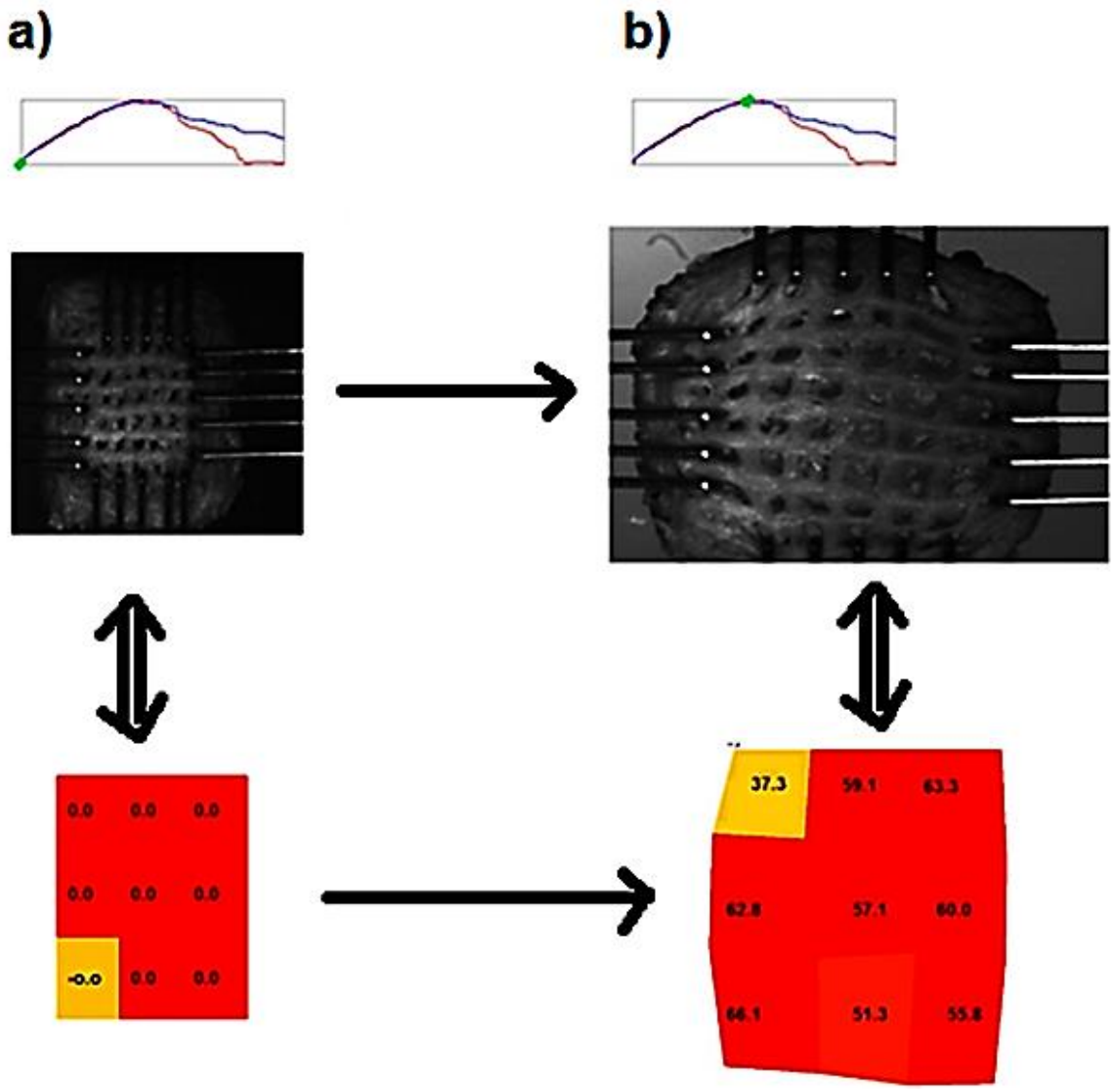


Figure 3.9: BioTester images and corresponding real-time image analysis and force-displacement graphs representing scaffold strength (a) before application of force and (b) during maximum stretch.

Alginate was investigated as a preferred material for bone tissue engineering compared to other materials because it can be easily modified, it can be introduced into the body in a less invasive manner due to its biocompatibility, and it enables controlled release of tissue induction factors (e.g., MBP). However, due to their less sufficient mechanical properties they cannot bear loads at the initial stages of regeneration without fixation (Lee and Mooney, 2012). Thus formation of a PEC with 3D printing was applied. In this study, a BioTester was employed for biaxial determination of the stiffness or the ability of the bioprinted scaffolds to resist deformation under an applied tensile load. Figure 3.9(a) depicts the scaffold while it was at rest (before force was applied, indicated by the green dot on the force-displacement curve). Figure 3.9(b) shows the maximum stretching of the scaffold with biaxial testing before breakage (indicated by the green dot on the force-displacement curve). The stress-

strain curve generated highlighted the elastic behaviour of the scaffold. The Young's modulus (representative of material stiffness) of the bioprinted scaffold was calculated from the linear elastic portion of the stress-strain curve generated from the average forces and displacements in both x and y-directions, and was determined to be 18.37MPa (Figure 3.10). The bioprinted scaffold exhibited the linear elastic behavior recommended for bone tissue engineering (Hollister, 2009), and the Young's modulus attained is within values reported for hybrid and nanobiocomposite alginate scaffolds for bone tissue engineering (~1-30MPa) (Bharatham *et al.*, 2014; Lee *et al.*, 2012) highlighting that the scaffold in its current form possesses the mechanical capabilities for certain bone tissue engineering applications (e.g. cancellous bone repair). Further strengthening of the bioprinted scaffold by enhanced incorporation of silica or addition of alternative inorganic or biomineral components may be considered for enhancement of the scaffold' biomechanical properties.

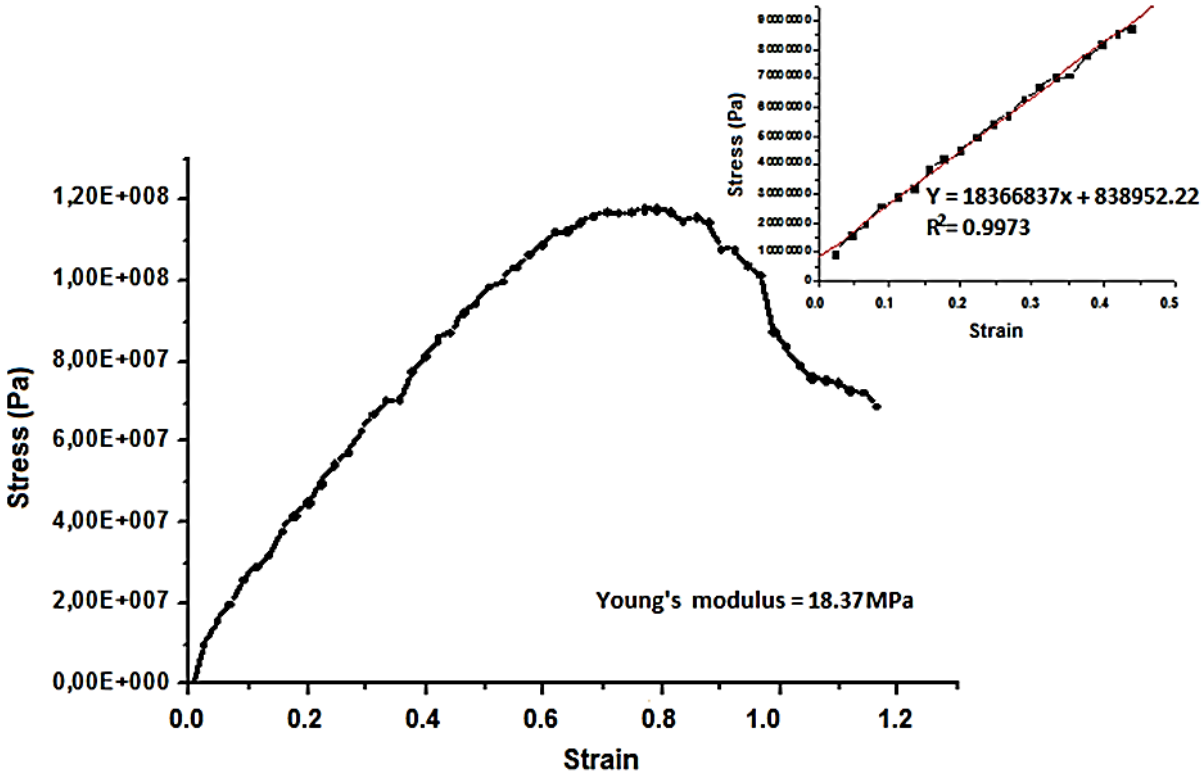


Figure 3.10: Stress-strain curve depicting Young's modulus of the bioprinted scaffold.

3.4. CONCLUDING REMARKS

The applications of autografts or allografts have shown limitations in repair or replacement of bone injuries. The 3D bioprinting technology was introduced as a promising approach for scaffold fabrication; however, limitations exist in terms of available printable biomaterials. Hence, a novel alternative method of scaffold fabrication *via in situ* conjugation-co-

fabrication for formation of a PEC-based 3D bioprinted scaffold for bone tissue engineering was employed. This single-step fabrication approach resulted in a scaffold based on an innovative Alg-PEI/Si biomaterial with appropriate pore size and porosity and maintenance of its 3D architecture over the 28 day period of investigation. The biomechanical properties of the 3D bioprinted scaffold highlighted the linear elastic behavior and a Young's modulus which was favorable for certain bone tissue engineering applications. The application of the 3D printing enable construction of scaffold layer-by-layer via low temperature processing for enhancing control over pore orientation, pore size distribution, pore volume and pore interconnectivity of the scaffold. This technique thus promotes customization of the spatial organization of the scaffold via variation of printing parameters for optimization of scaffold strength, nutrient transfer, and cellular infiltration for the required bone tissue engineering application. Further studies will focus on enhancement of the mechanical properties of the scaffold with evaluation of osteoblast attachment-, proliferation- and differentiation-promoting capabilities of the scaffold.

3.5. REFERENCES

Antony, R., Manickam, S. T. D., Kollu, P., V. Chandrasekar, P., Karuppasamy, K. and Balakumar, S. (2014) Highly dispersed Cu(ii), Co(ii) and Ni(ii) catalysts covalently immobilized on imine-modified silica for cyclohexane oxidation with hydrogen peroxide, *RSC Advances*, 4 (47), pp. 24820–24830. DOI:10.1039/C4RA01960A.

Bajaj, P., Schweller, R. M., Khademhosseini, A., West, J. L. and Bashir, R. (2014) 3D Biofabrication Strategies for Tissue Engineering and Regenerative Medicine, *Annual Review of Biomedical Engineering*, 16 (1), pp. 247–276. DOI:10.1146/annurev-bioeng-071813-105155.

Bharatham, B. H., Abu Bakar, M. Z., Perimal, E. K., Yusof, L. M. and Hamid, M. (2014) Development and Characterization of Novel Porous 3D Alginate-Cockle Shell Powder Nanobiocomposite Bone Scaffold, *BioMed Research International,* 23, pp. 1-11. DOI:10.1155/2014/146723.

Cohen, D. L., Lipton, J. I., Bonassar, L. J. and Lipson, H. (2010) Additive manufacturing for in situ repair of osteochondral defects, *Biofabrication*, 2 (3), pp. 035004. DOI:10.1088/1758-5082/2/3/035004.

Gu, B. K., Choi, D. J., Park, S. J., Kim, M. S., Kang, C. M. and Kim, C.-H. (2016) 3-dimensional bioprinting for tissue engineering applications, *Biomaterials Research*, 20, pp. 12. DOI:10.1186/s40824-016-0058-2.

Guvendiren, M., Molde, J., Soares, R. M. D. and Kohn, J. (2016) Designing Biomaterials for 3D Printing, *ACS Biomaterials Science & Engineering,* 2(10), pp. 1679-1693. DOI:10.1021/acsbiomaterials.6b00121.

Hashimoto, T., Suzuki, Y., Suzuki, K., Nakashima, T., Tanihara, M. and Ide, C. (2005) Review Peripheral nerve regeneration using non-tubular alginate gel crosslinked with covalent bonds, *Journal of Materials Science: Materials in Medicine*, 16 (6), pp. 503–509. DOI:10.1007/s10856-005-0524-1.

Hollister, S. J. (2009) Scaffold design and manufacturing: from concept to clinic, *Advanced Materials (Deerfield Beach, Fla.)*, 21 (32–33), pp. 3330–3342. DOI:10.1002/adma.200802977.

Inzana, J. A., Olvera, D., Fuller, S. M., Kelly, J. P., Graeve, O. A., Schwarz, E. M., Kates, S. L. and Awad, H. A. (2014) 3D printing of composite calcium phosphate and collagen scaffolds for bone regeneration, *Biomaterials*, 35 (13), pp. 4026–4034. DOI: 10.1016/j.biomaterials.2014.01.064.

Karageorgiou, V. and Kaplan, D. (2005) Porosity of 3D biomaterial scaffolds and osteogenesis, *Biomaterials*, 26 (27), pp. 5474–5491. DOI:10.1016/j.biomaterials.2005.02.002.

Kataoka, K., Suzuki, Y., Kitada, M., Hashimoto, T., Chou, H., Bai, H., *et al.* (2004) Alginate enhances elongation of early regenerating axons in spinal cord of young rats, *Tissue Engineering*, 10 (3–4), pp. 493–504. DOI: 10.1089/107632704323061852.

Khan, F., Tanaka, M. and Ahmad, S. R. (2015) Fabrication of polymeric biomaterials: a strategy for tissue engineering and medical devices, *Journal of Materials Chemistry B*, 3 (42), pp. 8224–8249. DOI: 10.1039/c5tb01370d.

Konwar, A., Gogoi, A. and Chowdhury, D. (2015) Magnetic alginate–Fe3O4 hydrogel fiber capable of ciprofloxacin hydrochloride adsorption/separation in aqueous solution, *RSC Advances*, 5 (99), pp. 81573–81582. DOI: 10.1039/C5RA16404D.

Landers, R., Hübner, U., Schmelzeisen, R. and Mülhaupt, R. (2002) Rapid prototyping of scaffolds derived from thermoreversible hydrogels and tailored for applications in tissue engineering, *Biomaterials*, 23 (23), pp. 4437–4447. DOI: 10.1016/S0142-9612(02)00139-4.

Lee, H., Ahn, S.-H. and Kim, G. H. (2012) Three-Dimensional Collagen/Alginate Hybrid Scaffolds Functionalized with a Drug Delivery System (DDS) for Bone Tissue Regeneration, *Chemistry of Materials*, 24 (5), pp. 881–891. DOI:10.1021/cm200733s.

Lee, K. Y. and Mooney, D. J. (2012) Alginate: properties and biomedical applications, *Progress in Polymer Science*, 37 (1), pp. 106–126. DOI:10.1016/j.progpolymsci.2011.06.003.

Levenberg, S., Rouwkema, J., Macdonald, M., Garfein, E. S., Kohane, D. S., Darland, D. C., *et al.* (2005) Engineering vascularized skeletal muscle tissue, *Nature Biotechnology*, 23 (7), pp. 879–884. DOI:10.1038/nbt1109.

Li, J., Tang, W., Yang, H., Dong, Z., Huang, J., Li, S., Wang, J., Jin, J. and Ma, J. (2014a) Enhanced-electrocatalytic activity of Ni 1−x Fe x alloy supported on polyethyleneimine functionalized MoS 2 nanosheets for hydrazine oxidation, *RSC Advances*, 4 (4), pp. 1988–1995. DOI:10.1039/C3RA42757A.

Li, X., Cui, R., Sun, L., Aifantis, K. E., Fan, Y., Feng, Q., Cui, F. and Watari, F. (2014b) 3D-Printed Biopolymers for Tissue Engineering Application, *International Journal of Polymer Science*, 2014, pp. e829145. DOI:10.1155/2014/829145.

Li, X., Liu, T., Song, K., Yao, L., Ge, D., Bao, C., Ma, X. and Cui, Z. (2006) Culture of Neural Stem Cells in Calcium Alginate Beads, *Biotechnology Progress*, 22 (6), pp. 1683–1689. DOI:10.1021/bp060185z.

Liu, C., Xia, Z. and Czernuszka, J. T. (2007) Design and development of three-dimensional scaffolds for tissue engineering, *Chemical Engineering Research and Design*, 85 (7), pp. 1051–1064. DOI: 10.1205/cherd06196.

Liu, X. and Ma, P. X. (2004) Polymeric Scaffolds for Bone Tissue Engineering, *Annals of Biomedical Engineering*, 32 (3), pp. 477–486. DOI:10.1023/B:ABME.0000017544.36001.8e.

Mallick, S., Tripathi, S. and Srivastava, P. (2015) Advancement in scaffolds for bone tissue engineering: A review, *IOSR J. Pharm. Biol. Sci*, 10, pp. 37–54. DOI: 10.9790/3008-10143754.

Mandrycky, C., Wang, Z., Kim, K. and Kim, D.-H. (2016) 3D bioprinting for engineering complex tissues, *Biotechnology Advances*, 34 (4), pp. 422–434. DOI:10.1016/j.biotechadv.2015.12.011.

Mehrban, N., Teoh, G. Z. and Birchall, M. A. (2016) 3D bioprinting for tissue engineering: Stem cells in hydrogels, *International Journal of Bioprinting*, 2 (1), pp. 1-14. DOI: 10.18063/IJB.2016.01.006.

Murakami, Y., Sugo, K., Hirano, M. and Okuyama, T. (2011) Surface chemical analysis and chromatographic characterization of polyethylenimine-coated hydroxyapatite with various amount of polyethylenimine, *Talanta*, 85 (3), pp. 1298–1303.

Naebe, M. and Shirvanimoghaddam, K. (2016) Functionally graded materials: A review of fabrication and properties, *Applied Materials Today*, 5, pp. 223–245. DOI:10.1016/j.apmt.2016.10.001.

Pan, T., Song, W., Cao, X. and Wang, Y. (2016) 3D Bioplotting of Gelatin/Alginate Scaffolds for Tissue Engineering: Influence of Crosslinking Degree and Pore Architecture on

Physicochemical Properties, *Journal of Materials Science & Technology*, 32 (9), pp. 889–900. DOI:10.1016/j.jmst.2016.01.007.

Prang, P., Müller, R., Eljaouhari, A., Heckmann, K., Kunz, W., Weber, T., *et al.* (2006) The promotion of oriented axonal regrowth in the injured spinal cord by alginate-based anisotropic capillary hydrogels, *Biomaterials*, 27 (19), pp. 3560–3569. DOI:10.1016/j.biomaterials.2006.01.053.

Qi, Y., Jiang, M., Cui, Y.-L., Zhao, L. and Zhou, X. (2015) Synthesis of quercetin loaded nanoparticles based on alginate for Pb (II) adsorption in aqueous solution, *Nanoscale Research Letters*, 10 (1), pp. 408. DOI: 10.1186/s11671-015-1117-7.

Sarkar, M. R., Augat, P., Shefelbine, S. J., Schorlemmer, S., Huber-Lang, M., Claes, L., Kinzl, L. and Ignatius, A. (2006) Bone formation in a long bone defect model using a platelet-rich plasma-loaded collagen scaffold, *Biomaterials*, 27 (9), pp. 1817–1823. DOI:10.1016/j.biomaterials.2005.10.039.

Shang, W., Liu, Y., Wan, W., Hu, C., Liu, Z., Wong, C. T., Fukuda, T. and Shen, Y. (2017) Hybrid 3D printing and electrodeposition approach for controllable 3D alginate hydrogel formation, *Biofabrication*. DOI:10.1088/1758-5090/aa6ed8.

Shen, J.-N., Yu, C.-C., Zeng, G.-N. and van der Bruggen, B. (2013) Preparation of a Facilitated Transport Membrane Composed of Carboxymethyl Chitosan and Polyethylenimine for CO2/N2 Separation, *International Journal of Molecular Sciences*, 14 (2), pp. 3621–3638. DOI:10.3390/ijms14023621.

Soares, J. P., Santos, J. E., Chierice, G. O. and Cavalheiro, E. T. G. (2004) Thermal behavior of alginic acid and its sodium salt, *Eclética Química*, 29 (2), pp. 57–64. DOI:10.1590/S0100-46702004000200009.

Sun, J. and Tan, H. (2013) Alginate-Based Biomaterials for Regenerative Medicine Applications, *Materials*, 6 (4), pp. 1285–1309. DOI:10.3390/ma6041285.

Suzuki, K., Suzuki, Y., Tanihara, M., Ohnishi, K., Hashimoto, T., Endo, K. and Nishimura, Y. (2000) Reconstruction of rat peripheral nerve gap without sutures using freeze-dried alginate gel, *Journal of Biomedical Materials Research*, 49 (4), pp. 528–533. DOI:10.1002/(SICI)1097-4636(20000315)49:4<528::AID-JBM11>3.0.CO;2-1.

Tabriz, A. G., Mills, C. G., Mullins, J. J., Davies, J. A. and Shu, W. (2017) rapid Fabrication of cell-laden alginate hydrogel 3D structures by Micro Dip-coating, *Frontiers in Bioengineering and Biotechnology*, 5, pp. 1-10. DOI: 10.3389/fbioe.2017.00013.

Tang, D., Tare, R. S., Yang, L.-Y., Williams, D. F., Ou, K.-L. and Oreffo, R. O. C. (2016) Biofabrication of bone tissue: approaches, challenges and translation for bone regeneration, *Biomaterials*, 83, pp. 363–382. DOI:10.1016/j.biomaterials.2016.01.024.

Venkatesan, J., Bhatnagar, I., Manivasagan, P., Kang, K.-H. and Kim, S.-K. (2015) Alginate composites for bone tissue engineering: A review, *International Journal of Biological Macromolecules*, 72, pp. 269–281. DOI:10.1016/j.ijbiomac.2014.07.008.

Wang, F., Liu, P., Nie, T., Wei, H. and Cui, Z. (2012) Characterization of a polyamine microsphere and its adsorption for protein, *International Journal of Molecular Sciences*, 14 (1), pp. 17–29. DOI:10.3390/ijms14010017.

Xia, B., Dong, C., Lu, Y., Rong, M., Lv, Y. and Shi, J. (2011) Preparation and characterization of chemically-crosslinked polyethyleneimine films on hydroxylated surfaces for stable bactericidal coatings, *Thin Solid Films*, 520 (3), pp. 1120–1124. DOI: 10.1016/j.tsf.2011.09.056.

CHAPTER FOUR
BIOCOMPATIBILITY AND BIOMINERALIZATION STUDY OF A NOVEL REINFORCED 3D PRINTED BIOMATERIAL SCAFFOLD

4.1. INTRODUCTION

There is a global clinical need for progressive approaches in bone tissue engineering to repair and regenerate bone defects resulting from trauma or disease. Bone tissue engineering in orthopaedics is aimed at regenerating/restoring/repairing bone defects or critical-sized defects from various pathological conditions (Amini *et al.,* 2012; Bankoff, 2012). The combination of biomaterial scaffolds with host cells or isolated cells and/ or bioactive molecules is the current approach in tissue engineering application. This methodology seeks to restore or enhance the natural processes of tissue development and regeneration. Furthermore, one of the significant aspects of bone tissue engineering is the introduction of osteoblast-like cells and cytokines (such as bone morphogenic proteins) into the biomaterial scaffold to generate *ex vivo* tissue construct for biocompatibility investigation (Karageorgiou and Kaplan, 2005; O'Brien, 2011; Orciani *et al.,* 2017; Rahyussalim *et al.,* 2017; Teixeira *et al.,* 2008). The nature of the interactions that occur at the biomaterial scaffold interface, such as cell proliferation, cell mobility, cell adhesion, and cell spreading is affected by the surface topography and the material type utilized in fabricating the biomaterial scaffold. It is significant to fabricate a controlled microtopographical surface that can be easily reproduced. The surface microtopography, microchemistry, and microtexture are associated with biocompatibility (Teixeira *et al.,* 2007). Cells isolated from human tissue/organs are normally used in investigating biocompatibility and cellular responses and believed to be anchorage dependent. Hence, supporting structures such as biomaterial scaffolds are important to act as a template for the cells to grow and proliferate among others. Therefore, the biomaterial scaffold should have good surface chemistry allowing the conjugation of Ca-P (biomineralization), cell proliferation and attachment. It should not only be biocompatible, but must be porous with interconnectivity allowing the transfer of nutrients amongst other things to take place when necessary (Salgado *et al.,* 2004).

The basic principle in tissue engineering is to combine osteoinduction and osteoconductive substances, biodegradable scaffold, and the matrix to mediate cell growth and proliferation in generating/regenerating tissue/organ (Bankoff, 2012). For safe implantation of biomaterial scaffolds to any living organism such as a human body, it must first undergo quantification/qualitative analyses of various cellular responses such as cell viability, cell proliferation, and cell adhesion investigations *in vitro*. Hence, cell viability needs to be carried

out before evaluating the facilitation of cell adhesion and cell proliferation amongst others in the biomaterial scaffold (Rubin and Rubin, 2006; Wang *et al.,* 2007; Wei *et al.,* 2013).

Osteoblast-like MG63 cells from human osteosarcoma derived from the malignant bone tumour were used in this study. Osteoblast-like MG63 cells were chosen because they have osteoblast features (Declercq *et al.,* 2004) which are necessary for the evaluation of various cellular responses in the novel 3D printed biomaterial scaffold. Sithole *et al.,* (2018) fabricated a novel 3D biomaterial scaffold through *in situ* 3D printing synthetic method using 3D Bioplotter® (EnvisionTEC, GmBH) and performed *in vitro* degradation studies amongst other characterization investigations. Proceeding from that study, this research chapter is aimed at evaluating various cellular responses (cell adhesion, cell viability, and cell proliferation) of the osteoblast-like MG63 cells seeded onto the novel 3D printed biomaterial scaffold. Therefore, the chapter verifies the effectiveness and feasibility of the novel 3D printed biomaterial scaffold's potential to be implanted into the bone defects of a living organism.

Therefore, this research chapter presents the generation of an *ex vivo* tissue construct through the combination of novel 3D printed biomaterial scaffold and osteoblast-like MG63 cells, aiming at critically evaluating the cell viability, cell proliferation and cell adhesion within the novel 3D printed porous biomaterial scaffold. Hence, this study highlighted the seeding of osteoblast-like MG63 cells onto the 3D printed novel biomaterial scaffold and evaluated cells behaviour in relation to the 3D printed biomaterial scaffold. The *in vitro* evaluation characteristic techniques such as light microscopy, scanning electron microscopy (SEM), energy-dispersive X-ray (EDX) analysis and fourier-transform infrared spectroscopy (FT-IR) were used to characterize the 3D printed biomaterial scaffold and methylene blue analysis was also used in this investigation for cell adhesion confirmation.

4.2. MATERIALS AND METHODS

4.2.1 Materials

Osteoblast-like MG63 cells were purchased from PromoLab (Pty) T/A separations and MTS cell Proliferation Colorimetric Assay Kit was purchased from Whitehead Scientific (Pty) Ltd. Fetal bovine serum (FBS; Biochrom, Berlin, Germany), alpha minimum essential medium (α-MEM) (Gibco), DAPI, methylene blue, amphotericin B solution, gentamicin solution, trypsin-EDTA solution, RNAse, triton X-100, silica gel (Si), Hydroxyapatite (HA), Nanoclay (surface

modified containing 05-5wt.% aminopropyl-triethoxysilane, 15-35wt.% octadecylamine), formaldehyde, phosphate buffer saline, vectashield®, glutaraldehyde solution, ethanol, Alexafluor-conjugate (Anti-Actin Antibody, clone C4, Alexa Fluor® 488 conjugated) were purchased from Sigma-Aldrich (Cleveland, OH). Chemicals were used without further purification unless stated.

4.2.2. Determination of the Biomaterials Complexation and Gelation Kinetics

The ElastoSens™ Bio^2 was used to investigate the complexation and gelation kinetics of Alg-PEI/Si, Alg-PEI/HAP, and Alg-PEI/nanoclay composite hydrogel compared to procures Alg/Si, Alg/HAP, Alg/nanoclay, and Alg hydrogels. The ElastoSens™ Bio^2 instrument enables contactless mechanical monitoring of composites hydrogel complexation and gelation. The measurements were made in seconds until a pre-defined time interval was achieved. Briefly, small amounts of the prepared hydrogels were poured in their initial state (using printing needles) into a cylindrical disposal cuvette, having a flexible bottom membrane. A vibration of few micrometres was gently applied to the sample, which triggered a slight perturbation in the sample creating a response signal. A laser probe was used to measure the response signal without any contact. Specialized models were used to process the samples response and the process continued repetitively depending on the number of measurements and time selected by the user.

4.2.3. Preparation of the Novel *in situ* 3D Printed Biomaterial Scaffolds

The 3D printed biomaterial scaffolds were fabricated using sodium alginate (NaAlg) impregnated/reinforced with bioceramics [silica gel (Si), Nanoclay and hydroxyapatite (HAP)] and printed onto PEI solution as previously reported by Sithole *et al.,* (2018). Briefly, AlgPEI/Si, Alg-PEI/HAP and Alg-PEI/Nanoclay 3D printed biomaterial scaffolds were engineered as follows: Ultra-filtrated purified deionized water (Millipore, France) was used in the preparation of the bio-ink, by hydrating sodium alginate (200mg/mL). A prepared bioceramic inorganic [Si or HAP or Nanoclay (200mg/mL)] solution was combined with sodium alginate hydrogel. Separately, poly (ethyleneimine) solution (PEI) was prepared by adding 40mL of PEI into 100mL of ethanol. The 3D porous biomaterial scaffolds were engineered using 3D Bioplotter® (EnvisionTEC, GmBH). To create the desired structure to be printed, the 3D Bioprinter uses a computer-aided design (CAD). Two moduli are contained in the software of STL and the control of the 3D Bioplotter® such as i) the visualMachine software for material parameters and machine control, and ii) the

3DBioplotter® software for STL data importation and structure (e.g. scaffold) fabrication. The biodegradable 3D porous biomaterial scaffolds were printed at a temperature of 37ºC and the 30cc cartridge was used to feed the bio-inks. Plastic needle (nozzle diameter 0.41mm) was used to dispense the bio-inks, under deposition speed of 10.1mm/s and pressure of 0.8Bar into a petri dish containing the solidifying solution of PEI dissolved in ethanol. The layers were deposited at 0 and 90-degree angle per double layer to the underlying layer in PEI solution. Layers were successively printed with the average solidification time per layer noted. The scaffolds were printed using parameters as modified and described in Table 4.1. The bioprinted scaffolds were subsequently washed thrice with ethanol/double deionized water and dried to constant weight at room temperature (25ºC).

Table 4.1: Modified parameters used for the 3D printing of the porous biodegradable scaffolds.

Parameters	**Values**
Temperature	37ºC
Pressure	0.8Bar
Speed	10.1mm.s^{-1}
Layers	15 layer
Platform temperature	20ºC
Pre-flow delay	0.15
Waiting time between layers	30s

4.2.4. Evaluation of the Biomechanical Properties of 3D Printed Biomaterial Scaffolds

Biomechanical properties of the three 3D printed porous biomaterial scaffolds were measured using BioTester 5000. The BioTester 5000 allows for biaxial testing of the 3D printed porous biomaterial scaffolds, this is significant for the evaluation of biomaterials mechanical properties due to their directionally oriented microstructure. Briefly as previously described by Sithole *et al.,* 2018, the 3D printed porous biomaterial scaffold samples were mounted into the BioTester utilizing BioRankers system. Before mounting, the 3D printed porous biomaterial scaffolds were equilibrated by soaking it in Dulbecco's Modified Eagle's Medium (DMEM), supplemented with 10% fetal bovine serum (FBS) and incubated at an atmosphere of 5% CO_2 at 37ºC (pH 7.4) for 24 h to allow equilibration. Sharp BioRankers pierces the most delicate and tough tissue samples or biomaterial scaffolds, to afford constant dispersing site of attachment across the shape of the samples. Following positioning of the samples, a manually-functioning crown press exerted pressure onto the sample.

4.2.5. Preliminary Mechanical Evaluation of the Different 3D Printed Biomaterial Scaffolds

Preliminary mechanical investigation was conducted, and the Bar Chart in Figure 4.1, provides the determined results of the preliminary investigations for Young's modulus of three different impregnated bioceramics inorganic materials (Si, HAP and Nanoclay) into the 3D printed porous biomaterial scaffolds. The Alg-PEI/Si 3D porous biomaterial scaffold, AlgPEI/HAP 3D porous biomaterial scaffold and Alg-PEI/Nanoclay 3D porous biomaterial scaffold were evaluated in order to determine the Young's modulus that's mostly preferable for bone tissue engineering application. Hence, the preferred 3D porous biomaterial scaffold composite was identified and subjected to further characterization. Therefore, the biomaterial scaffold impregnated with silica gel (Si) (Alg-PEI/Si) was identified (depicted in the Bar Chart Figure 4.1) as the preferred potential bone tissue engineering application scaffold, since it showed higher Young's modulus of 60MPa compared to nanoclay with Young's modulus of 30MPa and HAP with Young's modulus of 10MPa. The attained Young's modulus of 60MPa shown an improved alginate hybrid scaffolds strength for bone tissue engineering application which is within acceptable values reported for cancellous bone repair (∼20-500 MPa) (Velasco *et al.,* 2015). This highlighted that the 3D printed porous biomaterial scaffold in its current form possesses mechanical capabilities for certain bone tissue engineering applications (e.g., cancellous bone repair).

Scaffold porosity and pore size do not only have an effect on the cell behaviour and its potential to differentiate, but it also has an effect on the scaffolds mechanical properties (Loh and Choong, 2013). Therefore, the current 3D printed porous biomaterial scaffold has a higher Young's modulus of 60MPa compared to the previously 3D printed porous biomaterial scaffold by Sithole *et al.,* (2018), which was 18MPa. This difference is not just only because of the type of biomaterials used but it also furthered by the pore size of the current scaffold, since it is smaller (210±10µm) compared to the previous 3D printed porous biomaterial scaffold pore size of 360± 20µm. Therefore, it was observed that as the pore size decrease, Young's modulus of the 3D printed porous biomaterial scaffold increase vice versa.

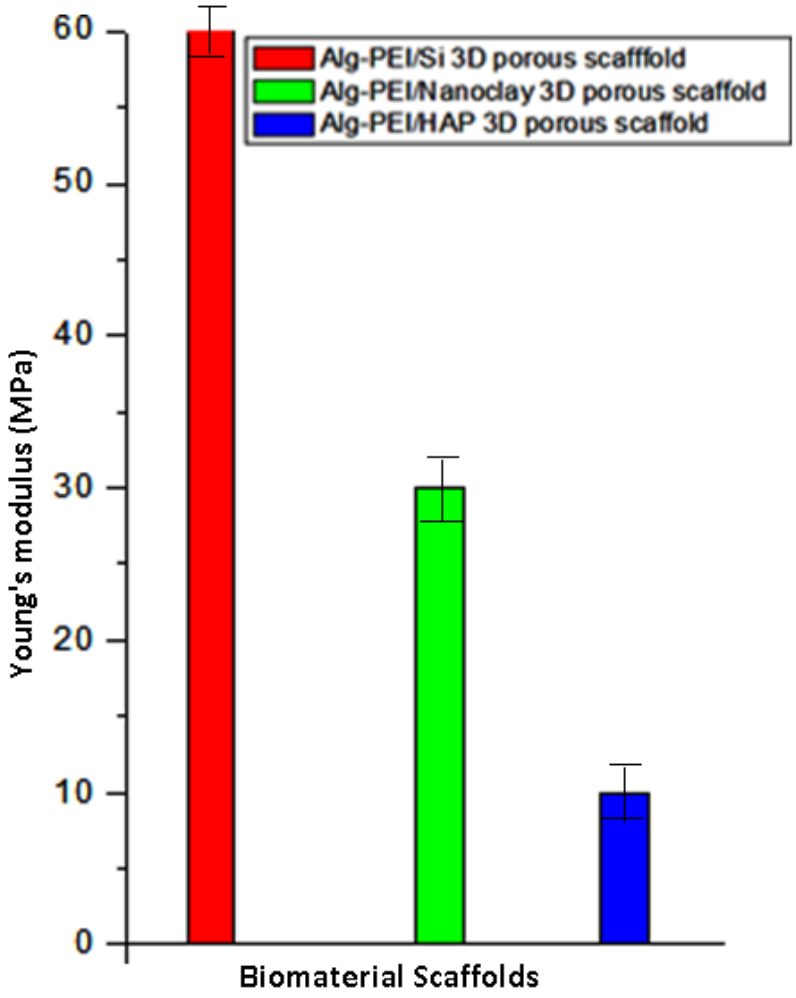


Figure 4.1: Bar Chart depicting Young's modulus of the three 3D printed biomaterial scaffolds.

4.2.6. Morphological Evaluation of the 3D Printed Porous Biomaterial Scaffold

Porosity morphology (pore size and pore interconnectivity) of the 3D printed porous biomaterial scaffold was examined using scanning electron microscopy (SEM) FEI Noval NanoLab SEM (FEI Company, Hillsboro, Oregon, USA). Briefly, gold isotope was used to sputter coat the 3D printed porous biomaterial scaffold samples. Aluminium spud with an EPI coater (SPI Model sputter-coater and control unit, Hester, PA, USA) was utilized to mount the 3D printed porous biomaterial scaffold samples. The coating of the samples took the 60s under constant nitrogen gas conditions, then the printed biomaterial scaffold samples were analyzed using an FEI Nova NanoLab SEM (FEI Company, Hillsboro, Oregon, USA) (Sithole

et al., 2018). An alternative method of calculating porosity is as follows; accordance to (Landers *et al.,* 2002) using Equation 4.1:

$$\boldsymbol{P = \frac{V_{scaffolds}}{V_{cube}} = 1 - \frac{\pi}{4}.\frac{(d)^2}{d_1 d_2}} \qquad \textbf{(Equation 4.1)}$$

Where;

P = scaffold porosity;

d = scaffold fiber diameter;

d_1 = scaffold fiber spacing and d_2 = layer thickness within each different structure (Pan *et al.*, 2016).

4.2.7. Biomineralization Evaluation of the 3D Printed Biomaterial Scaffold

The biomineralization investigation of the 3D printed porous biomaterial scaffold was performed using simulated body fluid (SBF). The analysis employed *in vitro* simulated body fluid (SBF). The immersion solution was prepared by dissolving reagents such as, $NaHCO_3$ (4.2mmol/L), $CaCl_2$ (2.6mmol/L), NaCl (14mmol/L), $MgCl_2.6H_2O$ (1.6mmol/L), Na_2SO_4 (0.5mmol/L), $K_2HPO_4.3H_2O$ (1mmol/L) and KCl (3.0mmol/L) in deionized water. The solution was adjusted to a pH 7.4 using tris (hydroxymethyl) aminomethane ($(CH_2OH)_3CNH_2$) and 1M HCl at 37^{o}C. The samples were immersed in a plastic bottle containing simulated body fluid (SBF) and placed in an orbital shaker (Thermo Forma, USA) (120rpm) at 37^{o}C. After 3 and 7 days of immersion, the samples were taken out of the solution and dried completely for 24 hours (Chen *et al.,* 2009). The dried samples were taken for FTIR and SEM analysis to do the XDE elementary analysis.

4.2.8. The *in vitro* Assessment using Osteoblast-like Cells

Cell viability of the developed novel 3D printed porous biomaterial scaffold was evaluated using MTS assay. The standard culture medium was used as a control medium in this investigation. The MTS assay aimed at evaluating cell viability of the novel 3D printed porous biomaterial scaffold in relation to osteoblast-like cells before implanting the scaffold in a living organism. Therefore, the objective of the MTS assay test was to determine whether the cells are metabolic active (Salgado *et al.,* 2004) on the 3D printed porous biomaterial scaffolds.

4.2.8.1. Cell culturing method for the osteoblast-like cell line

Osteoblast-like MG63 cells were used in this research study, which was derived from a human osteosarcoma. The osteoblast-like MG63 cells were chosen because they express a number of characteristic features of osteoblast and they have been found to be a great candidate for evaluation of cell viability, cell adhesion and cell proliferation in bone tissue engineering. Briefly, osteoblast-like MG63 cells were grown as a monolayer in a prepared cell culturing medium made of alpha minimum essential medium (α-MEM) (Gibco) supplemented with 20% fetal bovine serum (FBS; Biochrom, Berlin, Germany) and, 1mL of amphotericin B solution and 1mL of gentamicin. A 75cm^2 adhesive flask containing 15mL of prepared cell culturing medium was used to culture the osteoblast-like MG63 cells, at 37^{o}C, in a humidified atmosphere, containing 5%CO_2 in the air. The cell culturing medium was changed every second day (Linh *et al.,* 2013; Teixeira *et al.,* 2008).

4.2.8.2. Seeding osteoblast-like cells onto the 3D printed biomaterial scaffold

Novel 3D printed porous biomaterial scaffolds were sterilized prior placing them in 96-well plates (pre-cut 14mg/well scaffold, ca. 1cm^2 surface area). Briefly, as described above, the osteoblast-like MG63 cells were allowed to grow as a monolayer until they reach 60% to 90% confluence. The cells were harvested using trypsin-EDTA solution in accordance to the cells supplier's protocol. Then cells were centrifuged and re-suspended in a prepared cell culture medium and counted using haemocytometer. Aliquots (100µL) containing 3x10^5 cells were seeded on top of the novel printed scaffold which was prior placed in 96-well plates. The culture medium of 100µL was added in each well after two hours of seeding and then incubated in a humidified atmosphere at 37^{o}C, containing 5%CO_2, with medium changed every second day.

4.2.8.3. Cell viability assay assessment for the novel 3D printed biomaterial scaffold

The widely used cell viability testing method, the MTT assay, was substituted with an alternative MTS assay (Cell Titer 96 Ag Non-Radioactive Cell Assay, Promega) in this research study, to evaluate the cultured osteoblast-like MG63 cells on the 3D printed porous scaffold. The reason for not using the MTT cytotoxicity assay in this research study was

because the reaction product of MTT assay is water-insoluble formazan, which strongly attach to the surface of the 3D printed porous scaffolds and make it impossible to obtain a correct measurement. Hence, the MTS cytotoxicity assay was used because the formed reaction product is soluble in the culture medium, which makes it possible to get precise measurements. Briefly, in the different cell-scaffold cultured time interval, the medium was removed and replace with 10%v/v of MTS solution in culture medium to each well and incubated for 3 hours. All absorbance were measured at the wavelength of 490nm in a 96 multilabel reader Victor^{TM} X3 and the backgrounds of the well plates were measured at 690nm. The results were presented as percentage relative cell viability (mean±standard deviation) (Salgado *et al.,* 2004). Percentage relative cell viability was calculated using Equation 4.2 below:

$$\%\mathbf{Relative\ cell\ viability} = \frac{\mathbf{OD(sample)} - \mathbf{OD(blank)}}{\mathbf{OD(control)} - \mathbf{OD(blank)}}\ \mathbf{X\ 100} \qquad (\mathbf{Equation\ 4.2})$$

4.2.9. Osteoblast-like Cells Behaviour onto the 3D Printed Biomaterial Scaffold

Proliferation and adhesion of osteoblast-like MG63 cells that are seeded onto the novel 3D printed porous biomaterial scaffold were assessed using techniques such as light microscopy, methylene blue staining, scanning electron microscopy (SEM).

4.2.9.1. Visualization of cell adhesion onto the 3D printed biomaterial scaffold

After culturing for three or seven days, cell adhesion onto the 3D printed porous biomaterial scaffold was evaluated using light microscopy and scanning electron microscope (SEM). Briefly, the 3D printed porous biomaterial scaffolds were cut into portions of equal size in order to determine if the cells were attached in the scaffolds. Phosphate buffer saline (PBS) solution was used to wash the scaffold and then fixed in 1.5%v/v glutaraldehyde in PBS for 30minutes. The 3D printed porous biomaterial scaffolds were dehydrated by sequentially immersed to 50, 60, 70, 90 and 100%v/v ethanol series (15 minutes each) and dried in air. Finally, the samples were sputter coated with gold and analysed using SEM (Salgado *et al.,* 2004; Teixeira *et al.,* 2008; Yoo *et al.,* 2016).

4.2.9.2. Osteoblast-like cell staining using methylene blue

The 3D printed porous biomaterial scaffolds were cultured for three or seven days and removed from the culture medium to be washed with phosphate buffer saline (PBS) solution.

The 3D printed porous biomaterial scaffolds samples were then fixed with 1.5%v/v glutaraldehyde in PBS for 30 minutes. The 3D printed biomaterial scaffolds samples were washed with PBS twice and then immersed in methylene blue solution for five minutes. Finally, the samples were washed with PBS, the cell adhesion and cell proliferations were evaluated using light microscopy (Teixeira *et al.,* 2008).

4.3. RESULTS AND DISCUSSION

4.3.1. Complexation and Gelation Kinetics Evaluation of the Bio-Inks

Biomaterials inks (bio-inks) complexation and gelation kinetics are significant parameters to be investigation prior 3D bioprinting application. This is to have an idea of the approximate estimated time for the next layer to be printed and the confirmation of ionic interaction between the two ionic biomaterials inks (bio-inks). The complexation modulus and gelation time of the biomaterials inks used for 3D printing scaffolds for bone tissue application were evaluated using ElastoSens^{TM} Bio^{2}. The three biomaterial hydrogels samples of the same concentrations were prepared and poured in the sample holder to initiate complexation and gelation characterization process. The measurements were conducted at the constant temperature 37^{o}C over the entire period of investigation. Figure 4.2, depicture the three figures of the gelation kinetics (e.g. the speed of hardening and complexation) of a) AlgPEI/Si, b) Alg-PEI/HAP and c) Alg-PEI/Nanoclay. The result shows that all procured hydrogels (Alg, Alg/Si, Alg/HAP and Alg/Nanoclay) never changed their mechanical properties (includes, gelation, mechanical properties etc.). But there is an ionic interaction during the formation of complexes such as a) Alg-PEI/Si, b) Alg-PEI/HAP and c) AlgPEI/Nanoclay, evident by the increased shear complex modulus (Pa) leading to increase gelation time. These are good properties for the appropriate gelation time necessary for 3D bioprinting of the three biomaterial scaffolds.

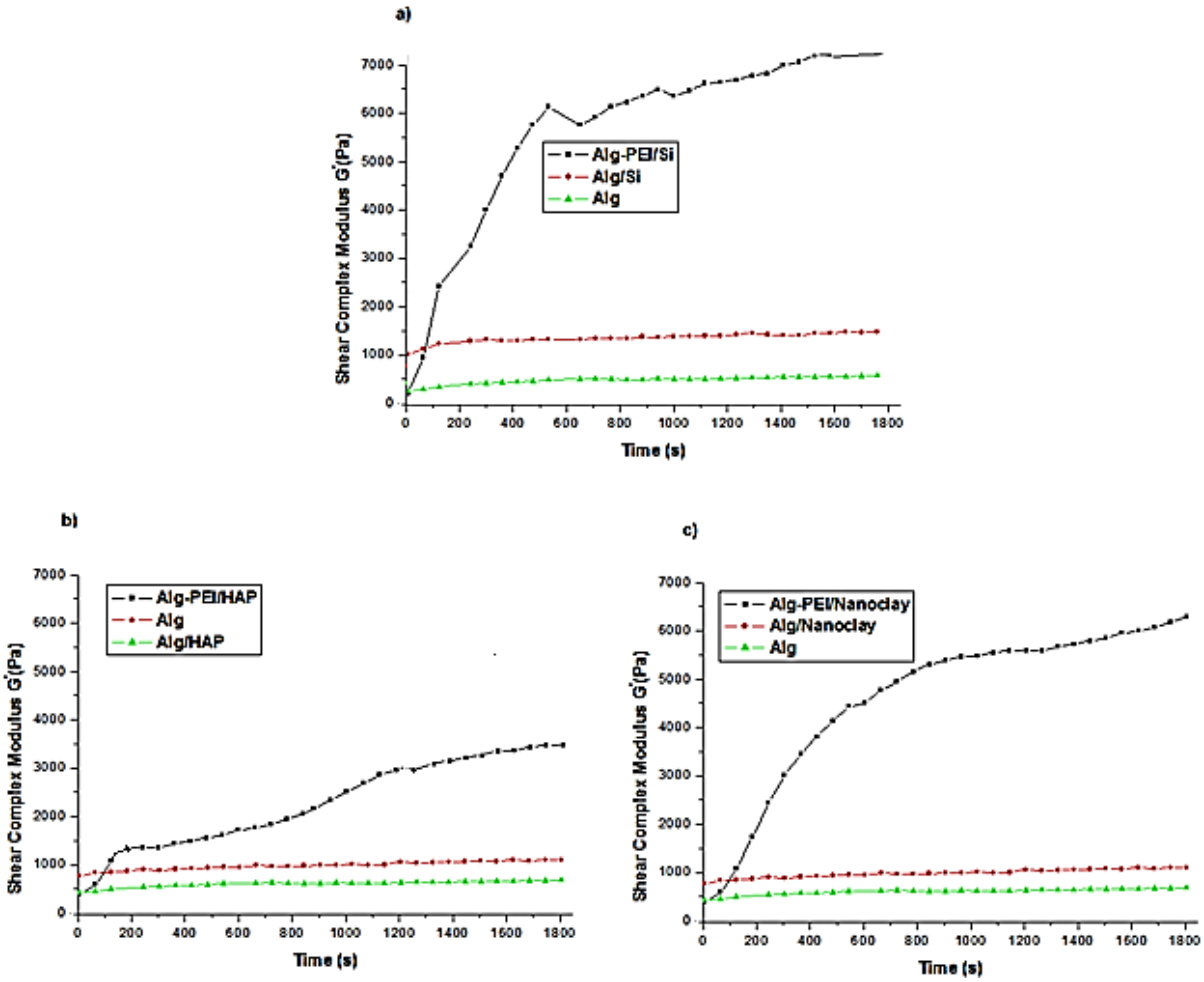


Figure 4.2: Complexation and gelation kinetics of the three biomaterial scaffolds, a) Alg-PEI/Si, b) Alg-PEI/HAP and c) Alg-PEI/Nanoclay.

4.3.2. Preliminary Mechanical Evaluation of the 3D Printed Biomaterial Scaffolds

Three-dimensional (3D) porous biomaterial scaffolds were successfully printed and impregnated with three different bioceramics inorganic materials (such as Si, HAP and Nanoclay) in order to investigate the appropriate complementary bioceramic inorganic component that will led to an acceptable Young's modulus for bone therapy. The Bar Chart in Figure 4.1 (section 4.2.5.), shown the resultant mechanical properties from the BioTester 5000 for the three impregnated inorganic components in our investigation. Hence, it was then found that the Young's modulus of Alg-PEI/Si is 60MPa and for Alg-PEI/HAP is 10MPa, whiles the Young's modulus for Alg-PEI/Nanoclay is 30MPa. The Alg-PEI/Si 3D porous biomaterial scaffold was the preferred scaffold, because the attained Young's modulus was higher than the other impregnated inorganic materials in the 3D printed porous biomaterial scaffolds. The Young's modulus of the preferred scaffold (Alg-PEI/Si) is within values reported for bone tissue regeneration (~20-500 MPa) such as cancellous bone repair. These

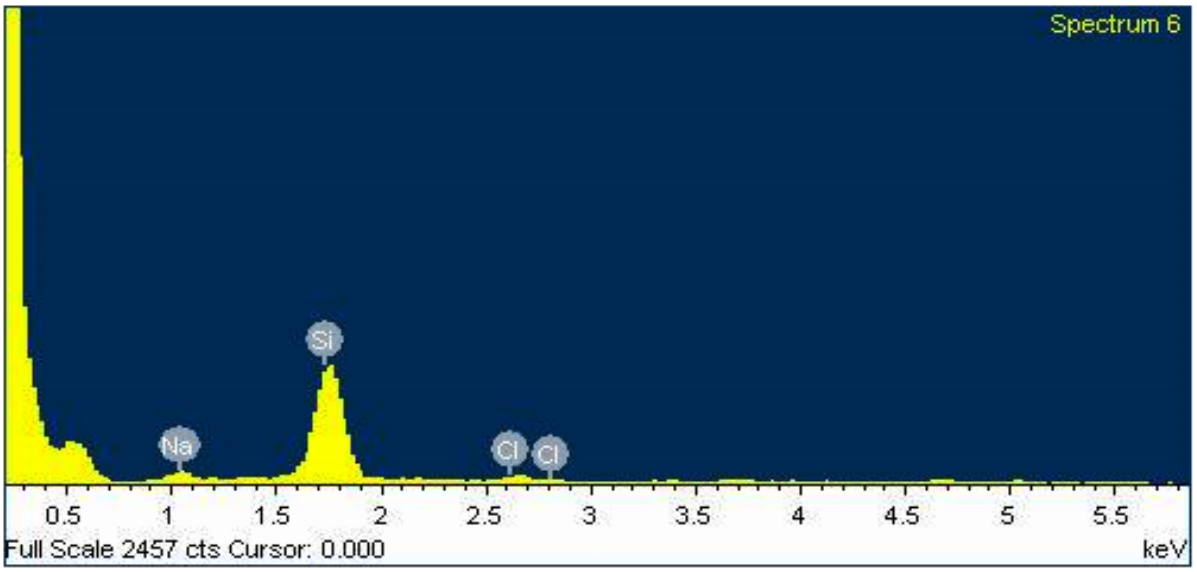
results highlighted that the 3D printed porous biomaterial scaffold in its current form possesses the mechanical capabilities for bone tissue engineering application. Therefore, due to the acceptable range of the Young's modulus, Alg-PEI/Si 3D porous scaffold was considered for further evaluation and cellular investigation.

4.3.3. Surface Biomineralization Evaluation of the 3D Printed Biomaterial Scaffold

There are many essential trace elements present in biological bone, that's includes, sodium (Na), chlorine (Cl), potassium (K), silicon (Si), calcium (Ca) etc., which play a significant role in bone growth or can have an effect on bone tissue metabolism. For instance, studies have revealed that silicon ions can induce angiogenesis and osteogenesis (Zhang *et al.,* 2018). The surface biomineralization analysis of the 3D printed porous biomaterial scaffold was evaluated using EDX and FT-IR characterization techniques after immersion in SBF (pH 7.4; 37^{o}C) for 7 days. The investigation shows that the 3D printed biomaterial scaffolds possess exceptional biomineralization abilities when immersed in SBF (Figure 4.3 and Figure 4.4). Figure 4.3, depictures a pictorial of the 3D printed biomaterial scaffold before immersed (elements; Cl, Na and Si) in SBF (Figure 4.3a) and the 3D printed biomaterial scaffold after immersed in SBF (Figure 4.3b). Hence, Figure 4.3b shown the EDX of the biomineralized scaffold containing elements such as Cl, Ca, Na, Si and P peaks which are essential for bone regeneration/healing while Figure 4.3a shown a control scaffold with only Cl, Na and Si elements.

Additionally, the FTIR, in Figure 4.4b, showed the gradual disappearance or gradual intensity decreasing from certain spectrum absorption of the scaffold after immersion in SBF (pH 7.4, 37^{o}C) compared to the control scaffold (Figure 4.4a) due to the interaction of additional ions (such as Ca and P) that hide certain functional groups. Despite, the visually noticeable changes in the two spectra, Figure 4.4 (spectrum b) had shown a characteristic band that may in part contribute to the biomineralization of the scaffold. Hence, the vibrational bands at 1590cm^{-1}, 1407cm^{-1} are partially assigned to CO_2^{3-} and furthermore, a vibration band observed at 1028cm^{-1} and 785cm^{-1} are in part attributing to PO_4^{3-} groups. These support that there may be a gradual precipitation of calcium phosphate layer on the surface of the scaffolds indicative of biomineralization of our scaffold. Hence, the EDX and FTIR analysis further confirmed the exceptional biominerals on the surface of the 3D printed biomaterial scaffold that is excellent for bone tissue engineering applications.

a)



b)

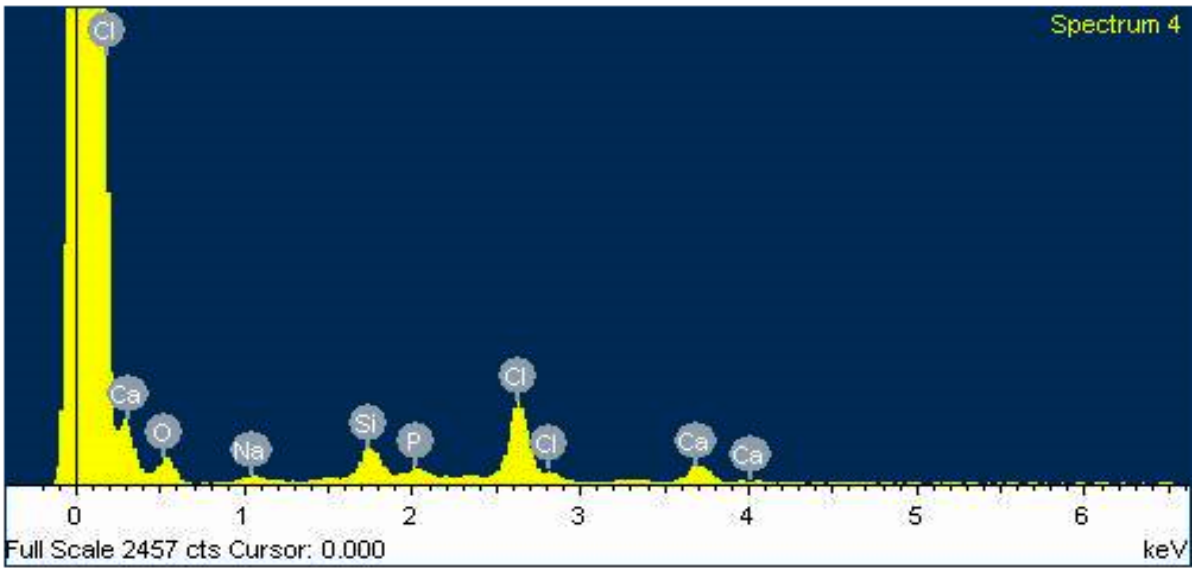


Figure 4.3: The EDX surface elements analysis of a) the scaffolds before immersion and b) scaffold after immerse in SBF (pH 7.4, 37ºC).

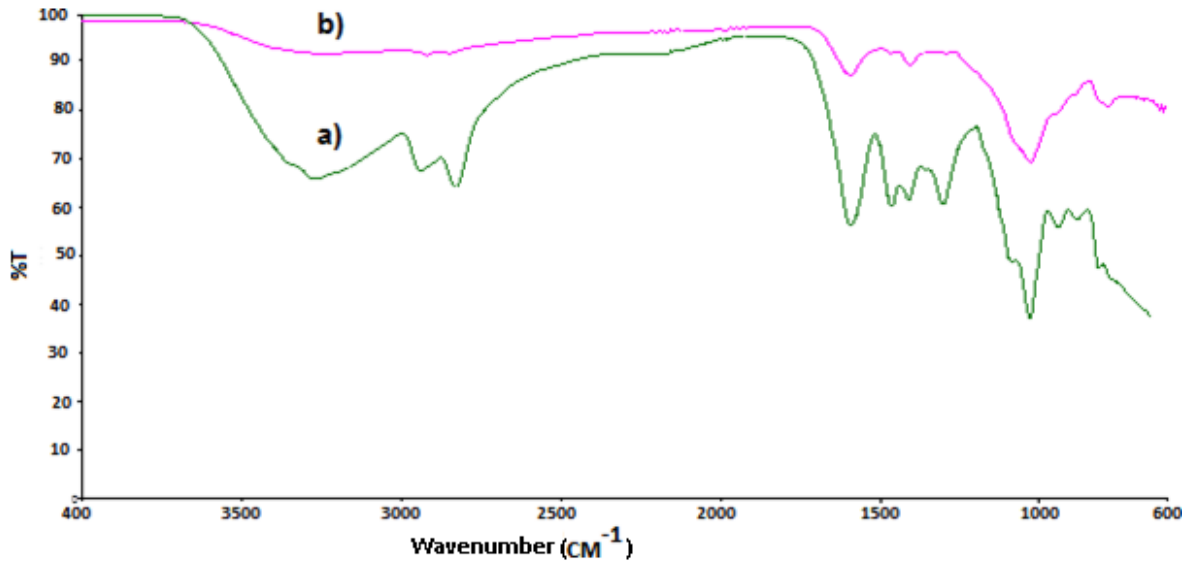


Figure 4.4: The FTIR spectra of a) scaffold before immersion as a control and b) scaffold after immerse in SBF (pH 7.4, 37°C).

4.3.4. Evaluation of the Scaffold Pore Size, Pore Interconnectivity and Morphology

The advantage of using the 3D printer as a 3D porous biomaterial scaffold fabricating tool is due to its potential to control scaffold's pore size amongst others. The pore size of the current fabricated 3D porous biomaterial scaffold was found to be 210µm, as observed in Figure 4.5 (a and b), which in general fall in an acceptable range of 50-1000µm (Li *et al.,* 2014) pore size for bone tissue engineering application. Figure 4.5 (c and d), depicted the cross-section part of the novel 3D printed porous biomaterial scaffold; highlighting the pore interconnectivity of the scaffold, for the transportation of nutrients and minerals amongst others. Pore interconnectivity within the 3D printed porous biomaterial scaffold is of a great significant parameter, measuring or influencing cell seeding, cell adhesion, cell migration and tissue ingrowth necessary for promoting tissue regeneration in three dimensions.

Figure 4.5, also depicted the surface roughness of the novel 3D printed porous biomaterial scaffold. The scaffolds surface roughness is also one of the significant facts or parameter that influences cell behaviour and cell adhesion. The surface roughness of materials modulates the biological response of the tissues that are in contact with it. It also directly influence *in vitro*, as well as *in vivo* cellular morphology, proliferation and phenotype expression (Chang and Wang, 2011). Literature has been reported that cells that grow on rough surfaces were stimulated towards differentiation, shown by their gene expression in comparison with cells growing on a smooth surface (Guptai *et al.,* 2015; Hatano *et al.,* 1999).

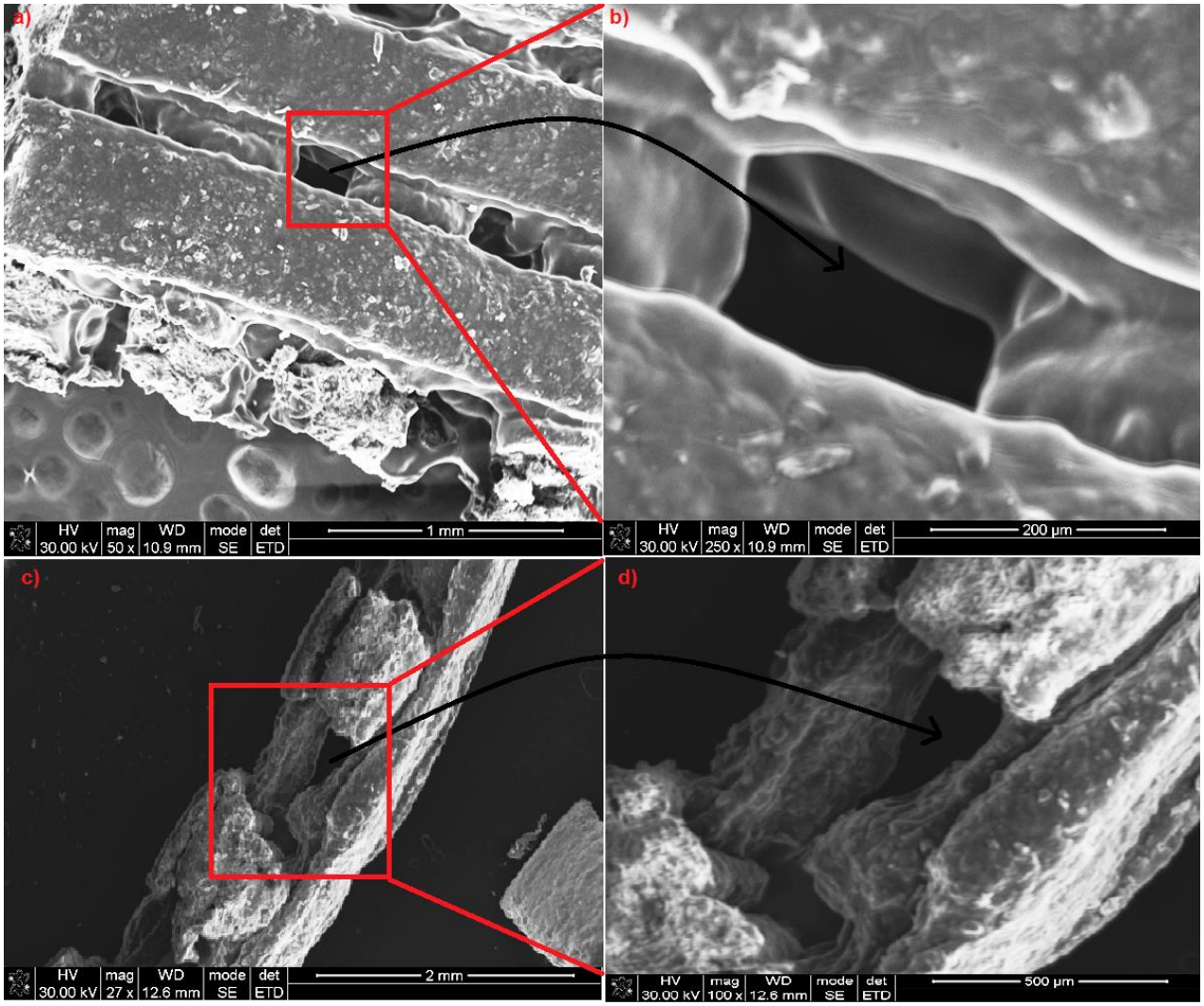


Figure 4.5: Scanning electron microscopy (SEM) pictures of the 3D printed porous scaffold (Alg-PEI/Si porous scaffold).

4.3.5. Evaluation of Cells Growth and Confluence before Seeding the Cells on the Scaffolds

Osteoblast-like MG63 cells were cultured successfully as depicted in Figure 4.6 in this research study. The initial culturing stage (day 0) of osteoblast-like MG63 cells is shown in Figure 4.6a, where the osteoblast-like MG63 cells appeared to be having a round-like shape. Figure 4.6b, depicted day 2 of the osteoblast-like MG63 cells growth, it is observed that the cells changed from their round-like shape and adapted a flat-like shape as they differentiate. The osteoblast-like MG63 cells were allowed to differentiate until they reached approximately 60 to 90% confluences as depicted in Figure 4.6c. Furthermore, cells were subcultured and stored (-80^{o}C) for future use and also cell seeding of scaffolds were conducted.

Proceeding from cells subculture, the osteoblast-like MG63 cells were successfully seeded onto the novel 3D printed porous biomaterial scaffolds after reaching approximately 60 to 90% confluence in day 3 or 7 (Figure 4.6c). Then cell-scaffold investigations were carried out; such as cell viability, cell proliferation, and cell adhesion.

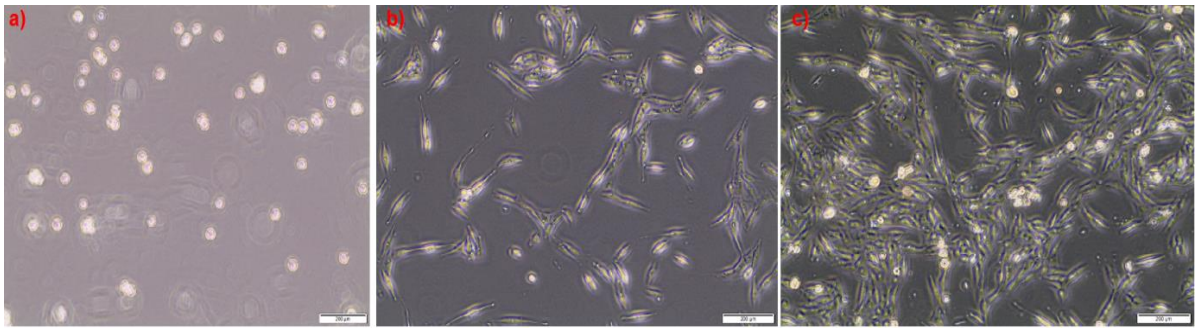


Figure 4.6: Assessment of osteoblast-like MG63 cells differentiation a) day zero, b) day 2 and c) day 3.

4.3.6. Cell Viability and Cell Proliferation Evaluation on the Printed Scaffold

The novel 3D printed porous biomaterial scaffold's cell viability was assessed using MTS cytotoxicity assay and the results are depicted in Figure 4.7. From the obtained analysed results, it was observed that the novel 3D printed porous biomaterial scaffolds were biocompatible in relation to osteoblast-like MG63 cells. Hence, Figure 4.7, is the investigation of the osteoblast-like MG63 cells on the 3D printed porous biomaterial scaffolds using MTS assay, it revealed that the growth rate of the osteoblast-like MG63 cells in the two groups (the control and cell-scaffolds) was not significantly different ($p>0.05$). Therefore, this result validated the biocompatibility of the 3D printed porous biomaterial scaffold, showing that the osteoblast-like MG63 cells are viable in the printed biomaterial scaffold over a period of seven days. It was also observed in both groups (control and cell-scaffolds) that in each day the cells are increasing in numbers compared to the previous days. This reveals/confirmed that the cells proliferate within the scaffold and differentiate over time.

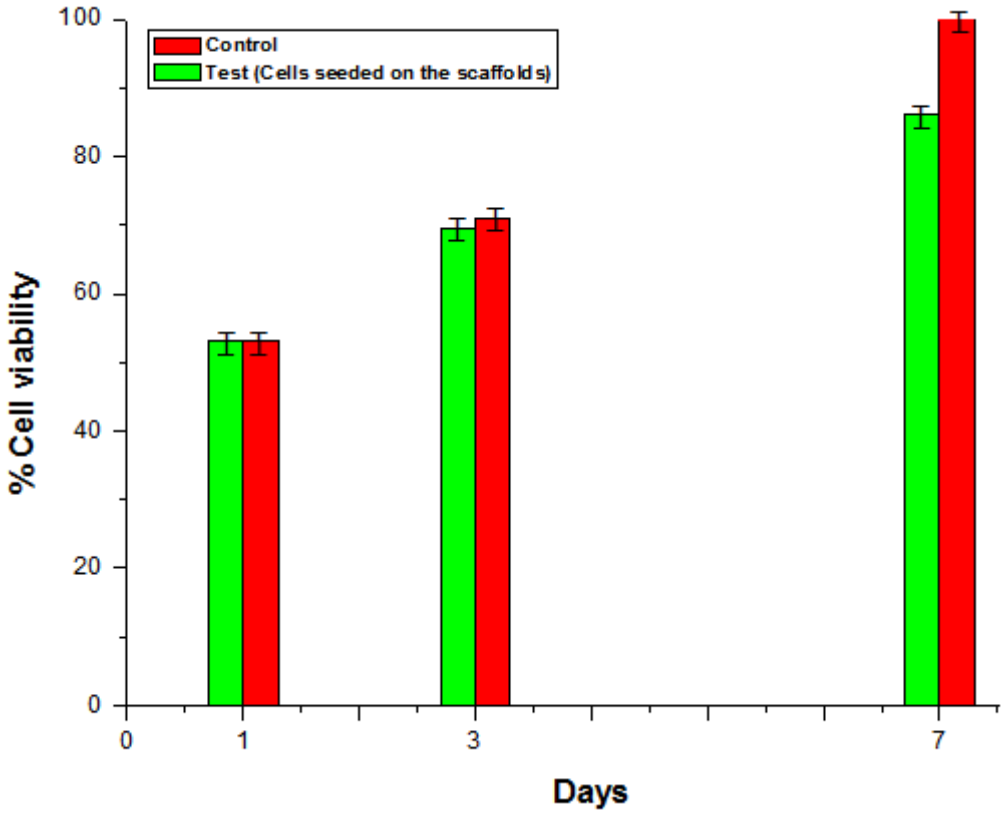


Figure 4.7: Cell viability performed on the 3D cell-scaffold within seven days

4.3.7. Evaluation of Cell Adhesion and Cells Confluence on the 3D Printed Porous Scaffold

Osteoblast-like MG63 cells were cultured on the 3D printed porous biomaterial scaffold for seven days. The 3D printed porous biomaterial scaffold surface was imaged using light microscopy to determine cell adhesion, cell confluence and cell proliferation on the 3D printed porous biomaterial scaffold, results are depicted in Figure 4.8.

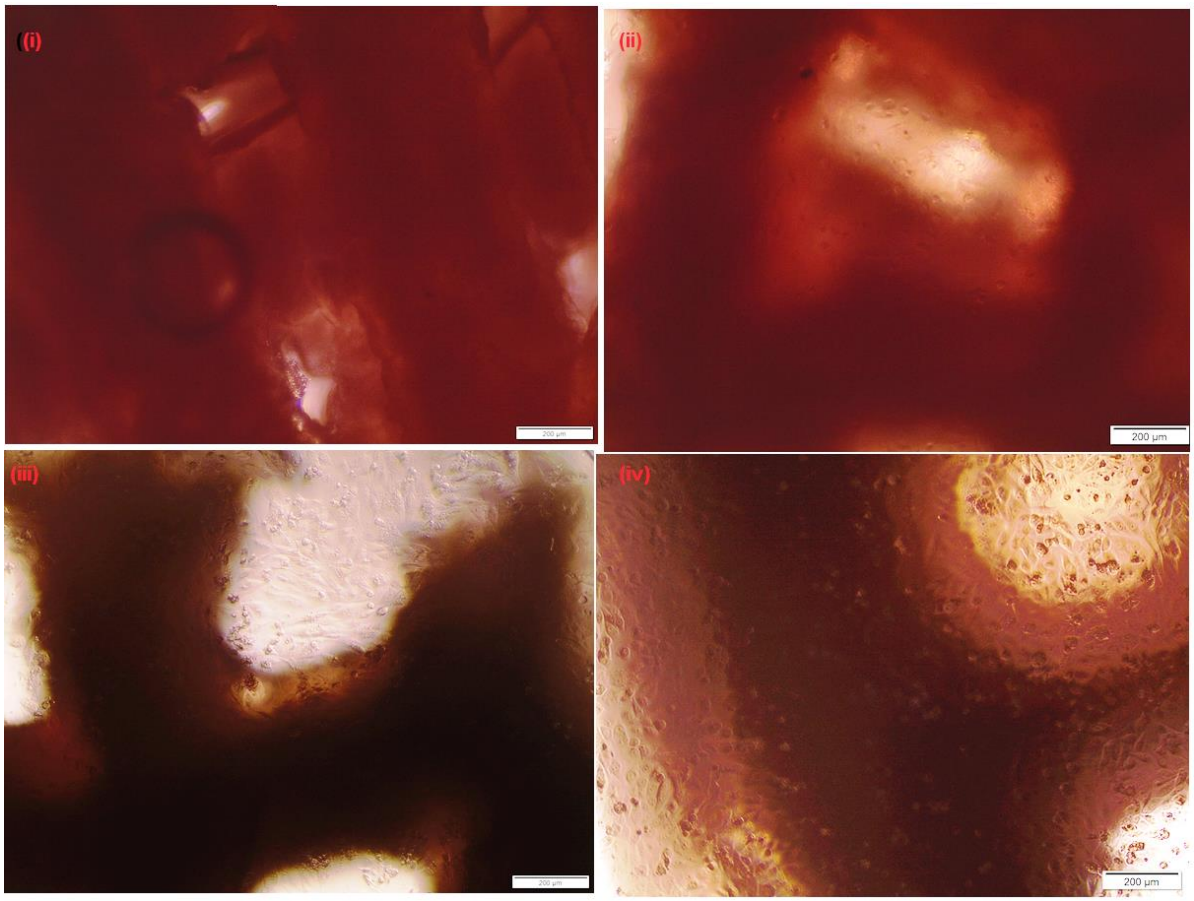


Figure 4.8: Light microscopy images of the cell-scaffolds (Alg-PEI/Si scaffolds) at different time intervals

Figure 4.8(i), depicted day zero; this is the 3D printed porous biomaterial scaffold without osteoblast-like MG63 cells. Figure 4.8(ii), depicted day 1 (24 hours) of the 3D printed porous biomaterial scaffold seeded with osteoblast-like MG63 cells and it appeared to show 5-10% confluence of osteoblast-like MG63 cells on the 3D printed porous biomaterial scaffold surface compared with the surface of the 3D printed porous biomaterial scaffold in day zero (Figure 4.8(i)). Figure 4.8(iii), depicted day 3 of the 3D printed porous biomaterial scaffold seeded with osteoblast-like MG63 cells and it appeared to show 60-70% confluence of osteoblast-like MG63 cells on the 3D printed porous biomaterial scaffold, while Figure 4.8(iv), which depicted day 7 shown approximately 90-100% confluence with near complete surface coverage of the 3D printed porous biomaterial scaffold.

Complementing these results, it was also observed that after day one, cells had adhered and grown onto the 3D printed porous biomaterial scaffold (Figure 4.8(ii)). Figure 4.8(iii) shows the osteoblast-like MG63 cells' starting to form colonies in day 3, and it was also observed that the colonies were larger and denser in day 7 (Figure 4.8(iv)) confirming cell growth, proliferation, and differentiation onto the 3D printed porous biomaterial scaffold.

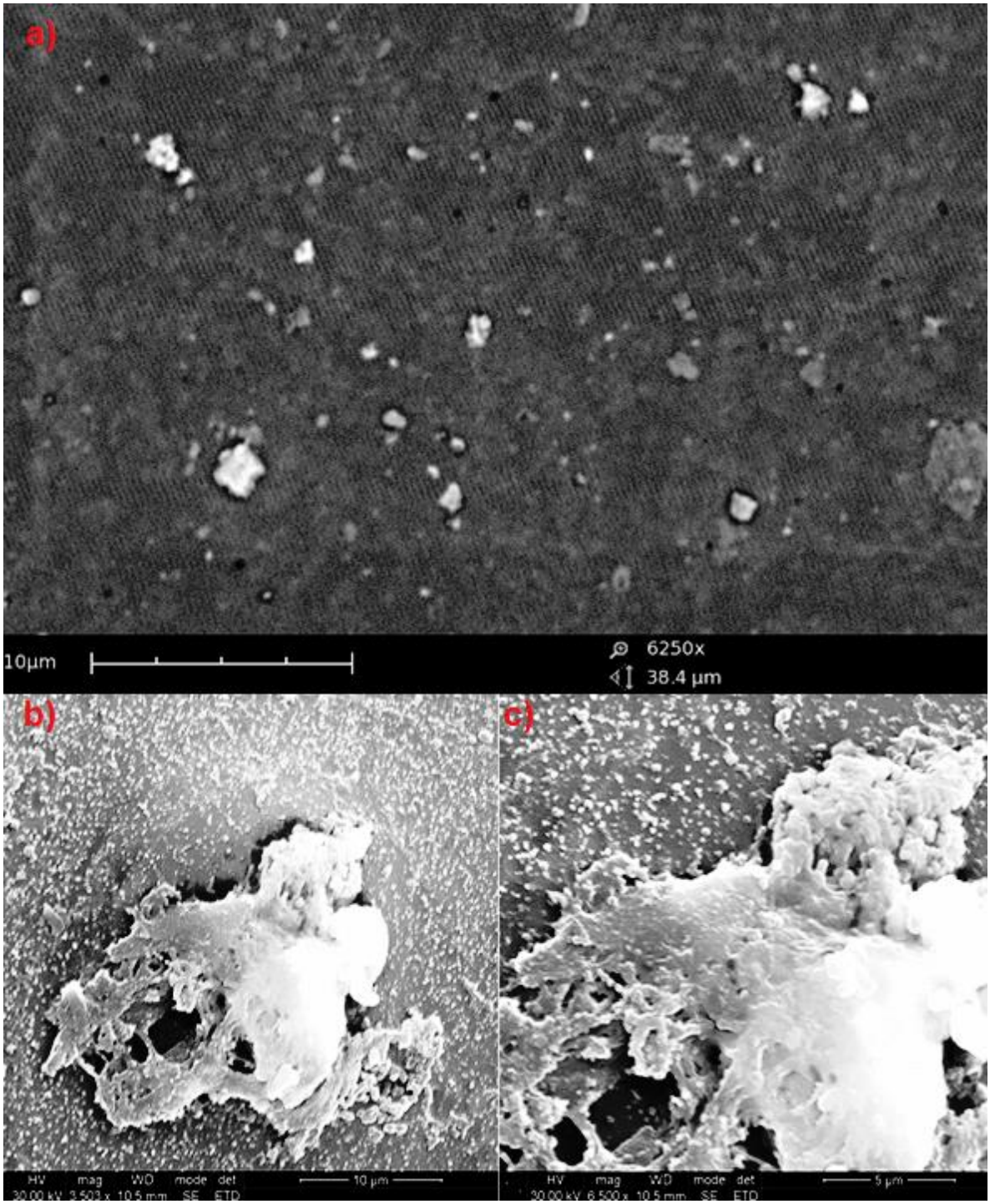


Figure 4.9: SEM images of osteoblast-like MG63 cells adhered to the 3D printed biomaterial scaffold at day seven.

Furthermore, supporting the above results, a scanning electron microscopic (SEM) image, Figure 4.9, was used to confirm cell attachment/cell adhesion onto the 3D printed porous biomaterial scaffold. However, observing cell adhesion/cell attachment is a complex process which is affected by a number of aspects such as materials surface properties, environmental factors and cell behaviour (Lee *et al.,* 2004). One problem that was

encountered during sample preparation is the issue of marking the samples. Hence, during sample preparation, it was observed that a sample marking is difficult to achieve. This lead to difficulties in identifying the cells seeded on the scaffold. Complications in determining the correct side to perform the SEM analysis where raised, but through trial and error, the cells were identified as observed in Figure 4.9. The registered SEM images on the 3D printed porous biomaterial scaffolds seeded with osteoblast-like MG63 cells and the 3D printed porous biomaterial scaffold without cells (control) are depicted in Figure 4.9. Where Figure 4.9a, depicted 3D printed porous biomaterial scaffold without cells (Control) subjected to similar conditions as the 3D printed porous biomaterial scaffold seeded with the osteoblast-like cells (Figure 4.9b and c). Hence, Figure 4.9b showed cell adhesion or cells attached on the surface of the 3D printed porous biomaterial scaffold compared to the control scaffold (Figure 4.9a). Therefore, cells adhesion on the rough surface could be highly advantageous for the development of *ex vivo* construct, since rough surface scaffold help cells to differentiate better.

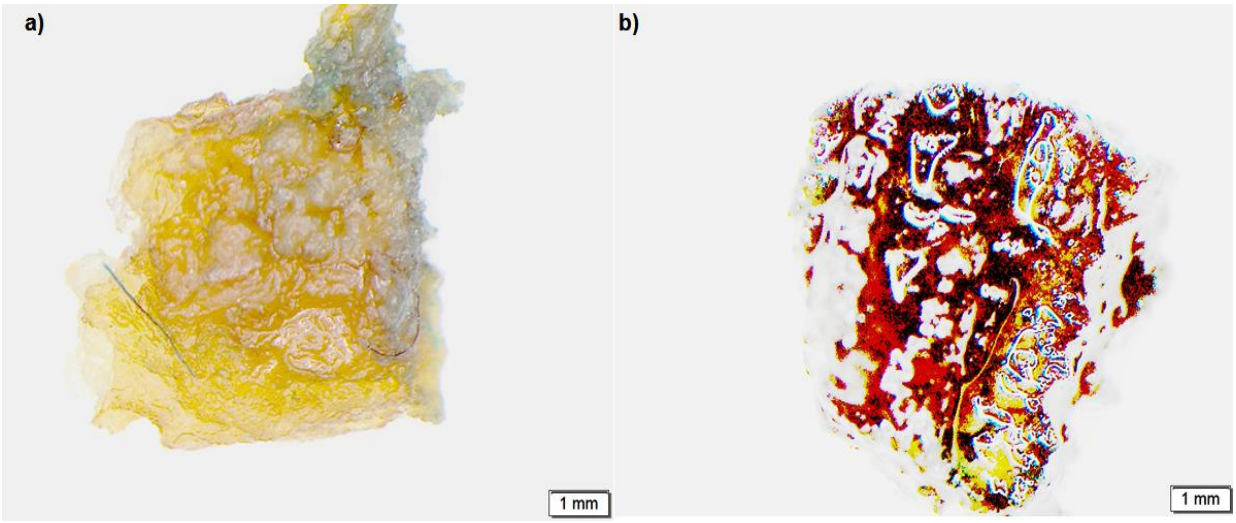


Figure 4.10: Images from light microscopy, a) the scaffold without cells (control) and b) the scaffold with cells both treated with methylene blue

Light microscopy was used to confirm cell proliferation, cell distribution along the surface and inner pores of the 3D printed porous biomaterial scaffold treated with methylene blue. This approach solves the need for marking the sample side to the scaffolds in order to identify osteoblast-like cells. With the Olympus software, it was possible to edit the images and observe the more detailed distribution of cells along the scaffold surface. The nuclei appeared stained red and the matric appeared yellowish allowing a more clearly accurate observation. Figure 10b represents day 7 of the scaffold seeded with cells corroborating the previous data presentation, showing cells spreading along the scaffold, while Figure 10a

represent the scaffold without cells (the control) subjected to similar condition as the scaffold seeded with the cells.

4.4. CONCLUDING REMARKS

Biocompatibility investigation for the 3D printed porous biomaterial scaffold is of great necessity in tissue engineering application. In our research, it was validated that the fabricated novel 3D printed porous biomaterial scaffold is biocompatible while using osteoblast-like MG63 cells. This study also proved that the fabricated novel 3D porous biomaterial scaffold gives positive results or shown great potential in their mechanical strength (e.g.bone tissue application), cell attachment, cell proliferation and biominaralization. Hence, these findings suggest that the current state of this novel 3D printed porous biomaterial scaffold have great potential in bone tissue engineering application and can be safely implanted in a living organism.

4.5. REFERENCES

Amini, A. R., Laurencin, C. T. and Nukavarapu, S. P. (2012) Bone Tissue Engineering: Recent Advances and Challenges, *Critical Reviews in Biomedical Engineering*, 40 (5), pp. 363–408. DOI: 10.1615/CritRevBiomedEng.v40.i5.10.

Gupta, A., Balani, K. and Mahoto, N. (2015) *Biosurfaces: A Materials Science and Engineering Perspective*. John Wiley & Sons, pp 170 – 200. DOI: 10.1002/9781118950623.ch6.

Bankoff, A. D. P. (2012) Biomechanical Characteristics of the Bone. DOI:10.5772/19690.

Chang, H.-I. and Wang, Y. (2011) Cell Responses to Surface and Architecture of Tissue Engineering Scaffolds. DOI:10.5772/21983.

Chen, J. D., Wang, Y. and Chen, X. (2009) In Situ Fabrication of Nano-hydroxyapatite in a Macroporous Chitosan Scaffold for Tissue Engineering, *Journal of Biomaterials Science, Polymer Edition*, 20 (11), pp. 1555–1565. DOI:10.1163/092050609X12464345036768.

Declercq, H., Van den Vreken, N., De Maeyer, E., Verbeeck, R., Schacht, E., De Ridder, L. and Cornelissen, M. (2004) Isolation, proliferation and differentiation of osteoblastic cells to study cell/biomaterial interactions: comparison of different isolation techniques and source, *Biomaterials*, 25 (5), pp. 757–768. DOI: 10.1016/S0142-9612(03)00580-5.

Hatano, K., Inoue, H., Kojo, T., Matsunaga, T., Tsujisawa, T., Uchiyama, C. and Uchida, Y. (1999) Effect of surface roughness on proliferation and alkaline phosphatase

expression of rat calvarial cells cultured on polystyrene, *Bone*, 25 (4), pp. 439–445. DOI:10.1016/S8756-3282(99)00192-1.

Karageorgiou, V. and Kaplan, D. (2005) Porosity of 3D biomaterial scaffolds and osteogenesis, *Biomaterials*, 26 (27), pp. 5474–5491. DOI:10.1016/j.biomaterials.2005.02.002.

Landers, R., Hübner, U., Schmelzeisen, R. and Mülhaupt, R. (2002) Rapid prototyping of scaffolds derived from thermoreversible hydrogels and tailored for applications in tissue engineering, *Biomaterials*, 23 (23), pp. 4437–4447. DOI:10.1016/S0142-9612(02)00139-4.

Lee, S. J., Choi, J. S., Park, K. S., Khang, G., Lee, Y. M. and Lee, H. B. (2004) Response of MG63 osteoblast-like cells onto polycarbonate membrane surfaces with different micropore sizes, *Biomaterials*, 25 (19), pp. 4699–4707. DOI:10.1016/j.biomaterials.2003.11.034.

Li, X., Cui, R., Sun, L., Aifantis, K. E., Fan, Y., Feng, Q., Cui, F. and Watari, F. (2014) 3D-Printed Biopolymers for Tissue Engineering Application, *International Journal of Polymer Science*, 2014, pp. 1-13. DOI:10.1155/2014/829145.

Linh, N. T. B., Min, Y. K. and Lee, B.-T. (2013) Fabrication and in vitro evaluations with osteoblast-like MG-63 cells of porous hyaluronic acid-gelatin blend scaffold for bone tissue engineering applications, *Journal of Materials Science*, 48 (12), pp. 4233–4242. DOI:10.1007/s10853-013-7236-6.

Loh, Q. L. and Choong, C. (2013) Three-Dimensional Scaffolds for Tissue Engineering Applications: Role of Porosity and Pore Size, *Tissue Engineering Part B: Reviews*, 19 (6), pp. 485–502. DOI:10.1089/ten.teb.2012.0437.

O'Brien, F. J. (2011) Biomaterials & scaffolds for tissue engineering, *Materials Today*, 14 (3), pp. 88–95. DOI:10.1016/S1369-7021(11)70058-X.

Orciani, M., Fini, M., Di Primio, R. and Mattioli-Belmonte, M. (2017) Biofabrication and Bone Tissue Regeneration: Cell Source, Approaches, and Challenges, *Frontiers in Bioengineering and Biotechnology*, 5. DOI:10.3389/fbioe.2017.00017.

Pan, T., Song, W., Cao, X. and Wang, Y. (2016) 3D Bioplotting of Gelatin/Alginate Scaffolds for Tissue Engineering: Influence of Crosslinking Degree and Pore Architecture on Physicochemical Properties, *Journal of Materials Science & Technology*, 32 (9), pp. 889–900. DOI:10.1016/j.jmst.2016.01.007.

Rahyussalim A., J., Kurniawati, T., Aprilya, D., Anggraini, R., Ramahdita, G. and Whulanza, Y. (2017) Toxicity and biocompatibility profile of 3D bone scaffold developed by Universitas Indonesia: A preliminary study, in: 1817, pp. 020004. DOI: 10.1063/1.4976756.

Rubin, C. and Rubin, J. (2006) . Biomechanics and Mechanobiology of Bone. *Primer on the metabolic bone diseases and disorders of mineral metabolism, 6th ed. American Society for Bone and Mineral Research, Washington, DC*, pp. 36-42..

Salgado, A. J., Coutinho, O. P. and Reis, R. L. (2004) Novel starch-based scaffolds for bone tissue engineering: cytotoxicity, cell culture, and protein expression, *Tissue Engineering*, 10 (3–4), pp. 465–474. DOI:10.1089/107632704323061825.

Sithole, M., Kumar, P., C du Toit, L., Marimuthu, T., Choonara, Y. and Pillay, V. (2018) *A 3D Bioprinted In Situ Conjugated-co-Fabricated Scaffold for Potential Bone Tissue Engineering Applications*. DOI:10.1002/jbm.a.36333.

Teixeira, S., Ferraz, M. P. and Monteiro, F. J. (2008) Biocompatibility of highly macroporous ceramic scaffolds: cell adhesion and morphology studies, *Journal of Materials Science. Materials in Medicine*, 19 (2), pp. 855–859. DOI:10.1007/s10856-007-3005-x.

Teixeira, S., Monteiro, F. J., Ferraz, M. P., Vilar, R. and Eugénio, S. (2007) Laser surface treatment of hydroxyapatite for enhanced tissue integration: surface characterization and osteoblastic interaction studies, *Journal of Biomedical Materials Research. Part A*, 81 (4), pp. 920–929. DOI:10.1002/jbm.a.31073.

Velasco, M. A., Narváez-Tovar, C. A. and Garzón-Alvarado, D. A. (2015) Design, materials, and mechanobiology of biodegradable scaffolds for bone tissue engineering, *BioMed Research International*, 2015, pp. 729076. DOI:10.1155/2015/729076.

Wang, H., Li, Y., Zuo, Y., Li, J., Ma, S. and Cheng, L. (2007) Biocompatibility and osteogenesis of biomimetic nano-hydroxyapatite/polyamide composite scaffolds for bone tissue engineering, *Biomaterials*, 28 (22), pp. 3338–3348. DOI: 10.1016/j.biomaterials.2007.04.014

Wei, X., Yang, X., Han, Z., Qu, F., Shao, L. and Shi, Y. (2013) Mesenchymal stem cells: a new trend for cell therapy, *Acta Pharmacologica Sinica*, 34 (6), pp. 747–754. DOI:10.1038/aps.2013.50.

Yoo, C.-K., Jeon, J.-Y., Kim, Y.-J., Kim, S.-G. and Hwang, K.-G. (2016) Cell attachment and proliferation of osteoblast-like MG63 cells on silk fibroin membrane for guided bone regeneration, *Maxillofacial Plastic and Reconstructive Surgery*, 38 (1). DOI:10.1186/s40902-016-0062-4.

Zhang, D., Wu, X., Chen, J. and Lin, K. (2018) The development of collagen based composite scaffolds for bone regeneration, *Bioactive Materials*, 3 (1), pp. 129–138. DOI:10.1016/j.bioactmat.2017.08.004.

CHAPTER FIVE
IN VIVO ASSESSMENT OF THE NOVEL *IN SITU* 3D PRINTED BIOMATERIAL SCAFFOLD FOR BONE REGENERATION IN NEW ZEALAND WHITE RABBITS

5.1. INTRODUCTION

Bone defects/fractures are amongst the main cause of morbidity and disability in most elderly patients (Wang *et al*., 2014). Therapy for damaged (defects) bone tissue remains a major challenge, and is the focus of bone tissue engineering research (Liu *et a*l., 2017). Bone tissue has the natural ability to self-regenerate or heal, but critical-sized (large-sized) bone defects do not heal to completion without external intervention (Kim *et al.,* 2017; Seitz *et al.,* 2005). The development of methods and 3D biomaterial scaffolds that can permanently and perfectly repair/regenerate damaged bone tissue is of great significance for clinical interest in patients with critical-sized bone defects (Liu *et al.,* 2017). Hence, the previously developed 3D biomaterial scaffolds showed great potential as a solution in repairing/regenerating bone tissue defects. The selection of biomaterials to be used for the fabrication of 3D biomaterial scaffolds must be such that, they reduce tissue rejection by the body since they have to be non-toxic and biodegradable (Seitz *et al.,* 2005). Nonetheless, fabricating a “perfect” defect-filling and extracellular matrix (ECM) mimicking biodegradable 3D biomaterial scaffolds is a challenge, since most conventional methods of 3D biomaterial scaffolds fabrication lack’s tailor-made fabrication capabilities (Tang *et al.,* 2016). However, the 3D printing fabrication method is been used as a solution and an alternative fabrication technique compared to the conventional methods of fabrication, to fabricate novel 3D printed biomaterial scaffolds through novel printing methods (Bandyopadhyay *et al.,* 2015). In the previous chapters (Chapter 3 and 4), Sithole *et al.,* (2018) successfully 3D printed a novel 3D Alg-PEI/Si scaffold and investigated the *in vitro* cell responses (cell adhesion, cell proliferation, and cell cytotoxicity analysis). The results of the fabricated novel 3D printed biomaterial scaffold showed potential to be a bone regeneration therapy. Therefore, attainment of research objectives at an *in vivo* level will aid in accentuating the clinical translational potential of the proposed novel 3D biomaterial scaffold for the treatment of bone tissue defects.

The *in vitro* analysis of novel 3D printed biomaterial scaffold therapy is expected to differ from the *in vivo* analysis studies. This difference is due to the fact that the *in vitro* assessment is not the exact replication of realistic biological conditions, as the analysis/assessments are not done in a living organism where there are multiple physiological and biomechanical interactions. However, the *in vivo* assessments allows for

the clinical translation of the novel 3D printed biomaterial scaffold intervention to be subjected to realistic conditions (Jurga *et al.,* 2011). Experimental animal models have been developed and used as an effective platform to explore the therapeutic potential of different developed novel therapeutic systems. This is in part because animals share both physiological and genetic similarities to humans, and this aids in assessing the clinical translation potential of the therapeutic agent being investigated for later clinical studies in humans (Marklund, 2016; Nyanzu *et al.,* 2017).

Numerous studies have used rabbits as the animal model of choice for inducing critical-sized nasal bone defects and for the study of bone regeneration. Rabbits were found to be an effective platform in progressing the understanding of the pathophysiology of the developed novel intervention for bone tissue application (Alam *et al.,* 2009; Higuchi *et al.,* 2016; Ishihara *et al.,* 2014; Mukozawa *et al.,* 2011). Therefore, the current study aimed at determining the therapeutic efficiency of the previously fabricated novel one step *in situ* 3D printed biomaterial scaffold using New Zealand White Rabbits. Critical-sized nasal bone defects were induced in rabbits. Therefore, this chapter investigate two types of novel printed biomaterial scaffolds: the scaffold supplemented with growth factor (Bone Morphogenetic Protein 7 human also known as osteogenic protein 1) and the scaffold without growth factors. Bone morphogenetic proteins (BMPs) are active bone-inducing growth factors that act on immature mesenchymal cells, including osteoblasts, resulting in osteogenesis (Wozney *et al.,* 1988). Hence, one of the novel 3D printed biomaterial scaffold was seeded with growth factor (osteogenic protein 1) to enhance the hybrid system functional properties to augment its performance *in vivo*. The 3D printed biomaterial scaffolds were positioned at the critical-sized defect site, and then the healing process was monitored.

The novelty of the 3D printed biomaterial scaffold (Alg-PEI/Si) in chapter 3, leads to new information from this chapter investigation, therefore, contributing toward the advancement in bone repair/regeneration tissue engineering research. Therefore, this chapter reports on an *in vivo* assay to verify that the novel 3D printed biomaterial scaffold properties can be engineered to match the bone regeneration cascade using rabbit's critical-sized nasal bone defect model. The objective of the rabbit critical-sized nasal bone defect model study was also to confirm the biocompatibility and bone regeneration of the 3D printed biomaterial scaffold supplemented with bone morphogenic protein 7 in a living organism. Therefore, the final hybrid 3D printed biomaterial scaffold is anticipated to provide a pro-regenerative platform, rich in mechanical, topographical and biological cues to guide cells towards functional regeneration.

5.2. MATERIALS AND METHODS

5.2.1. Materials

Ketamine HCL (a dissociative anesthetic) and lignocaine were purchased from Bayer (Pty) Ltd Animal Health Div (Wrench, Isando, SA). Xylazine HCl (sedation, anesthesia, muscle relaxation, and analgesia) was purchased from in vervet S.A. (Pty) Ltd. (Isando, SA), sodium pentobarbitone, antisedan, meloxican were purchased from Dechra Veterinary Products Limited (Hadnall, Shrewsbury, UK) and temgesic® was purchased from Mundipharma (Pty) Ltd. (Claremont, Cape Town, SA). Fetal bovine serum (FBS; Biochrom, Berlin, Germany), dulbecco's modified eagle's medium (DMEM), bone morphogenic protein 7 (Osteogenic protein 1) were purchased from Sigma-Aldrich (St. Louis, MO, USA). All other reagents were of standard analytical grade and were used as procured.

5.2.2. Animal Welfare, Housing and Habituation Prior to Scaffold Study Experiment

New Zealand White Rabbits were bred at the University of the Witwatersrand Central Animal Service (CAS) unit. Seventeen male New Zealand White Rabbits (12-16 weeks, 2.5 – 3.0Kg) were used for this study. Figure 5.1(a – b) depicted the digital photograph of the rabbits, housed individual in cages. Daily habituation process at Wits CAS under the care of trained CAS staff and the researcher was carried out for seven days. The cages were under a 12 hours light/12 hours dark cycle. Habituation is a significant process prior to the surgical experimental method so as to improve animal handling during the actual procedures and reduce the challenges that could delay the implantation of the scaffolds. The process of habituation included visitation of the animals twice per day for a routine check-up, ensuring their water and food were intact, and the animals were weighted before the surgical procedure and during the experimental study period (Figure 5.1c). Environmental enrichments for the rabbits were provided as per CAS SOPs for rabbits. Ethics approval for the use of the New Zealand White Rabbits for this study was obtained from the Animal Ethics Screening Committee of the University of the Witwatersrand (Clearance Certificate No. 2017/10/64/D).

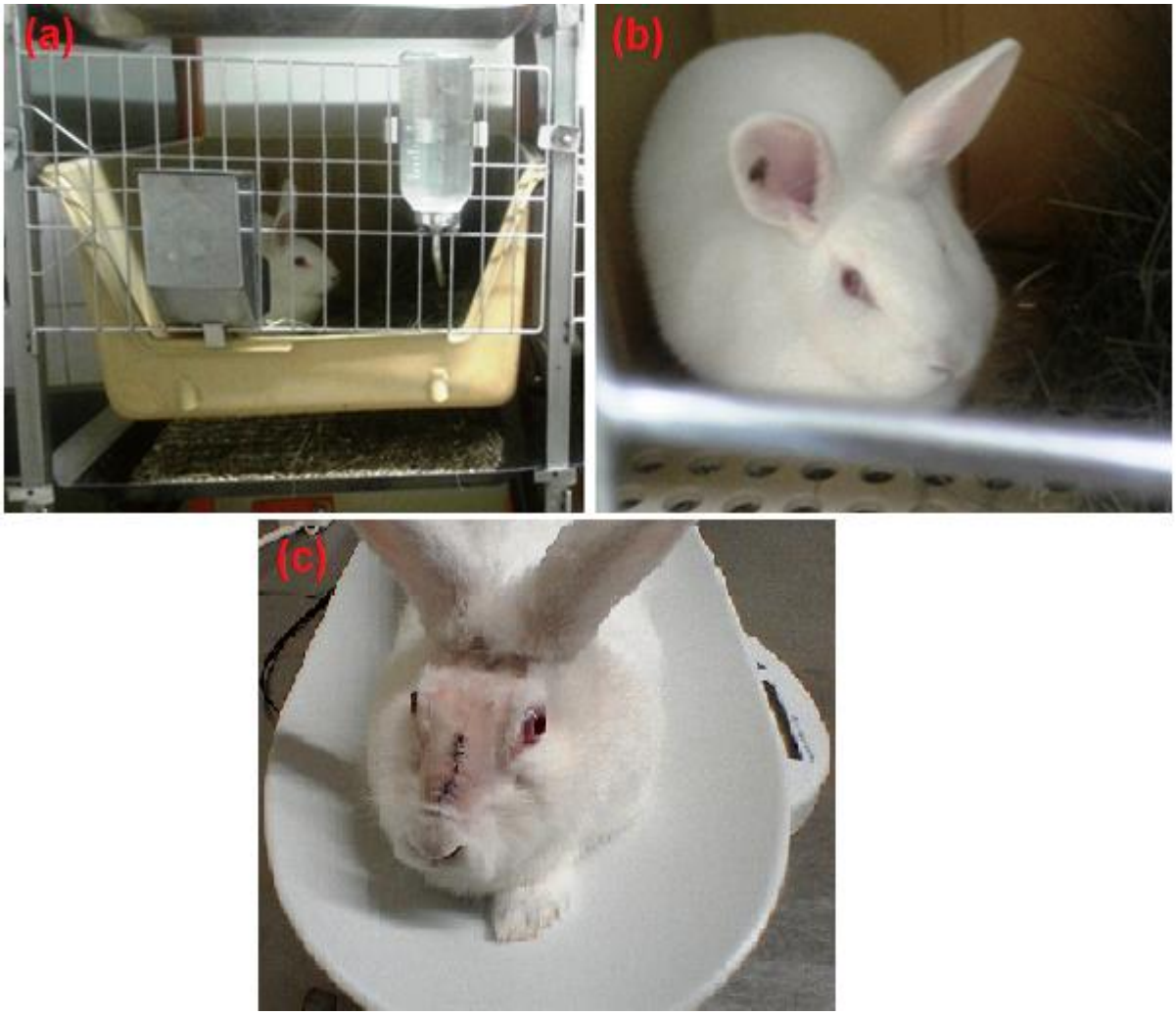


Figure 5.1: Photographic representation of (a – b) housing of the New Zealand White Rabbits, (c) measurement of rabbit's weight at Wits CAS unit.

5.2.3. The 3D Printed Biomaterial Scaffolds Preparation Prior Implantation

The 3D printed biomaterial scaffolds were sterilized using ethanol followed by exposure to UV light for 24 hours. After the sterilization process, the 3D printed biomaterial scaffolds were soaked in Dulbecco"s modified Eagle"s medium (DMEM), supplemented with 10% fetal bovine serum (FBS) and incubated at an atmosphere of 5% CO_2 at 37^{o}C (pH 7.4) for 24 hours to equilibrate prior implantation to the rabbit's induced critical-sized nasal bone defects.

5.2.4. Design and Surgical Procedure for the Main Intervention

The study was designed to comprise of four experimental groups (1, 2, 3, and 4), each with a sample size n = 3. The 3D printed biomaterial scaffolds were evaluated in each group at

different time intervals (1, 2, 4 and 8 weeks) after each rabbit's termination. In the experimental groups, 3D printed biomaterial scaffolds were utilized for the healing/regeneration of the induced critical-sized bone defects. *Ex vivo* toxicity studies of the 3D printed biomaterial scaffolds were performed prior *in vivo* experimental animal study. Furthermore, cell proliferation and cell adhesion were investigated as presented in previous chapters.

The study used seventeen New Zealand White Rabbits which were randomly assigned into groups, where 5 rabbits were assigned for a pilot study. The main study was conducted using 12 rabbits to observe bone healing over time.

5.2.4.1. The procedure for the pilot study

To perfect the surgical technique method for the induction of the critical-sized bone defects (5mm diameter), control rabbit's cadavers from previous study which were destined for incineration were used. There was no need for ethical committee approval, given that the procedure was performed on sacrificed rabbits which were previously been used in another rabbits testing project. Hence, following the perfection for the induction of the critical-sized bone defect technique, living rabbits were used to create the defects and implanted with the 3D printed biomaterial scaffolds (the rabbits from the approved ethics).

Therefore, the pilot study validated the feasibility of the experimental (surgical) procedures. The results revealed that the rabbits are a great model for the study and they survived for the whole period of this study. Therefore, the surgical procedures did not have noticeable side effect and the rabbit behaviour was usual. Hence, the results suggested that we can move on with the main study using 12 rabbits within a period of 1,2, 4 and 8 weeks as proposed in the approved ethics application

5.2.4.2. The design of the main study

Group 1 (Week 1, experimental group 1, n = 3): 3D printed biomaterial scaffolds containing growth factors (Bone Morphogenic Protein 7) and 3D printed biomaterial scaffolds without growth factors were implanted in an induced nasal critical-sized bone defect (please see section 5.2.4.3, Figure 5.3e). Two defects were empty (without any scaffolds as a control for the purpose of observing the bone self-healing ability in relation to the created defect size and also for comparison with scaffolds). The implantation of the 3D printed biomaterial

scaffolds was expected to demonstrate the regenerative potential of bone tissue by the scaffolds. These groups were used to obtain the effectiveness of the scaffolds in the healing process of the induced bone critical-sized defects compared with the control group. Group 1 was terminated in week 1.

Group 2 (Week 2, experimental group 2, n = 3): The implantation is the same as for group 1, but group 2 was terminated in week 2.

Group 3 (Week 4, experimental group 3, n = 3): The implantation is the same as for group 1, but group 3 was terminated in week 4.

Group 4 (Week 8, experimental group 4, n = 3): The implantation is the same as for group 1, but group 4 was terminated in week 8.

Therefore, each rabbit was induced with four bone defects as depicted in Figure 5.3d below (section 5.2.4.3); Where two bone defects were implanted with the novel 3D printed biomaterial scaffolds (e.g. one defect with scaffold contained growth factors and the other defect with scaffold without growth factors), the remaining two bone defects were empty for control, depictured in Figure 5.3e below (section 5.2.4.3).

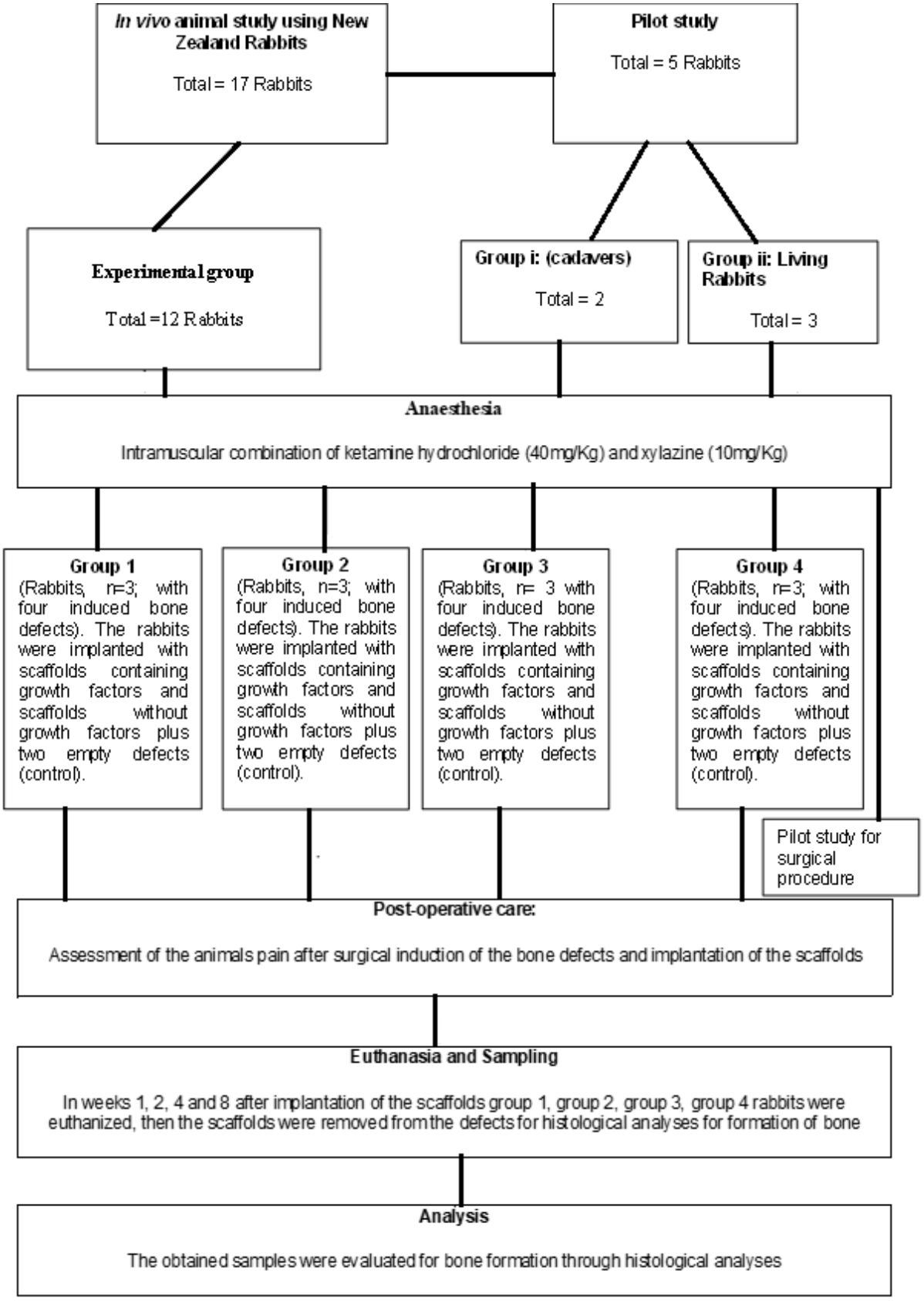


Figure 5.2: Schematic showing the *in vivo* studies model for the implanted scaffold

5.2.4.3. Surgical procedure for the intervention

The surgical procedures were performed in sterile conditions at all time. Briefly, the New Zealand White Rabbits were anaesthetized using an intramuscular combination of ketamine hydrochloride (40mg/Kg) and xylazine (10mg/Kg). The anaesthesia was maintained with isoflurane plus oxygen. The hair above the nasal bone was shaved and the skin was surgically prepared using F10 skin prep solution. Thereafter, 1.8mL of 2% lidocaine containing 1:80,000 epinephrine was administered subcutaneously. Both the nasoincisinal suture line and nasal bone via perpendicular incision were exposed. A critical-sized nasal bone defect (5mm in diameter) approximately 2mm thickness was induced (while preserving the nasal membrane) using a fissure bur with continuous saline irrigation. The 3D printed biomaterial scaffolds were then implanted into the defects. Following the creation of the critical-sized nasal bone defects and the implantation of the 3D biomaterial scaffolds, the surgical site was sutured closed. Great care was provided to avoid nasal bone infections and antibiotics were administered. The pain was managed with meloxicam (Alam *et al.,* 2009; Ishihara *et al.,* 2014). Therefore, Figure 5.3(a-f) depicts photos taken at each stage of the surgical procedure, from the preparation of the surgical site to the closing of the surgical site. Figure 5.3(a), the shaved rabbit forehead and muzzle; (b) the incision to expose the site for creation of the defect; (c), the first 5mm defect; (d), the four critical-sized nasal bone defects; (e), the scaffolds in place in two of the defects and an additional two open empty defects (control) and (f) the surgical site after closure of the wound. The surgical procedure was undertaken as previously described by Alam *et al.,* (2009).

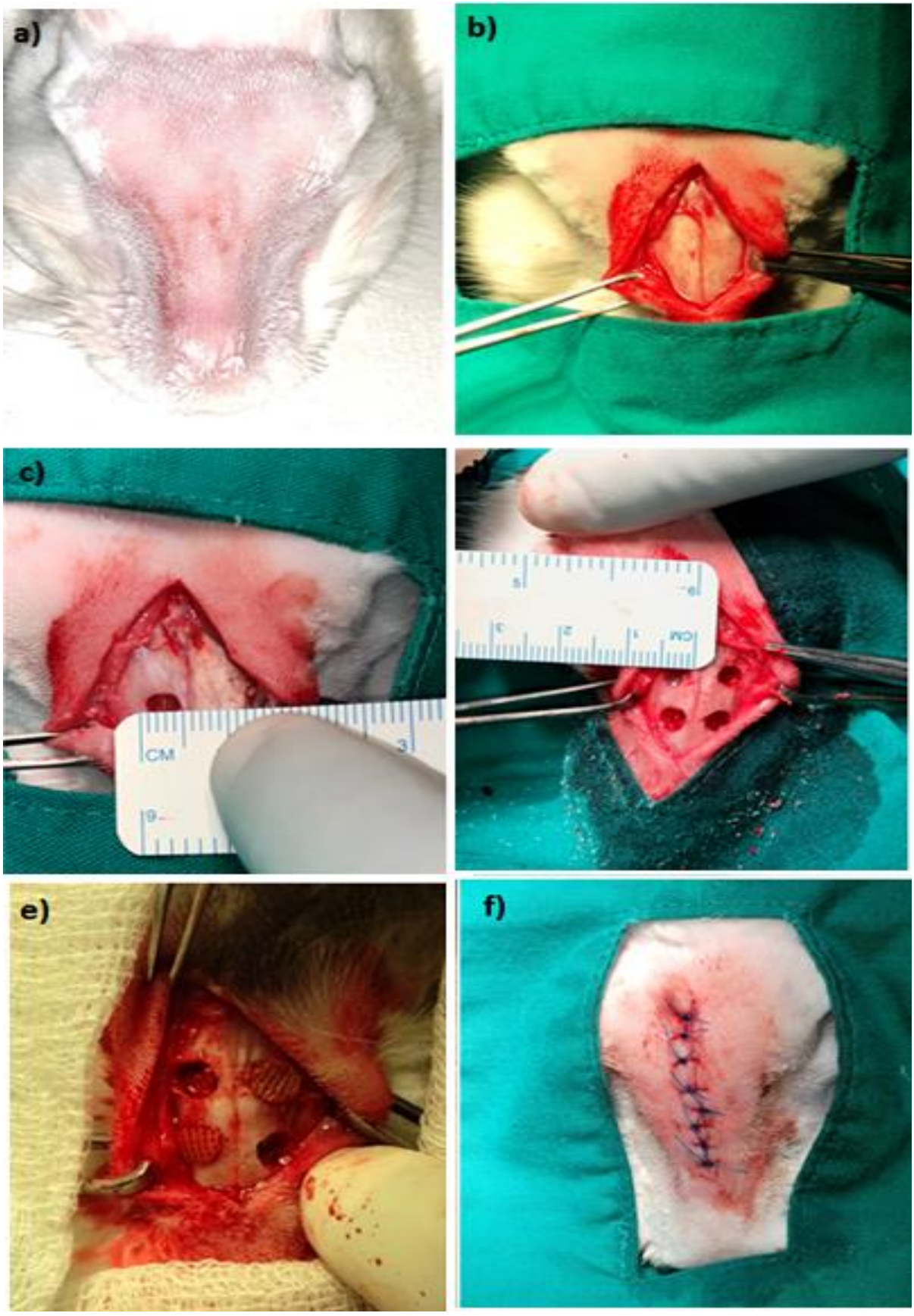


Figure 5.3: Schematic representation of the surgical procedure for induction of nasal critical-sized bone defects in the New Zealand White Rabbit.

5.2.5. Post-operative Care of the New Zealand White Rabbits

Post-surgery, the rabbits were under strict observation immediately after any surgical procedures, ensuring they recovered well. Rabbits were still kept individually in separate cages at ±25^{o}C and were maintained under 12 hours light: 12 hours dark cycle. The rabbits were fed in accordance to Wits CAS feeding SOPs throughout the duration of the study. There was no advance sign of lack of food and water intake by the rabbits noted for the duration of the study. The rabbits were weighed twice weekly during the period of the study. The rabbits were cared for according to the CAS protocol and observed by the researcher and veterinarian until the end of the study. There was no necessity for supportive orthotic devices and no need for postoperative restriction on the rabbit's activity. The rabbits were inspected twice daily for their welfare and other parameters for systemic complications such as animal behaviour, posture, weight, feeding and drinking pattern and then recorded for future references.

5.2.6. Procedure for Euthanasia and Sample Collection

The rabbits were euthanized using IV sodium pentobarbitone (2mL/Kg) in their ear vein with minimal damage to the anatomic and physiological structure and minimal discomfort. The euthanization happened at 1, 2, 4, and 8 weeks after the scaffolds implantation. The implanted scaffolds and the empty defects samples specimens were immediately removed from the nasal bone defects of the rabbits. The removed specimens were temporarily stored in 10% buffered formalin until the performance of the histological procedure as described in section 5.2.7 below.

5.2.7. Samples Preparation for Histological Examination

The specimens were fixed with 10% buffered formalin and following the fixation, the specimens were demineralized with 14%EDTA for 4 weeks. Representative samples from the induced defects were cut down according to Idexx standard operative procedure (IdexxSA-AP-26) and processed according to routine histological tissue processing in an automated tissue processor with standard operating procedures (IdexxSA-AP-SOP-27). Following tissue processing, embedded transverse sections were cut at a thickness of 5µm (IdexxSA-AP-SOP-30), mounted onto slides and were stained in an automated Haematoxylin and Eosin tissue stainer (IdexxSA-AP-SOP-205) before histological evaluation.

5.3. RESULTS AND DISCUSSION

5.3.1. Pilot Study Assessment

The pilot study validated the feasibility of the experimental (surgical) procedures. The results confirmed the previous studies (Alam *et al.,* 2009; Higuchi *et al.,* 2016; Ishihara *et al.,* 2014; Mukozawa *et al.,* 2011), that rabbits are feasible experimental model for the proposed study and these rabbits tolerated the intervention without any observable ill-effects within the two weeks of the pilot study. The rabbits survived the entire period of 2 weeks of the pilot study. Following the success and satisfactory results of the methodological surgical procedures and upon the approval of the reviewed report of the pilot study by the ethics committee of the University of the Witwatersrand, we proceeded with the proposed main study and its intervention.

5.3.2. Clinical and Histological Analysis

5.3.2.1. Clinical examination

There was no post-operative complication or adverse reaction such as abnormal bleeding during the healing of all surgical sites. There was a minimal sign of inflammation (e.g. swelling) and after resting for 3-6 days post-operation, the rabbits could move and leap without any notable pain or limitation. The 3D biomaterial scaffolds confirmed to be intact within the defects at the time of termination and sample collection. Healing progressed without major incident in all the rabbits during the 8 weeks observation period.

5.3.2.2. Histological analysis

5.3.2.2.1. Histological examination for group 1 (week 1)

Figure 5.4, depicts photographic images of an embedded transverse section of 3D printed biomaterial scaffold with growth factors, 3D printed biomaterial scaffold without growth factors and the defect without any scaffold (control) respectively (Figure 5.4a, b, and c), at week one post-operative histology. Reported histological results for Figure 5.4a (3D printed biomaterial scaffold with growth factors), revealed a visible large induced nasal defect and is filled with mixed eosinophilic and basophilic material (the 3D printed biomaterial scaffold) which is surrounded by inflammation reaction and granulation tissue. The inflammation is

mixed with macrophages and heterophils (Inflammation is a crucial biological process for eradication of pathogens and maintenance of tissue homeostasis (Loi *et al.,* 2016) predominating and a few of macrophages contain granular basophilic material. Necrotic bone fragments are present in the granulation tissue with surrounding macrophages (necrotic bone fragments could have resulted from the pieces of bones remains during the induction of the nasal bone defect (Fondi and Franchi, 2007)). Figure 5.4b (scaffold without growth factors), a large defect in the nasal bone is noted which is filled with granulation tissue as well as specular to amorphous, mixed eosinophilic and basophilic material (the scaffold). Necrotic bone is prominent and there is a marked inflammatory reaction with numerous degenerate heterophils. Figure 5.4c (an empty defect without any scaffold), there is a largely visible defect in the nasal bone which is filled with hemorrhage and fibrin, but there are areas with necrotic bone fragments and surrounding inflammation which includes macrophages and multinucleated giant cells. Early granulation tissue formation is noted as well. Therefore, all the defects in week 1 indicated no osteoblastic activities and a negligible amount of bone tissue formation were observed

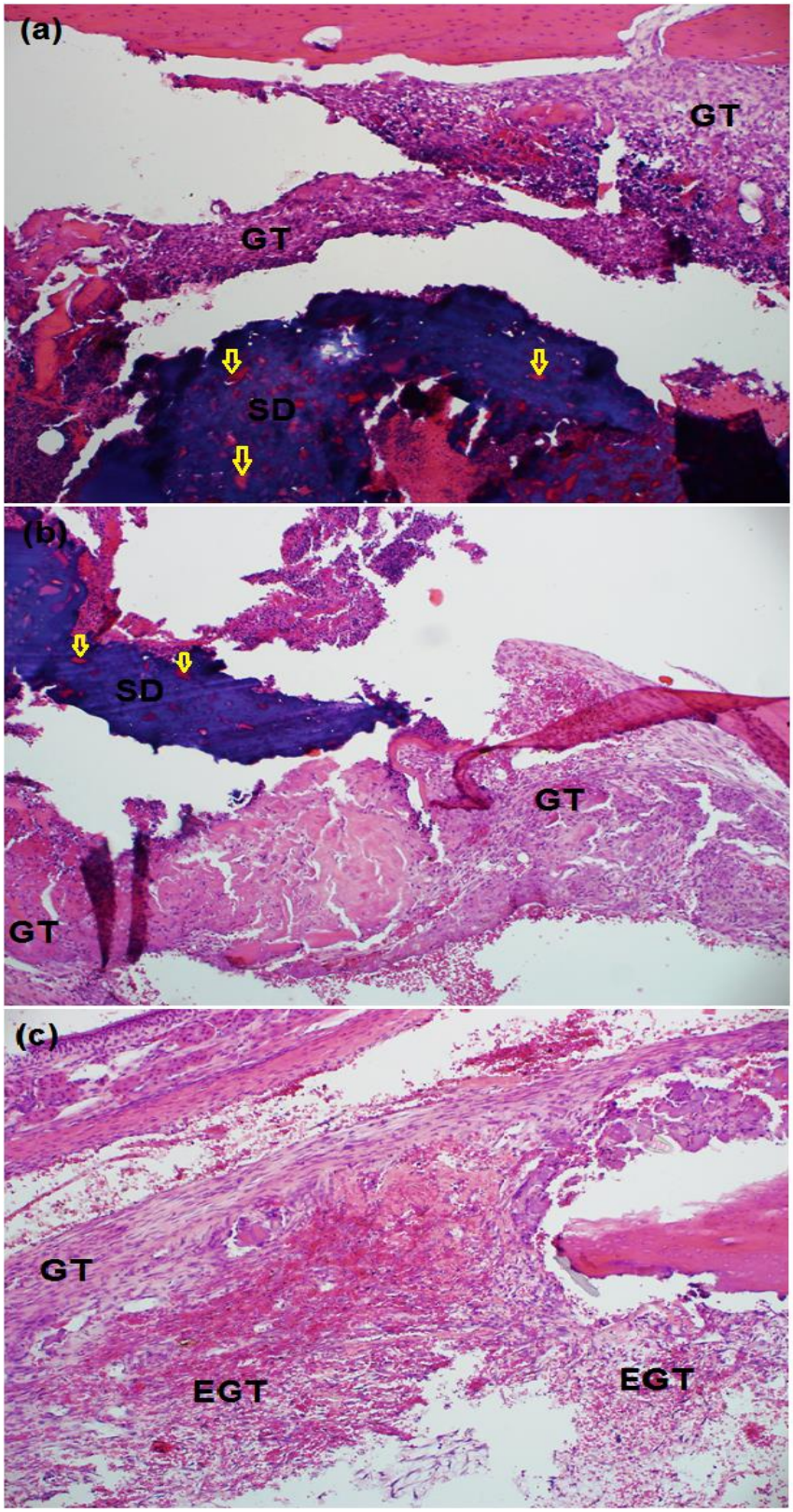


Figure 5.4: Histological images, a) scaffold with growth factors, b) scaffold without growth factors, c) an empty nasal defect at week one post-operation, H&E staining (x10 magnification): GT = granulation tissue; SD = scaffold mostly represent by the empty space; yellow arrows = blood vessels within the scaffold. There was negligible osteoblastic activity observed in all the defects.

5.3.2.2.2. Histological examination for group 2 (week 2)

Figure 5.5, depicts photographic images of the embedded transverse section of the 3D printed biomaterial scaffold with growth factors, 3D printed biomaterial scaffold without growth factors and the empty defect (control) respectively (Figure 5.5a, b, and c) at week two postoperatively. Reported histological results for Figure 5.5a (3D printed biomaterial scaffold with growth factors), a focal defect in the nasal bone is noted, which is filled primarily by similar amorphous to spicular, mixed eosinophilic and basophilic material (the scaffold). There is surrounding inflammation consisting of mixed macrophages and heterophils with surrounding fibrosis and granulation tissue development. Early new bone development with osteoblast activity is noted as well. Figure 5.5b (3D printed biomaterial scaffold without growth factors), the defect in the nasal bone is still visible which is filled with mixed eosinophilic and basophilic material (the scaffold) with inflammation consisting of macrophages, some of which contain phagocytosed basophilic granular material. There is mild early surrounding fibroplasia, but spicules of necrotic bone with surrounding macrophages are noted as well. A few heterophils and scattered lymphocyte and plasma cells are noted as well. Moderate periosteal reactions with active osteoblasts are noted on the edge of the bone defect. Figure 5.5c (an empty defect), a visible defect which is filled granulation tissue and clusters of lymphocytes and plasma cells with few interspersed adipocytes. Moderate haemorrhages and fibrin deposition is noted. The edge of defect shows mild osteoblastic activity and there is a marked periosteal reaction. Focally, there is a fragment of necrotic bone with surrounding macrophages and multinucleated cells. Therefore, the defects in week 2 indicated osteoblastic activities, though in Figure 5.5a (scaffold with growth factors) early bone formation was thought to more prominent compared the other defects.

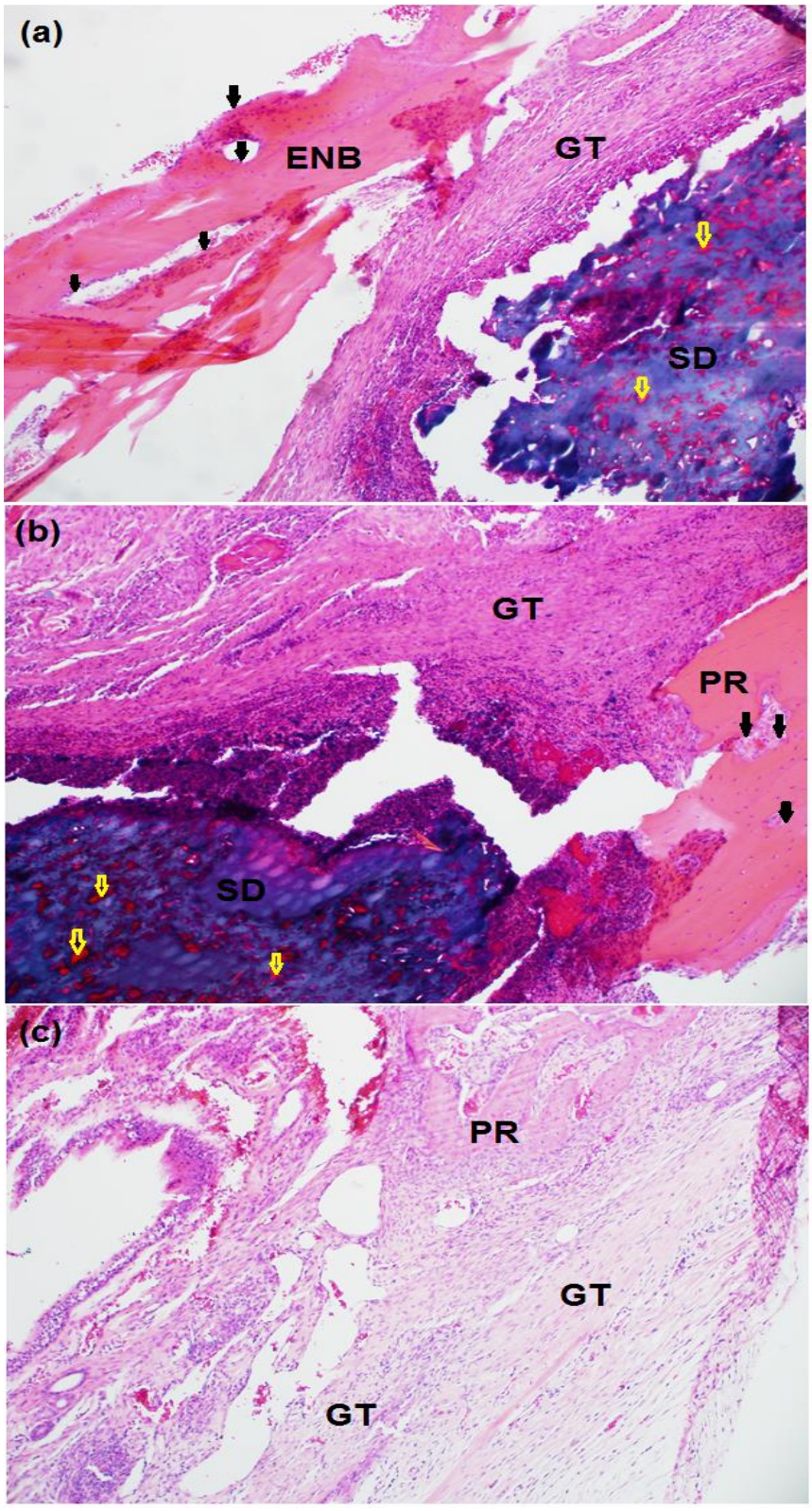


Figure 5.5: Histological images of the, a) scaffold with growth factors, b) scaffold without growth factors, c) an empty nasal defect at week 2 post-operation, H&E staining (x10 magnification): GT = granulation tissue; SD = scaffold mostly represent by the empty space; Yellow arrows = blood vessels within the scaffold, ENB = early new bone development, Black arrows = osteoblast, PR = periosteal reactions. Osteoblastic activity was observed in all the defects.

5.3.2.2.3. Histological examination for group 3 (week 4)

Figure 5.6, depicts photographic images of the embedded transverse sections of the 3D printed biomaterial scaffold with growth factors, 3D printed biomaterial scaffold without growth factors and the empty defect (control) respectively (Figure 5.6a, b, and c) at week 4 post-operatively. A reported histological result for Figure 5.6a (3D printed biomaterial scaffold with growth factors), a defect is visible in the nasal bone which is filled by granulation tissue and mixed, eosinophilic and basophilic material (the scaffold). There is surrounding inflammation lesion consisting of heterophils and macrophages. A few of the macrophages contain granular basophilic material. New bone formation with prominent osteoblastic activity is noted between the edge of the defect and the foreign material (The scaffold). Figure 5.6b (3D printed biomaterial scaffold without growth factors), a segment of the nasal bone is interrupted and filled with large quantities of granulation tissue and inflammation. New bone formation is prominently visible between the defect and the granulation tissue with marked osteoblastic activity. Figure 5.6c (an empty defect), the lesion is visible but this one is very subtle and consists of a focal segment of bone thinning and new bone formation. This new bone shows increased osteocytes density and there is osteoblastic activity on the periosteal surface with the production of thin bone spicules.

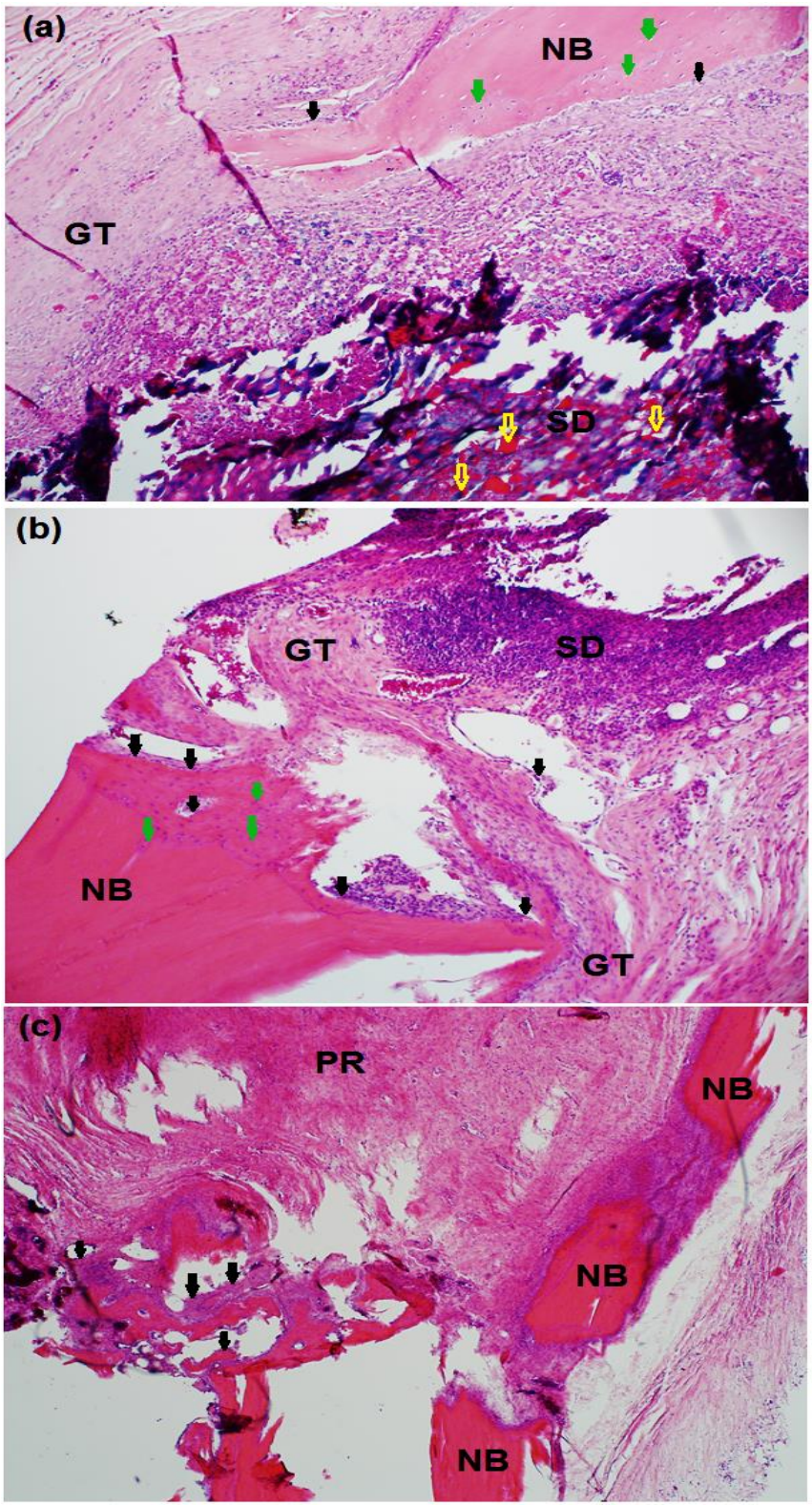


Figure 5.6: Histological images of the, a) scaffold with growth factors, b) scaffold without growth factors, c) an empty nasal defect at week 4 post-operation, H&E staining (x10 magnification): GT = granulation tissue; SD = scaffold mostly represent by the empty space; Yellow arrows = blood vessels within the scaffold, NB = new bone development, Black arrows = osteoblast, PR = periosteal reactions, Green arrows = osteocytes. There was a major osteoblastic activity accompanied by new bone formation observed in all the defects.

5.3.2.2.4. Histological examination for group 4 (week 8)

Figure 5.7, depicts photographic images of the embedded transverse sections of the 3D printed biomaterial scaffold with growth factors, 3D printed biomaterial scaffold without growth factors and the empty defect (control) respectively (Figure 5.7a, b, and c) at week 8 post-operatively. A reported histological result for Figure 5.7a (3D printed biomaterial scaffold with growth factors), the nasal bone is complete (with bone formation) but there is an area showing thinning and depression into the sinus space. This is associated with a focus of inflammation in the adjacent subcutis consisting primarily of macrophages heterophils and this is associated with foreign material of mixed basophilic and eosinophilic type. There is marked surrounding fibrosis. The adjacent thin bone segment is new with increased number of osteocytes as well as osteoblast activity. Figure 5.7b (3D printed biomaterial scaffold without growth factors), there marked thickening of the bone with the production of mature bony spicules and medullary cavities containing adipocytes and this bordered by a thinner segment but there is prominent new bone formation an increased osteocyte density. This section is associated with a moderate periosteal reaction and there are small medullary cavities containing prominent lining osteoblasts. A small defect is visible but this is filled with fibrous connective tissue and fibroblasts however osteoblastic activity is still present on the edges. Figure 5.7c (an empty defect), a small segment with thin, new bone formation was noted showing increased osteocyte density and osteoblastic activity on the periosteal surfaces and perivascular.

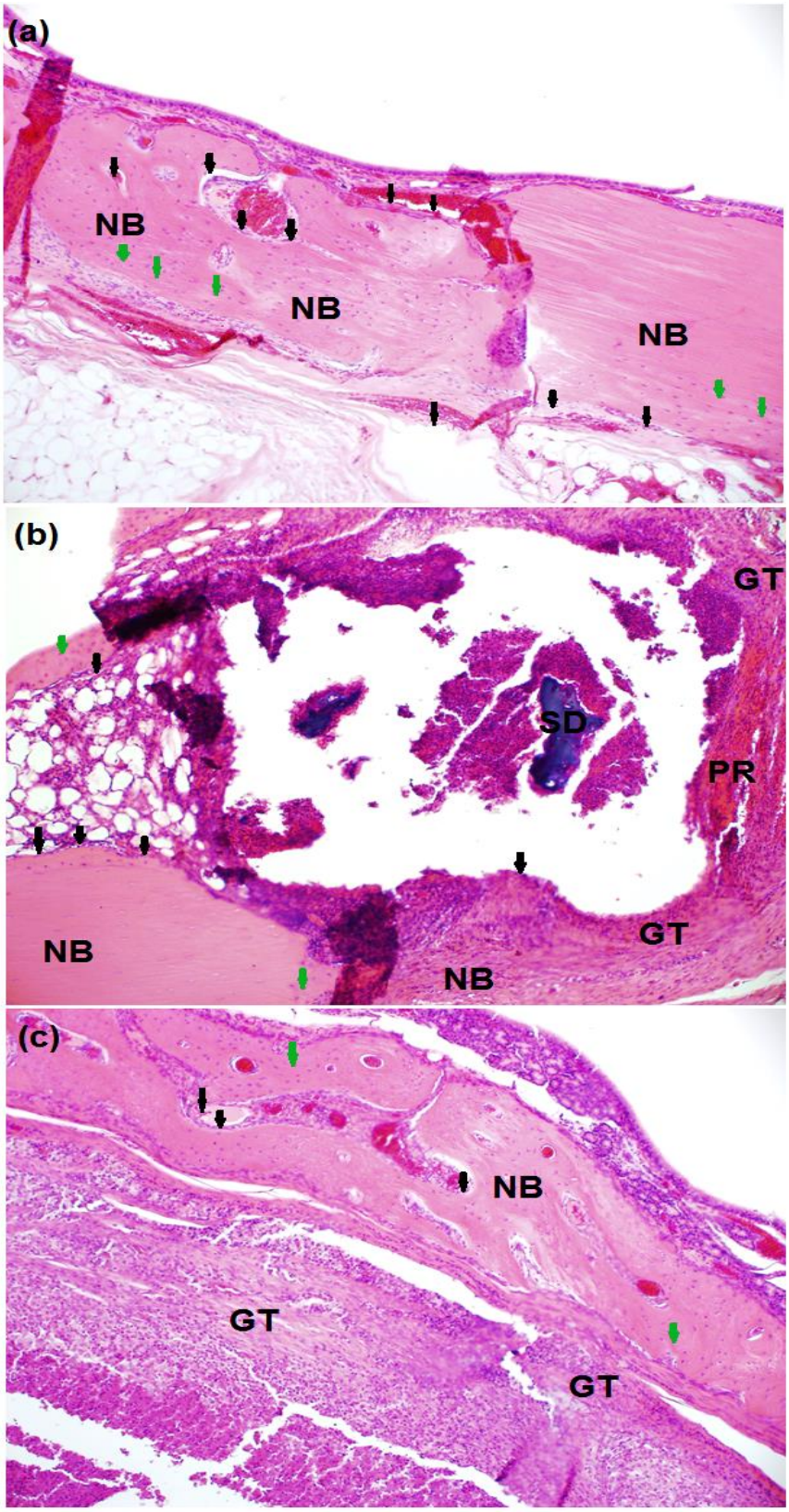


Figure 5.7: Histological images of the, a) scaffold with growth factors, b) scaffold without growth factors, c) an empty nasal defect at week 8 post-operation, H&E staining (x10 magnification): GT = granulation tissue; SD = scaffold mostly represent by the empty space; NB = new bone development, Black arrows = osteoblast, PR = periosteal reactions, Green arrows = osteocytes,. There was major osteoblastic activity observed in all the defects**.**

5.4. DISCUSSION

The previously 3D printed Alg-PEI/Si scaffold have the characteristics required for bone tissue engineering application, because of its tested biocompatibility, porous architecture and excellent mechanical strength acting as an artificial extracellular matrix. The purposes of this study was to evaluate the 3D printed Alg-PEI/Si construct's efficacy for bone defects regeneration and *in vivo* determining the effect of the added growth factors component. The experimental animal (rabbits) model that is been current used in this study chapter have previously shown the potential and suitability for bone substitutes, for the evaluation of early stage of healing. Furthermore, 5mm diameter in the rabbits nasal bone defects was previously suggested as an adequate size to observe the bone regeneration investigation. It was considered that the rabbits animal model and location and the dimension of the defects were valid (Mukozawa *et al*., 2011). Biomaterial scaffolds were used as implants of approximately the same size in all groups excluding the control group so that the same amount of space would be available for bone regeneration.

Bone defects/fractures are the most usual body injury, and their repair/healing is typically controlled and organized by a process involving signalling molecules and specialized cells that are precisely coordinated in space and time (Liu *et al.,* 2018). The success in bone healing/repair depends on complex interaction between immune cells and the bone tissue. Bone healing is a physiological complex process, involving both mechanical and biological aspect (Sandberg *et al*., 2017; Ghiasi *et al.,* 2017). Hence, after the defect/fracture on the body, cell migration, cell/tissue differentiation, tissue synthesis, and cytokine and growth factor release occur, controlled by the mechanical and the surrounding environment (Ghiasi *et al.,* 2017). Infiltration of inflammatory cells to the defect/fracture site, which combat infection and clear debris and dead cells initiate defect/fracture healing (Street *et al.,* 2002).

Inflammation is amongst the most significant biological process during defect/fracture healing/repair for maintenance of tissue homeostasis and eradication of pathogens (Loi *et al.,* 2016). Furthermore, the inflammatory cells also secrete various growth factors and cytokines significant for guiding neovascularization (Street *et al.,* 2002) and cell recruitment (Bourque *et al.,* 1993; Einhorn, 1998; Gerstenfeld *et al.,* 2003). Inflammatory macrophages are positioned anatomically to support significant events in early anabolic phases (Kaur *et al.,* 2017) and were required for maintenance of mature osteoblast *in vivo* (Raggatt *et al.,* 2014). Macrophages have a great role also in host defence and inflammatory and they are present in all phases of defect/fracture repair/healing and associated with significant repair/healing event in human tissue and animal model (Gu *et al*., 2017; Kaur *et al.,* 2017).

Therefore, macrophages are present during the inflammatory phase of fracture healing in humans (Andrew *et al.,* 1994; Oni, 1997) and animals (Alexander *et al.,* 2011; Hankemeier *et al*., 2001; Xing et al., 2010). Macrophages are located within the defects/fractures associated tissue and the required molecular repertoire can be express to influence, initiate and coordinate both bone anabolic outcome and inflammatory processes (Wu and Zeng, 2013). Osteoblast differentiation *in vivo* can be induced by macrophages (Chang et al., 2008; Vi *et al.,* 2015). Osteoblast yielding osteocytes are common cells in bone and bone development (O'Brien *et al.,* 2013). Osteocytes are on the surface of bone and distributed in the mineralized bone matrix, and form an interconnected network with osteoblasts, and the bone marrow, as result, osteocytes possess the most potent ability to regulate bone metabolism through direct cell-cell contacts and the release of soluble molecules (O'Brien *et al.,* 2013). Osteocyte, immune cells, and endocrine system tightly controlled the balance between bone resorption and bone formation (Gu *et al*., 2017).

Briefly, the histological results revealed that in group one, almost all of the defects showed no signs of osteoblastic activities, these are the rabbits terminated in week one. Healing and osteoblastic activities have started unevenly in different defects in forming new bone growth in the margins of the defect in animals terminated in week two. As the weeks' progress, there was more bony island observed compared with the histological results observed from previous weeks. Parts of this newly formed bone had an appearance of the lamellar structure. The fibroconnective tissue filled the porous structure of the scaffold, and occasionally observe the ingrowth of the maturing bone to the scaffold. Dense fibrous connective tissue surrounds these bony islands. The connective tissue ingrowth into the pores of the scaffold was also noted. The formation of bone seemed to progress gradually inside the scaffolds from the dense fibroconnective tissue to the newly formed bone through the mineralization of the tissue. There was an observed inflammation reaction with foreign body giant cells, and macrophages. Inflammation response was strong in the side of the scaffold facing the periosteum and skin. Therefore, foreign-body-type inflammation reactions composed of giant cells, macrophages, granulocytes, and lymphocytes as well as plasma cells were mostly found inside the upper part of the scaffold. Despite the presence of the inflammatory reaction, fibrous connective tissues were formed and also bone tissue was formed.

In this study, a subjective visual assessment of bone regeneration process was carried out; using two different implants (the scaffold with growth factors and scaffold without growth factors) and compared the bone regenerative capacity of these materials histological in a rabbit animal model. The defects appeared to be becoming progressively smaller with time.

In week 8, it was observed that, the defect implanted with the scaffold that contains growth factors healed completely as compared to the defect implanted with the scaffold without growth factor and an empty defect. This support the reported histological results for week 8 and the report also highlighted an evidence of scaffold being resorbed, hence, the scaffold appeared to make a significant difference in healing time required.

5.5. CONCLUDING REMARKS

Animal models have played an indispensable role over the years, for the evaluation of biomaterial scaffolds for bone tissue engineering application, in understanding their regenerative potential and interaction with host bone tissue. In our study, the composite 3D printed Alg-PEI/Si porous scaffold incorporated with growth factors, was found to be an acceptable candidate bone tissue regenerative implant. It induced no adverse tissue reaction and effectively supported and acted as a platform for the host cell to adhere, proliferate, differentiate and form new bone tissue *in vivo*. This indicates that the composite 3D printed biomaterial scaffold with growth factors can be a useful and beneficial implant for bone tissue regeneration to be introduced for clinical tests. Therefore, our study confirmed the healing potential of the implant through the 5mm diameter induced critical-sized nasal bone defects in rabbits.

5.6. REFERENCES

Alam, S., Ueki, K., Nakagawa, K., Marukawa, K., Hashiba, Y., Yamamoto, E., Sakulsak, N. and Iseki, S. (2009) Statin-induced bone morphogenetic protein (BMP) 2 expression during bone regeneration: an immunohistochemical study, *Oral Surgery, Oral Medicine, Oral Pathology, Oral Radiology, and Endodontics*, 107 (1), pp. 22–29. DOI:10.1016/j.tripleo.2008.06.025.

Alexander, K. A., Chang, M. K., Maylin, E. R., Kohler, T., Müller, R., Wu, A. C., *et al.* (2011) Osteal macrophages promote in vivo intramembranous bone healing in a mouse tibial injury model, *Journal of Bone and Mineral Research: The Official Journal of the American Society for Bone and Mineral Research*, 26 (7), pp. 1517–1532. DOI:10.1002/jbmr.354.

Andrew, J. G., Andrew, S. M., Freemont, A. J. and Marsh, D. R. (1994) Inflammatory cells in normal human fracture healing, *Acta Orthopaedica Scandinavica*, 65 (4), pp. 462–466. DOI: 10.3109/17453679408995493.

Bandyopadhyay, A., Bose, S. and Das, S. (2015) 3D printing of biomaterials, *MRS Bulletin*, 40 (2), pp. 108–115. DOI:10.1557/mrs.2015.3.

Bourque, W. T., Gross, M. and Hall, B. K. (1993) Expression of four growth factors during fracture repair, *The International Journal of Developmental Biology*, 37 (4), pp. 573–579.

Chang, M. K., Raggatt, L.-J., Alexander, K. A., Kuliwaba, J. S., Fazzalari, N. L., Schroder, K., *et al.* (2008) Osteal tissue macrophages are intercalated throughout human and mouse bone lining tissues and regulate osteoblast function in vitro and in vivo, *Journal of Immunology (Baltimore, Md.: 1950)*, 181 (2), pp. 1232–1244. DOI: 10.4049/jimmunol.181.2.1232.

Einhorn, T. A. (1998) The cell and molecular biology of fracture healing, *Clinical Orthopaedics and Related Research*, (355 Suppl), pp. S7-21. DOI: 10.1097/00003086-199810001-00003.

Fondi, C. and Franchi, A. (2007) Definition of bone necrosis by the pathologist, *Clinical Cases in Mineral and Bone Metabolism*, 4 (1), pp. 21–26.

Gerstenfeld, L. C., Cullinane, D. M., Barnes, G. L., Graves, D. T. and Einhorn, T. A. (2003) Fracture healing as a post-natal developmental process: molecular, spatial, and temporal aspects of its regulation, *Journal of Cellular Biochemistry*, 88 (5), pp. 873–884. DOI:10.1002/jcb.10435.

Ghiasi, M. S., Chen, J., Vaziri, A., Rodriguez, E. K. and Nazarian, A. (2017) Bone fracture healing in mechanobiological modeling: A review of principles and methods, *Bone Reports*, 6, pp. 87–100. DOI:10.1016/j.bonr.2017.03.002.

Gu, Q., Yang, H. and Shi, Q. (2017) Macrophages and bone inflammation, *Journal of Orthopaedic Translation*, 10, pp. 86–93. DOI:10.1016/j.jot.2017.05.002.

Hankemeier, S., Grässel, S., Plenz, G., Spiegel, H. U., Bruckner, P. and Probst, A. (2001) Alteration of fracture stability influences chondrogenesis, osteogenesis and immigration of macrophages, *Journal of Orthopaedic Research: Official Publication of the Orthopaedic Research Society*, 19 (4), pp. 531–538. DOI:10.1016/S0736-0266(00)00044-9.

Higuchi, M., Moroi, A., Yoshizawa, K., Kosaka, A., Ikawa, H., Iguchi, R., *et al.* (2016) Comparison between various densities of pore titanium meshes and e-polytetrafluoroethylene (ePTFE) membrane regarding bone regeneration induced by low intensity pulsed ultrasound (LIPUS) in rabbit nasal bone, *Journal of Cranio-Maxillo-Facial Surgery: Official Publication of the European Association for Cranio-Maxillo-Facial Surgery*, 44 (9), pp. 1152–1161. DOI:10.1016/j.jcms.2016.06.029.

Ishihara, Y., Ueki, K., Sotobori, M., Marukawa, K. and Moroi, A. (2014) Bone regeneration by statin and low-intensity pulsed ultrasound (LIPUS) in rabbit nasal bone, *Journal of Cranio-Maxillo-Facial Surgery: Official Publication of the European Association for Cranio-Maxillo-Facial Surgery*, 42 (3), pp. 185–193. DOI:10.1016/j.jcms.2013.05.002.

Jurga, M., Dainiak, M. B., Sarnowska, A., Jablonska, A., Tripathi, A., Plieva, F. M., *et al.* (2011) The performance of laminin-containing cryogel scaffolds in neural tissue regeneration, *Biomaterials*, 32 (13), pp. 3423–3434. DOI:10.1016/j.biomaterials.2011.01.049.

Kaur, S., Raggatt, L. J., Batoon, L., Hume, D. A., Levesque, J.-P. and Pettit, A. R. (2017) Role of bone marrow macrophages in controlling homeostasis and repair in bone and bone marrow niches, *Seminars in Cell & Developmental Biology*, 61, pp. 12–21. DOI:10.1016/j.semcdb.2016.08.009.

Kim, B. S., Shkembi, F. and Lee, J. (2017) In Vitro and In Vivo Evaluation of Commercially Available Fibrin Gel as a Carrier of Alendronate for Bone Tissue Engineering, *BioMed Research International*. Research article, 2017, pp. 1-10. DOI:10.1155/2017/6434169.

Liu, C., Carrera, R., Flamini, V., Kenny, L., Cabahug-Zuckerman, P., George, B. M., *et al.* (2018) Effects of mechanical loading on cortical defect repair using a novel mechanobiological model of bone healing, *Bone*, 108, pp. 145–155. DOI:10.1016/j.bone.2017.12.027.

Liu, M., Zeng, X., Ma, C., Yi, H., Ali, Z., Mou, X., Li, S., Deng, Y. and He, N. (2017) Injectable hydrogels for cartilage and bone tissue engineering, *Bone Research*, 5, pp. 17014. DOI:10.1038/boneres.2017.14.

Loi, F., Córdova, L. A., Pajarinen, J., Lin, T., Yao, Z. and Goodman, S. B. (2016) Inflammation, fracture and bone repair, *Bone*, 86, pp. 119–130. DOI:10.1016/j.bone.2016.02.020.

Marklund, N. (2016) Rodent Models of Traumatic Brain Injury: Methods and Challenges, *Methods in Molecular Biology (Clifton, N.J.)*, 1462, pp. 29–46. DOI:10.1007/978-1-4939-3816-2_3.

Mukozawa, A., Ueki, K., Marukawa, K., Okabe, K., Moroi, A. and Nakagawa, K. (2011) Bone healing of critical-sized nasal defects in rabbits by statins in two different carriers, *Clinical Oral Implants Research*, 22 (11), pp. 1327–1335. DOI:10.1111/j.1600-0501.2010.02135.x.

Nyanzu, M., Siaw-Debrah, F., Ni, H., Xu, Z., Wang, H., Lin, X., Zhuge, Q. and Huang, L. (2017) Improving on Laboratory Traumatic Brain Injury Models to Achieve Better Results, *International Journal of Medical Sciences*, 14 (5), pp. 494–505. DOI:10.7150/ijms.18075.

O'Brien, C. A., Nakashima, T. and Takayanagi, H. (2013) Osteocyte control of osteoclastogenesis, *Bone*, 54 (2), pp. 258–263. DOI:10.1016/j.bone.2012.08.121.

Oni, O. O. A. (1997) The early stages of the repair of adult human diaphyseal fractures, *Injury*, 28 (8), pp. 521–525. DOI:10.1016/S0020-1383(97)00062-4.

Raggatt, L. J., Wullschleger, M. E., Alexander, K. A., Wu, A. C. K., Millard, S. M., Kaur, S., *et al.* (2014) Fracture healing via periosteal callus formation requires macrophages for both initiation and progression of early endochondral ossification, *The American Journal of Pathology*, 184 (12), pp. 3192–3204. DOI:10.1016/j.ajpath.2014.08.017.

Sandberg, O. H., Tätting, L., Bernhardsson, M. E. and Aspenberg, P. (2017) Temporal role of macrophages in cancellous bone healing, *Bone*, 101, pp. 129–133. DOI:10.1016/j.bone.2017.04.004.

Seitz, H., Rieder, W., Irsen, S., Leukers, B. and Tille, C. (2005) Three-dimensional printing of porous ceramic scaffolds for bone tissue engineering, *Journal of Biomedical Materials Research Part B: Applied Biomaterials*, 74B (2), pp. 782–788. DOI:10.1002/jbm.b.30291.

Sithole, M., Kumar, P., C du Toit, L., Marimuthu, T., Choonara, Y. and Pillay, V. (2018) *A 3D Bioprinted In Situ Conjugated-co-Fabricated Scaffold for Potential Bone Tissue Engineering Applications,* 106(5), pp. 1311-1321. DOI:10.1002/jbm.a.36333.

Street, J., Bao, M., deGuzman, L., Bunting, S., Peale, F. V., Ferrara, N., *et al.* (2002) Vascular endothelial growth factor stimulates bone repair by promoting angiogenesis and bone turnover, *Proceedings of the National Academy of Sciences of the United States of America*, 99 (15), pp. 9656–9661. DOI:10.1073/pnas.152324099.

Tang, D., Tare, R. S., Yang, L.-Y., Williams, D. F., Ou, K.-L. and Oreffo, R. O. C. (2016) Biofabrication of bone tissue: approaches, challenges and translation for bone regeneration, *Biomaterials*, 83, pp. 363–382. DOI:10.1016/j.biomaterials.2016.01.024.

Vi, L., Baht, G. S., Whetstone, H., Ng, A., Wei, Q., Poon, R., Mylvaganam, S., Grynpas, M. and Alman, B. A. (2015) Macrophages promote osteoblastic differentiation in-vivo: implications in fracture repair and bone homeostasis, *Journal of Bone and Mineral Research: The Official Journal of the American Society for Bone and Mineral Research*, 30 (6), pp. 1090–1102. DOI:10.1002/jbmr.2422.

Wang, P., Zhao, L., Liu, J., Weir, M. D., Zhou, X. and Xu, H. H. K. (2014) Bone tissue engineering via nanostructured calcium phosphate biomaterials and stem cells, *Bone Research*, 2, pp. 14017. DOI:10.1038/boneres.2014.17.

Wozney, J. M., Rosen, V., Celeste, A. J., Mitsock, L. M., Whitters, M. J., Kriz, R. W., Hewick, R. M. and Wang, E. A. (1988) Novel regulators of bone formation: molecular clones and activities, *Science (New York, N.Y.)*, 242 (4885), pp. 1528–1534.

Wu, A. and Zeng, Z. (2013) Anti-synchronization control of a class of memristive recurrent neural networks, *Communications in Nonlinear Science and Numerical Simulation*, 18 (2), pp. 373–385. DOI:10.1016/j.cnsns.2012.07.005.

Xing, Z., Lu, C., Hu, D., Yu, Y., Wang, X., Colnot, C., *et al.* (2010) Multiple roles for CCR2 during fracture healing, *Disease Models & Mechanisms*, 3 (7–8), pp. 451–458. DOI:10.1242/dmm.003186.

CHAPTER SIX
CONCLUSIONS, RECOMMENDATIONS AND FUTURE OUTLOOK

6.1. CONCLUSIONS

The advancement in the design and fabrication of novel composite 3D printed biomaterial scaffolds for bone tissue engineering application is an on-going research in confronting the limited treatment in critical-sized bone defects. The combined effort of the interdisciplinary field which includes applying the principles of life science, material science and engineering aids in the fabrication of the scaffolds that maintain, restore and improve the functioning of the biological tissue. Moreover, in this study, the integration of multi-biomaterial reinforcement and the use of 3D print technology as an innovative fabrication tool, serves as an ideal outcome to solve the challenge of ideal 3D biomaterial scaffold with appropriate mechanical and biological properties for bone tissue engineering application The composite 3D biomaterial scaffold was prepared using novel in situ co-fabrication by employing 3D bioprinted technology as an innovative fabrication tool.

A number of breakthroughs for critical-sized bone defects treatment strategies have been designed to surpass the current models, however, the common limitation (e.g. poor mechanical strength for bone tissue engineering) continue to exist and no system is fully proven to be efficient yet. Therefore, the design and development of the 3D printed biomaterials scaffold for the enhancement of bone repairing or regeneration with appropriate mechanical properties that match bone tissue regenerations is currently a significant research area. Hence, novel composite 3D printed biomaterial scaffolds were designed, developed, and fabricated through novel synthetic methods for bone tissue engineering application. During synthesis, sodium alginate (NaAlg), silica gel (Si), Nanoclay, hydroxyapatite (HAP) and poly(ethyleneimine) (PEI) and growth factor (OP-1) were identified as suitable components for the formation of the three novel composite 3D printed biomaterial scaffolds (Alg-PEI/HAP, Alg-PEI/Si and Alg-PEI/Nanoclay). But Alg-PEI/Si was identified as the scaffold with appropriate mechanical properties and biological properties for bone tissue engineering for further investigation. The growth factor (OP-1) was used as a model growth factor for forming the final composite through blending and coupling techniques. Therefore, the composite 3D printed biomaterial scaffold was successfully fabricated and characterized.

The composite 3D printed biomaterial scaffold was *in vitro, ex vivo* analysed, that which includes, the investigation of cell viability, cell adhesion and cell proliferation using

osteoblast-like MG63 cells. The difference in toxicity between the printed scaffold and the control allows for biocompatibility validation of the printed scaffold. Therefore, the osteoblast like MG63 cells were found to be biocompatible to the fabricated scaffold. In addition, cell proliferation and cell adhesion were confirmed by SEM and light microscopy

Furthermore, the novel composite 3D printed biomaterial scaffold was evaluated *in vivo* using a New Zealand White Rabbits model. The composite 3D printed biomaterial scaffold displayed significant results, which substantiate and surpassed the control bone defects, thereby demonstrating the major enhancement in new bone regeneration in the induced critical-sized bone defects.

6.2. RECOMMENDATIONS AND FUTURE OUTLOOK

The fabricated novel composite 3D printed biomaterial scaffold resulted to be a biomaterial system that fulfilled the aims and objectives of this study. The *in vitro*, *ex vivo* and *in vivo* analysis showed that the fabricated biomaterial system gave impressive outcome, however, additions to the study may have enhanced the data output.

- The developed composite 3D printed biomaterial scaffold is proposed to be not entirely limited to bone tissue engineering application. This implant can be investigated for other hard tissue defects such as cartilage amongst others using cartilage growth factors.

- There is also a requirement to investigate other types of bone or hard tissue growth factors effects on the regenerative potential of this novel scaffold.

- The *in vivo* study provides significant results concerning the progression of the new bone formation in the induced critical-sized bone nasal defects. These results could be enhanced if proper diet and antibiotics were provided to these animals, which in this instance may have possible accelerated enzymatic alteration of the composite biomaterial scaffolds.

- Pilot human bio-studies are recommended and depending on the results, Wits enterprise will market the product to pharmaceutical companies leading to commercializing the product.

- Quantitative histology results may also help enhancing data output.

STRICTLY CONFIDENTIAL

ANIMAL ETHICS SCREENING COMMITTEE (AESC)

CLEARANCE CERTIFICATE NO. 2017/10/64/D

APPLICANT: Mr M Sithole

SCHOOL: Pharmacy and Pharmacology
DEPARTMENT:
LOCATION:

PROJECT TITLE: In vivo assessment of 3D printed, in situ Conjugated-co-Fabricated, Alginate-PEI Scaffolds using New Zealand white rabbits

Number and Species

17X 12-16 weeks 2.5kg-3.0kg male New Zealand rabbits

Approval was given for the use of animals for the project described above at an AESC meeting held on 2017/10/31. This approval remains valid until 2019/12/04.
Unreported changes to the application may invalidate the clearance given by the AESC
An annual progress report must be provided

The use of these animals is subject to AESC guidelines for the use and care of animals, is limited to the procedures described in the application form and is subject to any additional conditions listed below:

Signed: _____ (Chairperson, AESC) Date: 7 December 2017

I am satisfied that the persons listed in this application are competent to perform the procedures therein, in terms of Section 23 (1) (c) of the Veterinary and Para-Veterinary Professions Act (19 of 1982)

Signed: _____ (Registered Veterinarian) Date: 05 December 2017

cc: Supervisor: Professor V Pillay
Director: CAS

Works 2000\lair\0015\AESCCert.wps

Society For Biomaterials

A 3D bioprinted *in situ* conjugated-*co*-fabricated scaffold for potential bone tissue engineering applications

Mduduzi N. Sithole, Pradeep Kumar, Lisa C. du Toit, Thashree Marimuthu, Yahya E. Choonara, Viness Pillay

Wits Advanced Drug Delivery Platform Research Unit, Department of Pharmacy and Pharmacology, School of Therapeutic Sciences, Faculty of Health Sciences, University of the Witwatersrand, Johannesburg, 7 York Road, Parktown 2193, South Africa

Received 27 September 2017; revised 8 December 2017; accepted 5 January 2018
Published online 23 January 2018 in Wiley Online Library (wileyonlinelibrary.com). DOI: 10.1002/jbm.a.36333

Abstract: There is a demand for progressive approaches in bone tissue engineering to repair and regenerate bone defects resulting from trauma or disease. This investigation sought to engineer a single-step *in situ* conjugated polymeric scaffold employing 3D printing technology as an innovative fabricating tool. A polymeric scaffold was engineered *in situ* employing sodium alginate as a bio-ink which interacted with a poly (ethyleneimine) solution on bioprinting to form a polyelectrolyte complex through ionic bond formation. Silica gel was included in the bio-ink as temporal inorganic support component and for ultimate enhancement of osteoinduction. Characterization of the biorelevant properties of the scaffold was undertaken via Fourier Transform Infrared Spectroscopy, Differential Scanning Calorimetry and Thermogravimentric Analysis, X-Ray diffraction, Scanning Electron Microscopy, and biomechanical testing. The scaffold maintained its 3D architecture for the duration of the 28-day degradation investigation, while potentially permitting the infiltration of nutrients, growth factor, and cells evident by the increased solvent penetration into the scaffold observed via Magnetic Resonance Imaging studies. The scaffold porosity and pore size were found to be 60% and 360 μm, respectively. Biomechanical evaluation revealed a Young's modulus of 18.37 MPa highlighting that the scaffold in its current form possesses the mechanical capabilities for certain bone tissue engineering applications. This investigation provided highlighted the applicability of alginate-poly(ethyeneimine)/silica for 3D bioprinting as a scaffold which could possess potential as a bone tissue engineering scaffold. © 2018 Wiley Periodicals, Inc. J Biomed Mater Res Part A: 106A: 1311–1321, 2018.

Key Words: bone tissue engineering, 3D printing, scaffold, polyelectrolyte complex

How to cite this article: Sithole MN, Kumar P, du Toit LC, Marimuthu T, Choonara YE, Pillay V. 2018. A 3D bioprinted *in situ* conjugated-*co*-fabricated scaffold for potential bone tissue engineering applications. J Biomed Mater Res Part A 2018:106A:1311–1321.

INTRODUCTION

The traditional repair treatments for critical-sized or nonunion bone defects due to trauma or disease have centered on orthopedic implants, allografts, and autografts. However, these techniques suffer from a number of limitations[1,2] such as lack of available donors and inadequate biomechanical properties.[3] Hence, bone tissue engineering employing scaffolds has emerged as an innovative and growing field of research in tissue engineering as an alternative technique to overcome the limitations of current approaches.[2] Tissue engineering techniques involve the use of an appropriate scaffold biomaterial, relevant growth factor and/or cells.[4,5] Polymers have been investigated as biomaterials for a range of medical applications due to their biological properties.[6] Major breakthroughs in tissue engineering is owing to the success in development of novel biomaterial-based approaches that simulate native organ and tissue parts.[7] Manipulation of materials and their biorelevant characterization has been the fundamental to their application in tissue engineering.[8]

The properties of the scaffold depend mainly on the fabrication methods and the nature of the biomaterial.[6] Two-dimensional (2 D) patterns of biochemical and mechanical cues have been generated through the development of numerous intricate methods, but for many cell types, the 2D culture condition may not be appropriate for propagating tissue regeneration. Additionally, 2D fabrication methods cannot be easily transformed into 3D methods, hence, there is a need for more progressive methods to precisely capture the intricate 3D cellular environment.[7] Scaffolds with controlled surface chemistry, pore size distribution, pore volume, pore interconnectivity, and architecture cannot be fabricated with traditional processing techniques[9,10] such as solvent casting or particle leaching, freeze-drying, and gas foaming.[7] Therefore, additive manufacturing processing technologies such as 3D printing have been explored as an innovative tool since

Correspondence to: V. Pillay; e-mail: viness.pillay@wits.ac.za
Contract grant sponsor: National Research Foundation (NRF) of South Africa

© 2018 WILEY PERIODICALS, INC.

APPENDIX C

Reinforced, Composite Biomaterial 3D Printed Scaffolds for Bone Tissue Engineering: Tuning Mechanical Properties and Cellular Affinity

Mduduzi N. Sithole[1], Pradeep Kumar[1], Yahya E. Choonara[1], Lisa C. du Toit[1], Viness Pillay[1*]

Wits Advanced Drug Delivery Platform Research Unit, Department of Pharmacy and Pharmacology, School of Therapeutic Sciences, Faculty of Health Sciences, University of the Witwatersrand, Johannesburg, 7 York Road, Parktown, 2193, South Africa

*Corresponding Author: viness.pillay@wits.ac.za

Abstract

Three dimensional (3D) printing technology have emerge with great potential in designing and fabricating novel biomaterial scaffolds for bone tissue engineering application. Most of the biomaterials (e.g. polymers, bioceramics, metals and composites) used for scaffold fabrication have been discussed in detail over the years in relation to bone tissue regeneration/repair/development. Consequently, this leads to an increase number of developed novel 3D biomaterial scaffolds for bone tissue engineering application. However, there is still an existing challenge in developing novel 3D biomaterial scaffolds with appropriate mechanical and biological properties that match native bone tissue. A number of reinforced multi-biomaterial 3D printed scaffolds have been developed and investigated as a key solution for the mechanical and biological properties challenge. But there is still a huge research gap to attempt new combination of biomaterials that will yield novel 3D printed biomaterial scaffolds with acceptable mechanical and biological properties for bone tissue engineering application. Biomaterials that are mostly investigated for bone tissue engineering application includes: alginate, silica, collagen amongst others, due to their partially/whole similar properties with bone tissue extracellular matrix (ECM). This review discusses the challenges faced by pure biomaterials (single-component) in their 3D printability and unsatisfactory properties for bone tissue engineering application, with selected examples to highlight their properties limitations. The review is aimed at describing the reinforced multi-biomaterial 3D printed scaffolds for bone tissue engineering application, and the rationality of 3D printing technology and the advantages of reinforced multi-biomaterial in tuning mechanical and biological properties of the printed scaffold.

Keywords: Bone tissue engineering, biomaterials, reinforced multi-biomaterial, 3D printed biomaterial scaffolds

APPENDIX D

3D bioprinted biomaterial scaffold for bone tissue engineering: *in vitro* cell assessment and *in vivo* animal studies

Mduduzi N. Sithole[1], Pradeep Kumar[1], Yahya E. Choonara[1], Lisa C. du Toit[1], Kennedy H. Erlwanger[2], Viness Pillay[1*]

[1]Wits Advanced Drug Delivery Platform Research Unit, Department of Pharmacy and Pharmacology, School of Therapeutic Sciences, Faculty of Health Sciences, University of the Witwatersrand, Johannesburg, 7 York Road, Parktown, 2193, South Africa

[2]School of Physiology, Faculty of Health Sciences, University of the Witwatersrand, Johannesburg, 7 York Road, Parktown, 2193, South Africa

*Corresponding Author: viness.pillay@wits.ac.za

Abstract

This research article aimed at substantiating the feasibility of using novel 3D printed biomaterial scaffold as a matrix platform to guide and enhance bone tissue regeneration. The scaffolds were cultured with osteoblast-like MG63 cells for 1, 3, and 7 days, thereafter, optical microscopy and electron scanning microscopy (SEM) were used to examine cell adhesion and surface morphology; MTS assay was used to determine cell viability, and cell proliferation was qualitatively evaluated using Olympus microscopy. The scaffold exhibited biomineralization (Ca-P) confirmed through the SEM-EDX and FTIR analysis. Optical microscopy and SEM revealed that the osteoblast-like MG63 cells attached to the surface of the scaffold. Viability of cells cultured on the scaffold and on control increased over time ($P < 0.05$), however, at respective time point, cell viability was not significantly different between the two groups ($P > 0.05$). The results suggested that the scaffold is biocompatible (non-toxic materials). The study was also conducted to verify that the scaffold properties were engineered to match bone regeneration cascade using rabbit's critical-sized nasal bone defect model. The final scaffold provided a pro-regenerative platform, rich in mechanical, topographical and biological cues to guided cells towards functional regeneration. Histology revealed that there was significant progress of new bone formation especially in week 8 of the study, in all induced bone defects. Therefore, scaffold containing growth factors showed high visual bone formation regenerative (week 8 complete) compared to the scaffold without growth factors and the empty defect (the control).

Keywords: Osteoblast-like MG63 cells, cell adhesion, cell proliferation, cell viability, bone regeneration

APPENDIX E

A 3D Bioprinted in situ Conjugated-co-Fabricated Scaffold for Bone Tissue Engineering Applications

Mduduzi N. Sithole[1], Pradeep Kumar[1], Yahya E. Choonara[1], Lisa C. du Toit[1], Viness Pillay[1*]

Wits Advanced Drug Delivery Platform Research Unit, Department of Pharmacy and Pharmacology, School of Therapeutic Sciences, Faculty of Health Sciences, University of the Witwatersrand, Johannesburg, 7 York Road, Parktown, 2193, South Africa

*Corresponding Author: viness.pillay@wits.ac.za

Purpose:

There is a global clinical need for progressive approaches in bone tissue engineering to repair and regenerate bone defects resulting from trauma or disease. The combination of biodegradable scaffolds, with either host cells, isolated cells and or bioactive molecules is the current approach in tissue engineering. This methodology seeks to restore or enhance the natural processes of tissue development and regeneration. The fabrication of novel 3D biodegradable scaffolds for application towards bone tissue engineering has recently generated intensive research. These novel 3D biodegradable scaffolds need to fulfil certain biological parameters (such as cell adhesion, cell proliferation and cell viability amongst others) before implanted to the human body/ living animal for further investigation. This research article sought to engineer a single-step in situ conjugated polymeric 3D biodegradable scaffold employing 3D printing technology as an innovative fabricating tool, depicted in Figure 1. The aim of this study was to substantiate the feasibility of using the novel printed 3D biodegradable scaffold as a potential matrix platform to guide and enhance bone regeneration

Methods:

A polymeric 3D biodegradable scaffold was engineered in situ employing sodium alginate as a bio-ink which interacted with poly(ethyleneimine) solution on bioprinting to form a polyelectrolyte complex through ionic bond formation. Silica gel was included in the bio-ink as temporal inorganic support component and for ultimate enhancement of osteoinduction. The quantification of various cellular responses (e.g. cell proliferation, cell attachment and viability) of osteoblast-like MG63 cells, cultured on the novel printed scaffold was carried out. The printed scaffolds were cultured with osteoblast-like MG63 cells for 1, 3, and 7 days. Characterization of the biorelevant properties of the scaffold was undertaken via Fourier Transform Infrared Spectroscopy, Differential Scanning Calorimetry and Thermogravimentric Analysis, X-Ray Diffraction, Scanning Electron Microscopy, and biomechanical testing. Optical microscopy and electron scanning microscopy (SEM) were also used to examine cell adhesion and surface morphology. The MTS assay was used to determine cell viability and cell proliferation.

Results:

The scaffold maintained its 3D architecture for the duration of the 28-day degradation investigation, while potentially permitting the infiltration of nutrients, growth factor, and cells evident by the increased solvent penetration into the scaffold observed via Magnetic Resonance Imaging studies. The scaffold porosity and pore size were found to be 60% and 360 µm, respectively. Biomechanical evaluation revealed a Young's modulus of 18.37 MPa highlighting that the scaffold in its current form possesses the mechanical capabilities for certain bone tissue engineering applications. Scanning electron microscopy revealed that the osteoblast-like MG63 cells cultured on the printed scaffold were clearly attached to the surface of the printed scaffold. The viability of cells cultured on the printed scaffold and on control increased over time ($P < 0.05$), however, at respective time points, cell viability was not significantly different between the two groups ($P > 0.05$).

Conclusion:

Therefore, a novel alginate-poly (ethyeneimine)/silica 3D bioprinted scaffold was fabricated, characterized and showed great potential for application in bone reconstruction in the future. These results suggest that the novel printed scaffold contain biocompatible material that could be used as a suitable bone application.

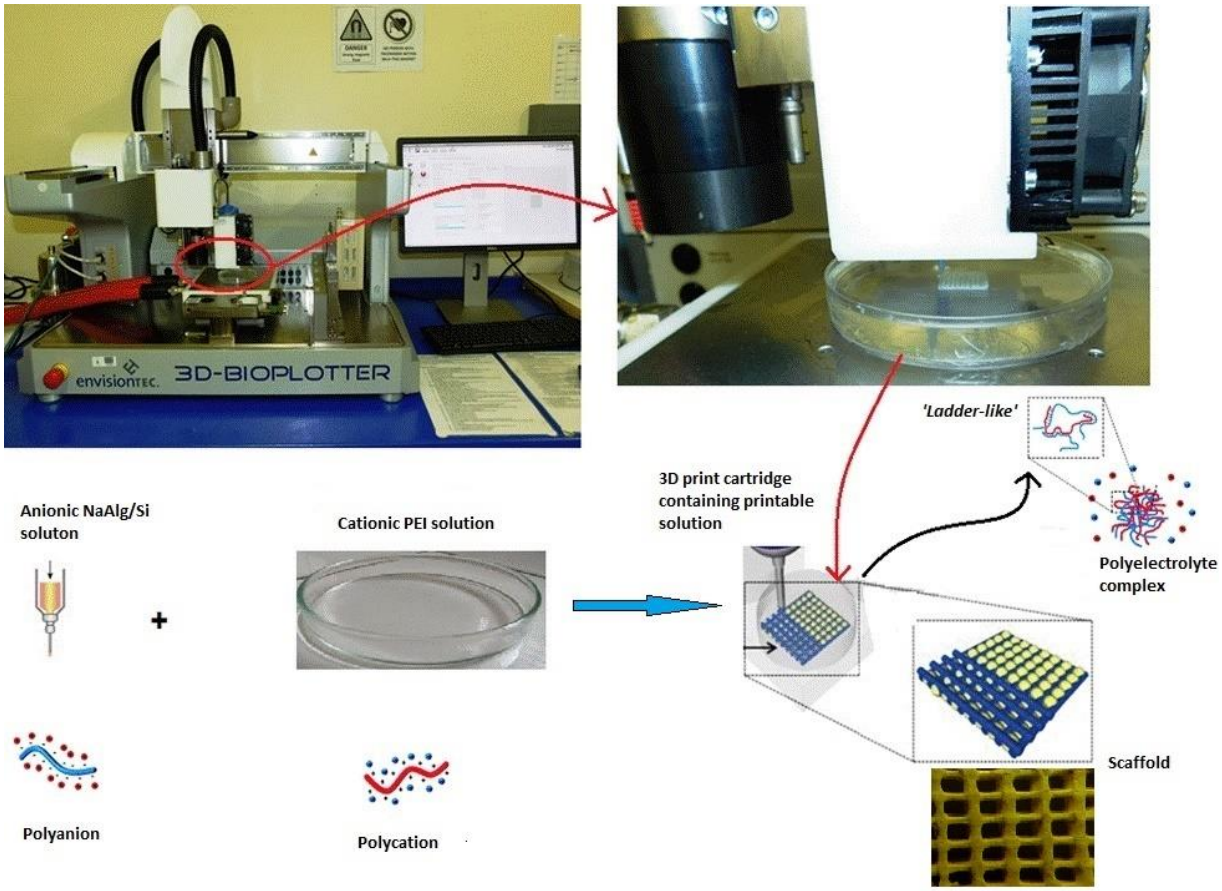


Figure 1: Schematic and photographic depiction of formation of the 3D bioprinted and *in situ* conjugated-co-fabricated scaffold